Flood Control 2015

SOLUTIONS FOR *SMART* FLOOD CONTROL

MODELS AND ANALYSIS FOR FLOOD CONTROL SYSTEMS

FLOOD CONTROL 2015 > STIELTJESWEG 2 > 2628 CK DELFT > THE NETHERLANDS > T: +31 (0)88 33 57 446 > F: +31 (0)15 261 0821
INFO@FLOODCONTROL2015 > WWW.FLOODCONTROL2015.COM

INFO

Title
Models and analysis for flood control systems

Commissioned by
Stichting Flood Control

Number of pages
102

Status
Final

Version	Date	Author	Signature	Reviewer	Signature
6.0	2010-12-16	Pauline Kruiver, Victor Hopman, Research team		J. Maccabiani	

Research team:

- Deltares: Pauline Kruiver, Victor Hopman, Marco Kleuskens, Han Knoeff, Hans Sellmeijer, Raymond van der Meij, André Koelewijn, Rogier Westerhoff (project number 1202195.002)
- TNO-ICT: Erik Langius, Matthijs Vonder, Bram van der Waaij, Wiltfried Pathuis, Arnoud de Jong
- IBM: Bram Havers, Marijke Bultsma, Ernst van Waning
- Stichting IJkdijk: Wouter Zomer
- Fugro; Martin van der Meer, Maarten Bomers, Charlotte Bishop, Richard Chiles, Harry McCormack, Richard Burren

Disclaimer

MANAGEMENT SUMMARY

The goal of the project is to define a framework for Smart Levees, including the development of new models for levee safety monitoring and underlying IT infrastructure.

The general goal can be subdivided into four subgoals, which are:
1. Define technical feasibility of Smart Levee concept.
2. Model development based on IJkdijk experiments and LiveDijk Eemshaven.
3. Real time levee monitoring with improvement of robustness.
4. Develop remote sensing levee monitoring techniques.

This report contains the findings of the research on the subgoals 2, 3 and 4 (Deliverable 2010.02.02.3). In combination with report 2010.02.01.01 ''Feasibility study on Smart levees and report 2010.02.05.02 ''Application inventory for levee management'' it is the backbone for the development of a Smart Levee concept.

Model development based on IJkdijk experiments and LiveDijk Eemshaven
Slope stability
For slope stability, both movements and pore pressures are key parameters. Humidity, soil moisture content, temperature and vibrations are not relevant for this type of failure mechanism. Time series analysis on pore pressure data from the LiveDijk Eemshaven provide a viable approach to convert raw data to useful information on slope stability for water boards. Stability calculations can be improved using observations from tilt meters. With the developed TimeLine Store, a statistical analysis of all parameters will be possible, but has not been performed yet.

Piping
For piping, the key parameters are pore pressure and discharge. Self Potential, temperature and sand volume are potentially useful parameters. A 2D model was explored to link pipe length to discharge, head drop and sand volume. The results are good for head drop and discharge. In future, these results can be expanded to cover generalized levee schematizations using Artificial Neural Networks. The link between Self Potential and discharge is complex and more research is needed.

For both piping and slope stability, the time dependent behavior of pore pressures at changing water conditions will be investigated in a Flood Control project in the future.

Real time levee monitoring with improvement of robustness
In order to gain real time information a TimelineStore is developed and implemented. Timelines are based on potential high available, high scalable, geodistributed database technology (Cassandra).

Pre-analysis techniques for detection of missing samples and value of the signal were designed. These techniques resulted in virtual sensors of sample changeability and number of dominant frequencies.

The possibilities of multi-sensor trendspotting need to be explored. The next step in the development of the TimeLineStore will be the implementation of the concept of forking timelines in order to do simulation and investigation of all the capabilities of the Cassandra database for the use of dike monitoring.

Develop remote sensing levee monitoring techniques
Deformation
In the case study of the Juliana Canal, many PS points were detected and regional deformation patterns could be inferred. However, only a small amount of PS points were identified on the levees. With more advanced PSI processing, the number of PS points can probably be increased. Also, higher resolution satellites such as

Terrasar-X are expected to provide higher PS point densities. In conclusion, PSI is considered a useful technique for levee monitoring. Due to the revisit times of satellites and the delay in availability of the precise orbit parameters (needed in processing), this monitoring will not be real-time.

Leakage and soil moisture content
Some of the detected anomalies using backscatter of SAR might be related to soil moisture variations. Differential Interferometry based on phase centre shifts also show encouraging results that some high spatial frequency effects could be the result of soil moisture. With the launch of future SAR missions at higher spatial and temporal accuracy, this technique might provide an operational soil moisture detection system in the future. Fully polarimetric data hold the most promise for further investigation at vegetated areas.

TABLE OF CONTENTS

1 INTRODUCTION

1.1 GENERAL

In recent years, sensor systems have been developed and tested on field-scale laboratory and existing operational levees. The development of underlying models, IT infrastructure and a vision on the use of sensors in levee monitoring needs to keep in pace with the market. During the 2009 Flood control project of “Robust Monitoring”, a start was made on the models and IT infrastructure. The vision on Smart Levees received less attention.

The 2010 Flood Control project “Monitoring of a Smart Levee” (2010.02) focuses on the vision of Smart Levees and is a continuation of model and IT development. Five parties of the Flood Control consortium joined forces. These were Deltares, TNO-ICT, Fugro, Stichting IJkdijk, IBM.

1.2 GOAL

The goal of the project is to define a framework for Smart Levees, including the development of new models for levee safety monitoring and underlying IT infrastructure.

The general goal can be subdivided into four subgoals, which are:
1. Define technical feasibility of Smart Levee concept.
2. Model development based on IJkdijk experiments and LiveDijk Eemshaven.
3. Real time levee monitoring with improvement of robustness.
4. Develop remote sensing levee monitoring techniques.

These project goals contribute to the Flood Control 2015 program goals:
> Improved prediction of short term risks.
> User friendly information and knowledge for end users and stakeholders.
> The expectation that innovation in sensor technology can produce a leap in operational protection against high water levels.

This report contains the findings of the research on the subgoals 2, 3 and 4 (Deliverable 2010.02.02.3). The technical feasibility of Smart Levees of subgoal 1 is reported in “Feasibility study of smart levees concepts” (Deliverable 2010.02.01.1).

1.3 AUDIENCE

This report on the models and analysis for flood control systems is useful for end user organizations such as water boards, STOWA and Rijkswaterstaat (RWS). The sensor suppliers can also benefit from the results of this study.

1.4 DOCUMENT STRUCTURE

The deliverables of the work packages concerning the contributions to the model and analysis report are reflected in the document structure and chapters. Chapter 2 describes the new and improved models for levee safety. Chapter 3 focuses in the long term real time monitoring of a real sensor equipped levee. In chapter 4, the potential use of remote sensing for levee monitoring is discussed. Chapter 5 combines the monitoring with the Smart Levee concept. In Chapter 6 the results are provided and recommendations made.

2 MODELS FOR DIKE SAFETY

2.1 INTRODUCTION

In this chapter, improved and new models are presented in which dike stability is related to sensor values. These models are based on sensor measurements performed during the two IJkdijk experiments (slope stability, September 2008 and backward piping erosion September-December 2009) and ongoing sensor measurements on the LiveDijk Eemshaven (from October 2009 onwards).

In various projects, research is performed to improve the understanding of the failure mechanisms of slope stability and piping [e.g. van Duinen, 2010 and Van Beek en Knoeff, 2010]. The FEWS-DAM model for slope stability and piping was adjusted in the Robust Monitoring project (FC2015 project 2009-02) to be able to cope with real-time sensor values of pore pressures [FC 2009]. In the STOWA reports of the IJkdijk experiments, the reference measurements and the individual sensor party reports have been incorporated [Weijers et al. 2009; Koelewijn et al. 2010]. However, various types of sensor data were not combined in models.

The goal of this part of the project is to improve existing and develop new models for dike safety predictions based on several types of sensor data from the two IJkdijk experiments which were performed in 2008 and 2009.

The approach for the development of new or improved models consists of several steps. First, general issues regarding data quality, extrapolation in time and space, types of models and processing techniques are considered. Subsequently, issues specific for a failure mechanism are considered, like the suitability of a parameter to monitor a process, available models and concepts. With models available to link slope stability to measurements, existing and future levee monitoring projects (e.g. LiveDijk type locations, where existing levees are monitored without failure occurring), the raw measurements can be translated into information which is useful for the levee manager at several levels in the national (Rijkswaterstaat) or water board organizations.

The failure mechanisms considered in this chapter are slope stability and backward piping erosion. When large scale slope stability is a problem in a levee, often not only the levee itself fails, but also the subsoil underneath the levee (Figure 2.1). The cut in a failed levee can often be described by a spherical form. At the crest of the levee at the upper part of the cut, a deep incision occurs. On the landside of the levee, the crest will subside. At the lower part of the levee, the land will rise or a ditch (if present) will be closed.

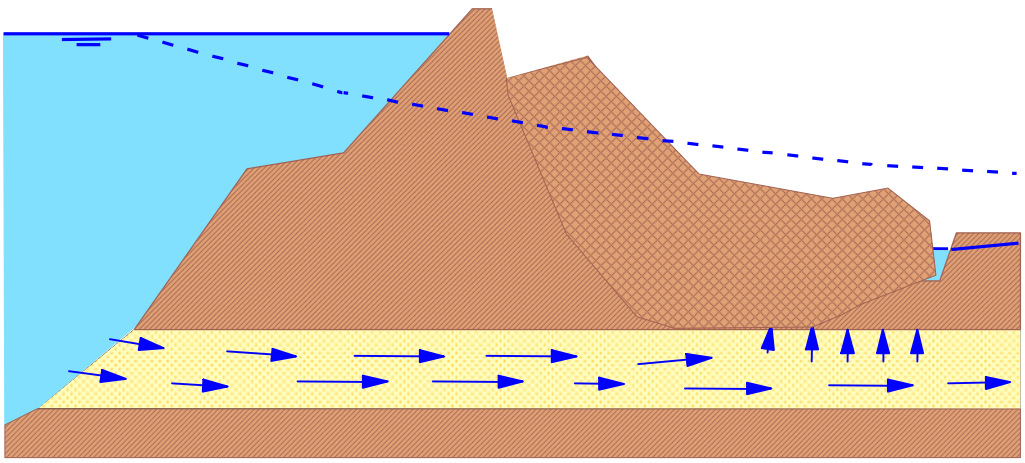

Figure 2.1 Schematic representation of failure by slope instability of a levee

Backward piping erosion (in short: piping) is defined as the process of backward internal erosion in sandy layers underneath clayey levees (Figure 2.2). This process is considered to be one of the most dominant failure mechanisms of levees in The Netherlands. The piping process is divided into four phases: seepage, backward erosion of a pipe, widening of the pipe and breakthrough.

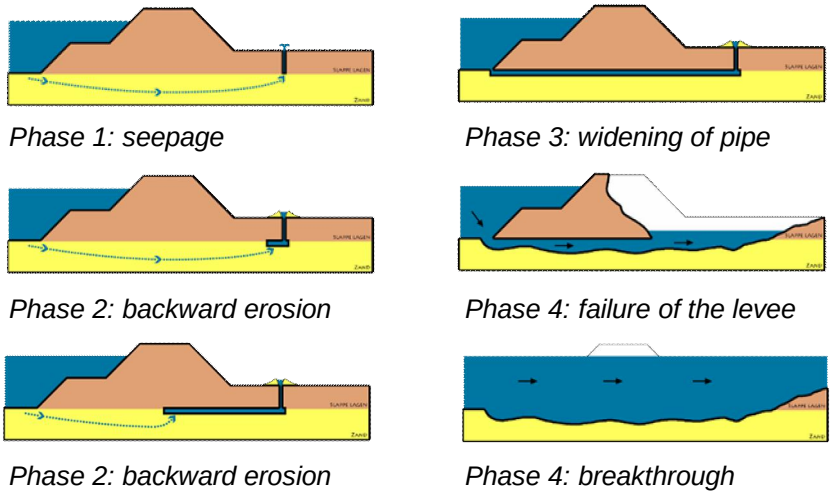

Phase 1: seepage *Phase 3: widening of pipe*

Phase 2: backward erosion *Phase 4: failure of the levee*

Phase 2: backward erosion *Phase 4: breakthrough*

Figure 2.2 Schematic representation of the piping process

In this chapter, the data acquired on both failure mechanisms is described, some considerations on interpolation and extrapolation are given, followed by a statistical analysis of the piping data and a description of several calculation models.

2.2 DATA

During the IJkdijk experiments, a wide variety of parameters was measured by several types of sensors. The parameters are summarized in Table 2.1. At the LiveDijk Eemshaven, temperature and pore pressures are measured.

The suitability of the parameters to describe and monitor slope stability and piping was judged by dike experts. The results are shown in the tables in Appendix 2 : and Appendix 3 : . For stability, both movements and pore pressures are key parameters. Humidity, soil moisture content, temperature and vibrations are not relevant for this type of failure mechanism. For piping, the key parameters are pore pressure and temperature. Self Potential, discharge and sand volume are potentially useful parameters.

During the various IJkdijk experiments, not all sensors worked during the entire experiment or gave reliable or stable results. From the first glance analysis of the piping experiment data in the Flood Control project Robust Monitoring (2009.02), several aspects concerning data quality appeared:

- The individual sensor values appear to be jumpy. The accuracy of the sensor needs to be checked against the expected order of deviating values indicating a change in circumstances related to stability. Some kind of averaging in time might be necessary.
- Changes in parameter values can be indicative of changes in safety level or they can be merely following (lagging in time). The predictive value needs to be assessed.
- It is difficult to distinguish between deviating sensor values because of malfunction, drift (e.g. by gas formation in the measurement chamber of a piezometer) or indications of changing safety level.
- The sensor values may depend on the way the sensor is incorporated in the dike (flexible or fixed).
- Some sensors are not stable in time. They may give fluctuating values, while the average value appears to be correct. The virtual sensor derived from a number of sensors gives erroneous results when one of the input sensors is an unstable one.
- The data set needs to be divided into parts with reliable and unreliable data.

Table 2.1 Parameters measured during the IJkdijk experiments

Slope stability experiment			Piping experiment	
Reference measurements	**Measurements by sensor parties**		**Reference measurements**	**Measurements by sensor parties**
Pore pressure	Pore pressure		Pore pressure	Pore pressure
Soil moisture content	Soil moisture content		Flow / discharge	Capacitive measurements
Movement (Tilt / Settlement)	Movement (Tilt/ Strain/ Deformation)		Sand volume	Movement (Strain/ Deformation)
Visual inspection	Vibration		Visual inspection	Vibration
Weather station	Electrical conductivity			Self Potential
Humidity	Temperature			Temperature

The participants were asked to state the quality of their data according to the following ranks:

1. High quality (in accordance with specifications)
2. Limited quality (oscillations, peaks)
3. Low quality (e.g. delayed response)
4. Unreliable
5. No data

In the further analysis, only high quality data was incorporated. Malfunctioning sensors were removed from the data set.

2.3 INTER- AND EXTRAPOLATION IN TIME AND SPACE

In a Flood Control System which uses different types of sensors, the data is inherently supplied at different times. This is because of the different frequencies with which they measure. Some sensors give values every 10 minutes, others twice a day, etc. Even if all sensors would be synchronized and set up to produce a value with a common frequency, drifts of internal clocks would desynchronize the system after some time. Therefore, models need to be able to cope with sensor values from different moments in time. Differences in timing of sensor values is solved using the timeline principle, described in § 3.3.

When running a model which has time dependent input parameters, several aspects deserve attention:

> Definition of a model clock-frequency. The right moment for the model calculation to start: e.g. after each new sensor value or after a new value for a selected parameter.
> Correct extrapolation of sensor values in time from the last registered sensor value to the time of the start of the model calculation. The sensor value at time X can be e.g. taking the last known value, linear extrapolation from the last two known values, kriging, curve-fitting, trendspotting etc.
> Reliability of the extrapolated sensor value related to the time span between the last measured sensor value and the moment of input in the model.

It is assumed that the sampling frequency is sufficiently high that the last known value is representative for the entire period between measurement and the next moment of measurement. Other techniques of extrapolation are not considered at this stage. If necessary, they can be added later.

In the IJkdijk experiments, an abundance of sensor types and numbers were implemented. An important question is how many sensors are needed to obtain a sensible dike safety prediction. The answer is of significance for the business case elaborated under subgoal 1, which is reported in the report “Feasibility study of smart levees concepts” (Deliverable 2010.02.01.1).

The spatial distribution of sensors depends on the scale of the phenomenon which is monitored. In the case of slope instability, the slip plane depends on the geometry of the levee and the composition of the subsoil. For a typical Dutch levee, the part that will slide down will have a length of several tens of meters. Therefore, the sensors monitoring the levee, can be in lines which are about 30 m apart. Piping is a process which occurs on a very small scale. The initial height of the pipes can be only about one millimeter. The pore pressures are affected by changes in hydraulic conductivity up to 1-2 m from the pipe. Therefore, a much denser sensor network is required for early detection of this mechanism.

2.4 STATISTICAL ANALYSIS

In order to reveal correlations between various parameters which were measured during the IJkdijk experiments, a statistical analysis was carried out. For this analysis, the software application SPSS was used.

The original goal of the statistical analysis was to find correlations between *all* parameters measured during one complete experiment. During the project, this appeared to be too ambitious. One of the problems encountered was the difference in recording times for the different parameters. During the SPSS analysis, the TimeLine Store was not yet developed. For the statistical analysis, it was vital that the recordings were done at identical moments in time for the parameters considered. Therefore, the SPSS analysis was carried out for two of the four piping experiments, for temperature and various types of pore pressure sensors. These were either measured at the same time (by one instrument) or resampled before carrying out the statistical analysis. The SPSS report is attached in Appendix 4 : and summarized in §2.4.1 and §2.4.2.

2.4.1 Piping experiment 1

In order to study the behavior of the sensors during pipe formation, the time sequence was truncated at about two hours before failure of the levee. The correlation matrix of three MEMS pore pressure sensors located close to the location of failure show a very high correlation, indicating that these sensors measure the same phenomenon.

Principal component analysis was performed on the correlation matrix of 54 pore pressure sensors, i.e. on 22 MEMS (series ASA001 and ASA002) and 32 piezoresistive pore pressure sensors (series WSMA300 and WSMA500). Before that, the measurements were first standardized to mean = 0 and variance = 1, which is shown in Figure 2.3. The first dimension describes 97.08% of the variance, enough to claim that the measurements by pr sensors and by MEMS are interchangeable. Both types of pressure sensors (pr and MEMS) in Piping Experiment 1 report on just one process (development of pressure), no other processes can be detected in this case.

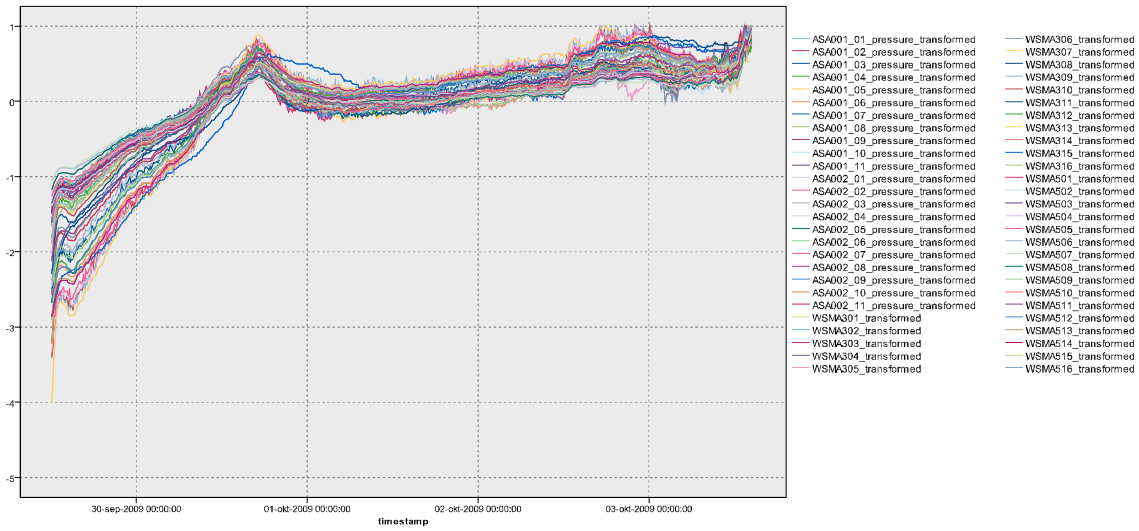

Figure 2.3 Standardized measurements by MEMS and pr pore pressure measurements during piping experiment 1. Input for Principal Component Analysis

During experiment 1, the temperature changes are much less consistent than changes in pressure. PCA was not performed on the temperature data of experiment 1.

2.4.2 Piping experiment 4

In piping experiment 4, several interfering actions of the Luisterbuis drainage tube took place. The actions are clearly visible in the observed pressures as dips (Figure 2.4). The three dips in the curves show the effect of drainage. Inside the levee, drainage seems to have more effect on ASB02 and ASB03 than on ASB04 and ASB05. This may be because ASB02 and ASB03 were closer to the drainage tube.

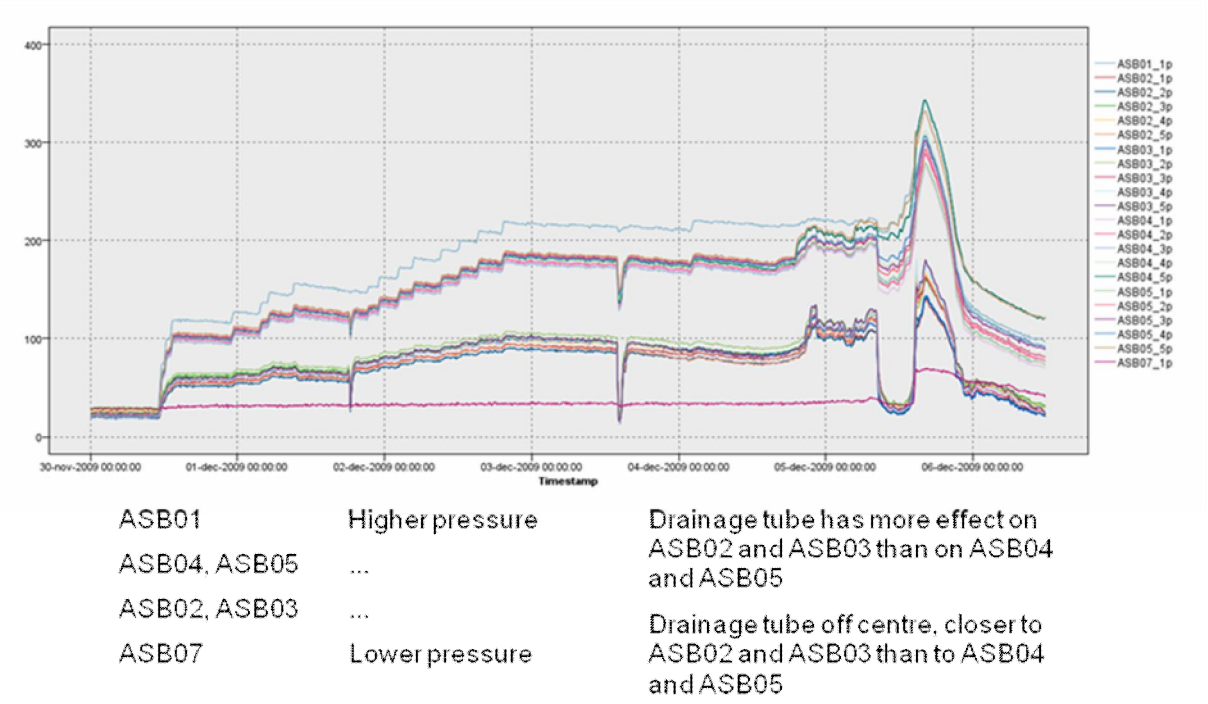

Figure 2.4 Measurements by MEMS pore pressure measurements during piping experiment 4. Actions from drainage are visible as dips in pore pressure.

The temperature measurements during experiment 4 are shown in Figure 2.5. Sensors ASB01 and ASB07, located at the toe of the levee, initially report similar temperatures which is well below the initial temperatures of the two sensor chains. They diverge during the experiment: ASB07 receives warmer water and ASB01

cooler. Temperature values from sensor chains ASB04 and ASB05 (high pressure) steadily decrease, while ASB02 and ASB03 remain constant with a sudden drop for some sensors. Sensor chains ASB04 and ASB05 steadily report colder water, most probably representing water from the high pressure side of the levee. Meanwhile, sensor chains ASB02 and ASB03 retain their high temperature, dropping sharply during collapse.

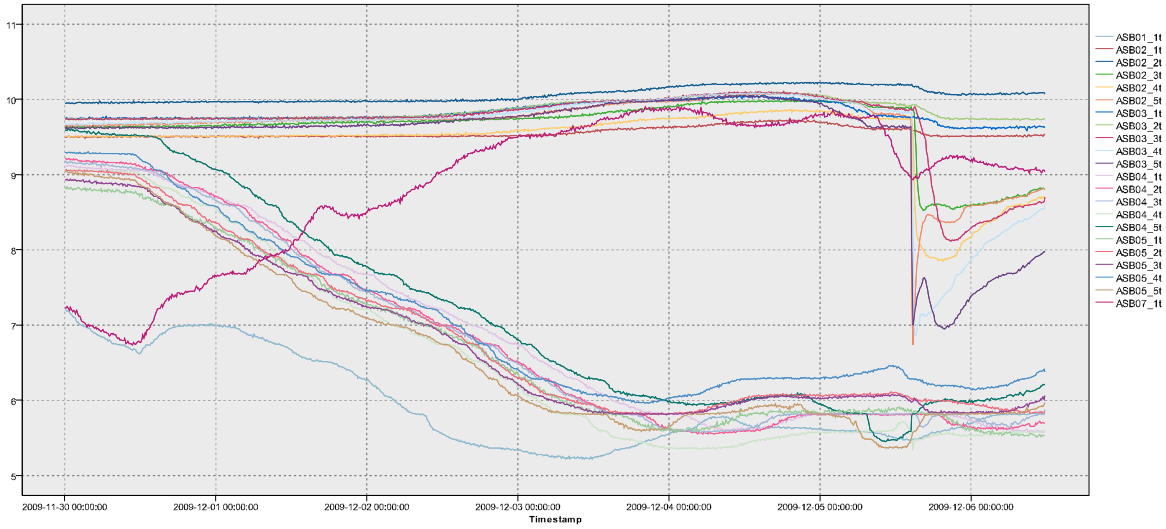

Figure 2.5 Measurement of temperature at the same locations as the MEMS pore pressure sensors during piping experiment 4.

Principal Component Analysis performed separately on the pressure and on the temperature measurements. In both cases, two principal components are needed to describe the largest part of the variance in the data. The components are shown in Figure 2.6. For pressure, almost 96% of the variations is described by two components: the first describes 88.5% and the second just over 7%. Both components are orthogonal. The first component (upper panel, blue line) shows a general trend, while the second, less important component (upper panel, red line) separates ASB02 and ASB03 from ASB04 and ASB05. The most striking features show during the periods of drainage. There are low scores for the general trend of the first component, showing the effectiveness of drainage. The second component has high and opposite scores. In the first component, the effect remains roughly constant during the three episodes of drainage action, while compensating effect in the second component grows with time until it reaches 4 standard deviations. This can be explained as if drainage has a diminishing effect for the high-pressure sensors of ASB04 and ASB05 relative to ASB02 and ASB03. From a physical point of view, it can easily be explained by the fact that the upstream reservoir level was kept constant during these three drainage periods, with an increasing effect on the pore pressures measured between this reservoir and the drainage tube, whereas downstream the situation each time approached to the same situation.

For temperature, almost 94% of the variations is described by two components: the first one describes 62% and the second one 31%. The first component separates the high pressure sensors without sudden cold water (ASB01, ASB04 and ASB05) from the sensors with lower pressure with a cold water wave. The first component (Figure 2.6 lower panel, blue line) shows the gradual lowering of temperatures measured at the high pressure sensors, the second component (lower panel, red line) displays the constant temperature of ASB02 and ASB03 with a rising tendency of ASB07 and especially the wave of cold water.

These findings may be useful for the development of models applicable to large scale monitoring of levees, applying Artificial Intelligence to detect anomalies from normal or expected behavior. Such models are for instance under development within the European 7th framework project “Urban Flood” (www.urbanflood.eu).

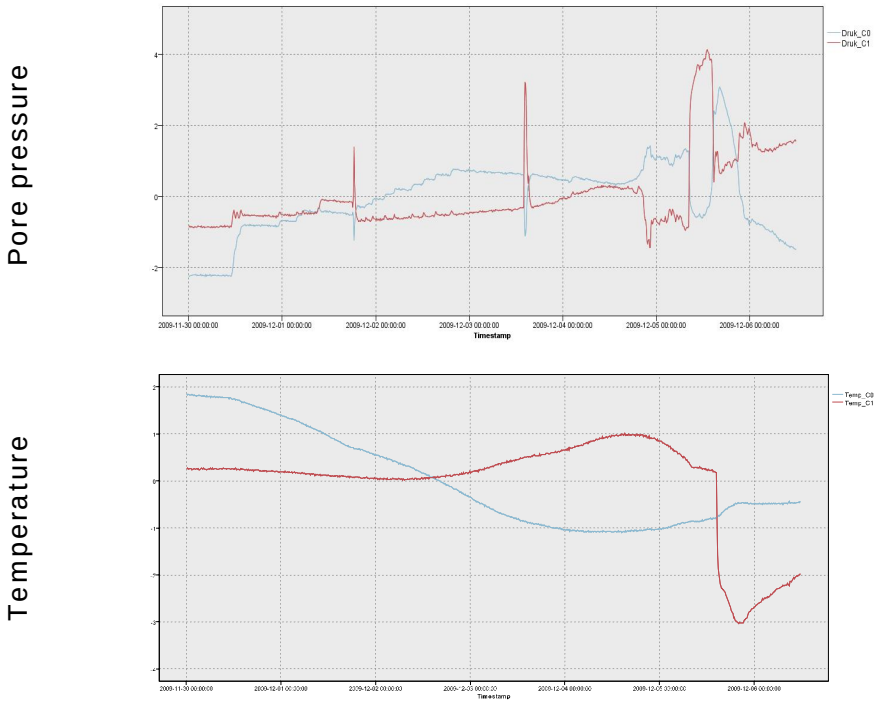

Figure 2.6 Two principal pressure components (upper panel) and two principal temperature components (lower panel) from the PCA of experiment 4. Blue represents the first component, red the second component.

2.5 MODELS

In this paragraph models, which link parameters which can be measured in or on a levee to a measure of safety, are described for slope stability and for piping. For slope stability, several types of models were investigated. They range from relatively simple analytical models to complex Finite Element Models. Intermediate in complexity is time series analysis. This last approach was successfully applied during this project (§2.5.2). The other two types of models are shortly described in §2.5.1 and §2.5.3. One model for piping is described in detail in §2.5.5, another method is described shortly in §2.5.6.

2.5.1 For slope stability – simple analytical models

To our knowledge, only one simple analytical method is available that links the safety of an embankment to its deformations. Bourges & Mieussens [1979] describe a method to predict horizontal deformations of an embankment as a result of loading. This method has proven to be the best method to predict horizontal deformations in the Dutch subsoil [CUR 228, 2010]. One of the parameters in this method is the safety with respect to slope instability of the embankment.

The safety factor of the embankment is derived following Bourges & Mieussens [1979] as:

$$f = \frac{4,85\left(8-m\right)}{\frac{7u}{0,73D}+7\times 1,15}$$ **Equation 2-1**

where *m* is a function of the slope angle of the embankment, *D* is the thickness of the soil layers and *u* is the maximum horizontal deformation at the toe of the embankment (Figure 2.7).

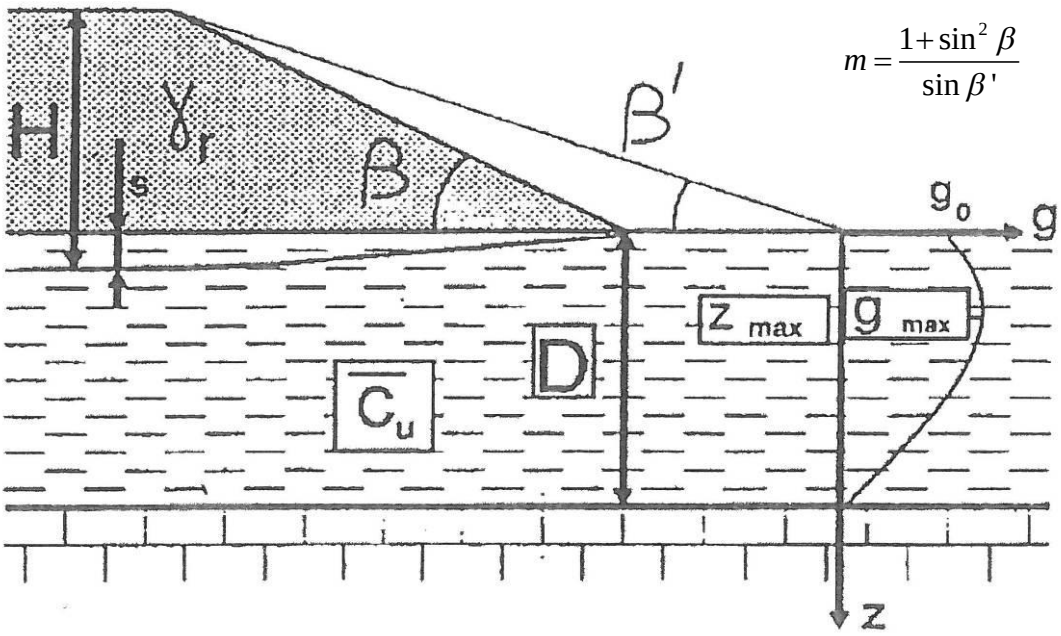

Figure 2.7 Horizontal deformations in Bourges & Mieussens' method [1979]

In Equation 2-1, the stiffness of the soil is not one of the parameters determining the safety factor. This means that regardless of the soil type (sand or peat), the embankment will have the same safety factor at a certain deformation. This is not realistic, because soft soils show larger deformations at a given safety factor than stiffer soils. A workaround might be possible by using normalized deformations to account for differences in stiffness. This will require more research. At this stage, this analytical approach is abandoned.

2.5.2 For slope stability – Time series analysis

The slope stability of a levee depends on the internal structure, and is unique for every case. In order to calculate the slope stability, it is necessary to estimate the water table inside the levee. The envelope of the water table is dependent on the internal structure, rainfall and the intensity of a flood. Since most levees in the Netherlands are very heterogenic, the changes in groundwater table are very unpredictable.

Therefore, much effort is spent on predicting the behavior of a levee using the minimum amount of sensors. This research covers the possibility to predict sensor information by means of time series analyses. In this way, it is possible to fill in gaps when a sensor is damaged, and to extrapolate data in order to predict the safety of a levee during a future hazard.

One of the most structural approaches of a time series analysis is the Box Jenkins model. This model covers several steps. First, autocorrelation and spectral analysis characterizes the temporal variability and periodicity respectively. The next step is to fit a time series to a regressive model, which means that it is assumed that a measurement is linearly dependent on the last state. The parameters of the following function are estimated:

$$o_t = i_t\alpha + o_{t-1}\delta \qquad \textbf{Equation 2-2}$$

Where *i* is the input time series, *o* the output time series, and α and δ are the parameters which are to be estimated. This equation can be used in two ways: the prediction of the output in the future is best when *o* is the real output time series. But when the output time series are temporarily unavailable, *o* can be replaced by the simulated output. In this case, the prediction is less accurate, but still useful as interpolation. The parameter α shows the rate between the magnitudes of the input signal and the output signal. The term δ is a memory term; it describes how much the output is dependent on the past data. This term becomes very important when the output time series show a substantial delay. If required, this equation can be expanded to a summation with a series of deltas, referring to different moments in the past. In this way, a more complex response in time can be simulated. Considering the usually relatively fast response in levees, these extra terms are redundant here.

Since the input and output can have different reference levels (e.g. pore pressure and height with respect to sea level), the data is corrected with respect to the mean value:

$$o_t = \bar{o}_t + (i_t - \bar{i})\alpha + (o_{t-1} - \bar{o})\delta$$ **Equation 2-3**

This mean value is taken over the time window that is used for the calculation. When the time window is substantially larger than the tidal period, this offers no problems.

Finally, it is calculated about how much of a time series can not be predicted from the past, the so-called white noise. A calculation takes in the order of 5 seconds, which eventually enables us to use the package in a real time mode (for instance by FEWS).

Time series analysis is performed on the sensor readings from the LiveDijk Eemshaven in the northeast of the Netherlands. The results of this analysis are presented in § 3.5. It is demonstrated that an external sensor of a different party (Rijkswaterstaat) can be used to predict pore pressures inside the levee. The relationship between the RWS values and the pore pressures is learned during times of relatively quiet weather and low water levels. The relationship cannot be extrapolated as such to conditions of e.g. severe storms and high water levels. In that case, the relationship should be learned anew. This also means that this method is not directly suitable to determine failure conditions, as this inevitably requires extrapolation – it can never be derived by interpolation. Although the analysis showed that the time series approach is successful in predicting the pore pressures inside the levee, it can not fully substitute the sensors.

2.5.3 For slope stability – Finite Element Methods

Models more complex than analytical or time series models are finite element methods. A finite element method can be used to derive a relation between the safety factor and deformations at a certain point in the geometry using a so-called phi-c reduction (Figure 2.8). In a phi-c reduction, the strength described by the internal friction phi and the cohesion c of the soil is reduced by an increasing factor until large deformations occur. The factor at which the strength is equal to the resistance is sought. That factor is in many ways comparable to a conventional analytical safety factor.

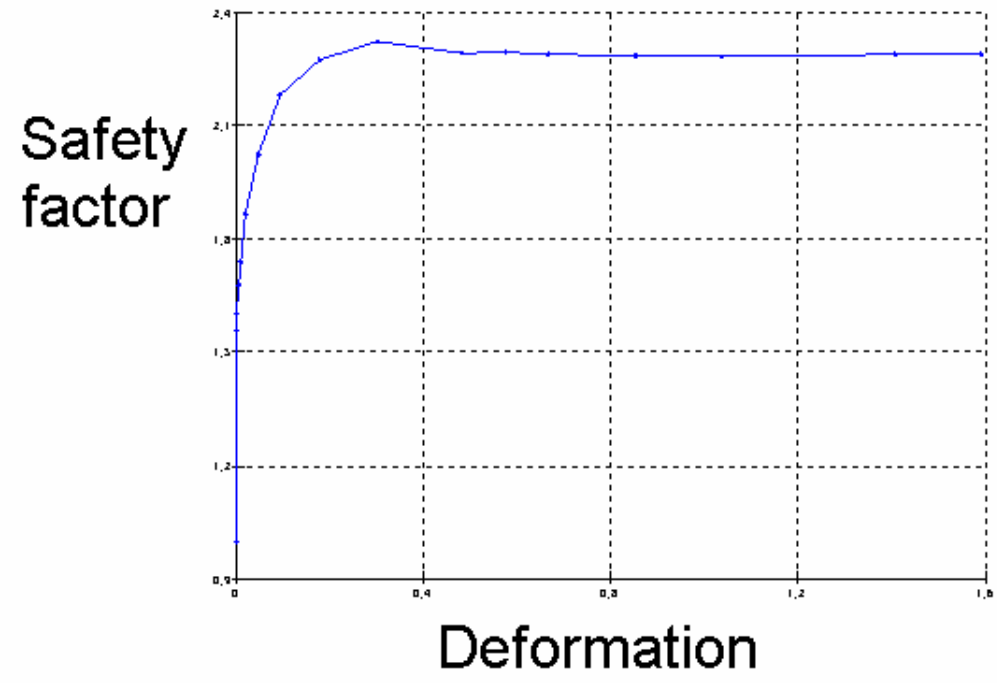

Figure 2.8 Result of a phi-c reduction analysis

A finite element model needs a constitutive model to describe the behavior of the material. Simple models like Mohr-Coulomb cannot describe soil behavior well. The Hardening Soil Models performs for stiff materials like rock and compact sand. The Soft Soil Creep model specifically models peat and clayey material, but only performs well if the material behaves isotropically. If the material has different properties in different directions,

an anisotropic model is required, such as the “Undrained Clay Model” [Vermeer et al., 2010]. The latter model, however, is still in an academic phase and not applicable during this stage of the project.

Table 2.2 Summary of a comparative study for failed or strongly deformed levees in the Netherlands. MStab calculations used Uplift Van model [van Duinen, 2010] and [den Haan and Feddema, 2009].

Site	Situation	Sensors in levee	Finite Element Model (Plaxis)	Result
Bergambacht (uplift induced instability experiment)	Failure of levee	Yes, full-height inclinometers and pore pressure meters	Hardening Soil and Mohr Coulomb models	Problems with Plaxis, because of low initial stability (low effective pressures, low cohesion, excavation of hinterland)
Wolpherense-dijk Gorinchem	Failure of levee	No, but measurements of horizontal and vertical movement are available	Hardening Soil and Mohr Coulomb models	Results appear to be highly sensitive to assumptions regarding time-dependent pore pressures in the aquitard above the aquifer connected to the river during flood.
Zuiderlingedijk Spijk	Failure of levee	No	Hardening Soil model	With some combinations of peak and end values for phi, no stable calculations with Plaxis were possible.
Lekdijk west Bergambacht (TAW-proefvak)	Large deformation, no failure	Yes, one full-height inclinometer	Hardening Soil and Mohr Coulomb models	Plaxis calculations are in agreement with observations.
Heinoomsvaart, Wilnis	Large deformation, no failure	No, but measurements of horizontal and vertical movement are available	Plaxis	Large difference in results for MStab and Plaxis for drained shear strength parameters. Good agreement for undrained shear strength parameters.
Lekdijk Streefkerk	Failure of levee	Yes, pore pressure meters	None	Calculated stability factors are too high to describe failure.
IJkdijk (slope stability experiment)	Failure of levee	Yes, pore pressure meters, full-height inclinometers, tilt meters, other	Soft Soil Creep	MStab calculations with undrained strength parameters give a slip circle in agreement with observations. Soft soil Creep calculations in agreement with observations, except when close to failure.

Based on a graph as in Figure 2.8, the safety can be inferred from the measured deformations at a certain location. There are, however, some difficulties in this approach. First, the finite element method does not predict the horizontal deformations well, whereas these are the main component of the total deformations. Second, relatively large displacements can be predicted from the graph, which results in large distortions of the finite elements, reducing the precision of the analysis. Lastly, many experimental laboratory results are required to determine reliable input parameters and good calibration of the model.

In recent years, Deltares has performed several studies which compared results for stability calculations with the models by Bishop and Van using MStab and the Finite Element Method using Plaxis. The results are compiled in [van Duinen, 2010] and summarized in Table 2.2. The IJkdijk slope stability experiment has been analyzed by den Haan and Feddema [2009] using the Soft Soil Creep model. In van Duinen [2010] it is also concluded that the soil parameters which are measured in the laboratory and which form the input for the Finite Element model need to be different for deformations or for maximum strength at failure. For deformations, drained parameters need to be selected. For maximum strength at failure undrained parameters are needed. For construction works, the ADP method or corrected drained methods performs best.

In some of the studies, the calculations with Finite Element Method were troublesome. This mostly occurs when the effective pressure in the soil near the failure plane is close to zero. Then the calculations in the zone of interest may become very sensitive to near-arbitrary variations in input values. Moreover, the calculation process easily diverges for this type of calculations, because the convergence process of the numerical solution is judged upon the accuracy of the calculation points (“integration points”) where plasticity occurs. Additionally, the criteria for plasticity are highly dependent on the precise stress level at low effective stresses and plasticity-driven deformations themselves will cause changes in the stress distribution. In a way, the stability of the calculation could be regarded as a measure for the stability of the slope.

Several techniques exist to improve the finite element predictions. The soil behavior can be described by constitutive models which exhibit better horizontal precision, like the anisotropic soft soil creep model. Since this model is still academic, experiences with real world data is rather limited. Cooperation with universities is possible, but the rapid use of these techniques in an operational system is not to be expected on the short term. Another possibility is the use of updated mesh calculations to increase precision with large deformations. However, in Plaxis updated mesh analysis cannot be combined with phi-c reduction analysis yet.

In literature, one other method arises which is explicitly designed to update the safety based on an finite element analysis [Sakurai et al., 2003]. This method is designed for stiff sands and rock. It is unclear whether the method is also suitable for soft, anisotropic sediments. The finite element part of the method has the same disadvantages as mentioned before. Some of the assumptions make the model more robust but at the same time (potentially) less accurate. For example, it assumes a correlation between strength and stiffness, which is not generally true for materials in levees. Therefore, the Sakurai et al. method is not useful in this context.

Overall, the quality of the update of the safety depends on the quality of the prediction of the horizontal deformations. At this stage, the current finite element methods are expected to be insufficiently accurate for this.

2.5.4 For slope stability – Updating the safety factor

For slope stability, the safety factor can be updated based on measurements and observations. The resistance against failure due to slope instability depends on the local strength parameters. Often, strength parameters of a certain trajectory are known statistically. Local differences can occur. The goal of this exercise is to use measurements and observations to fine-tune the safety factor. A good first estimate of the safety is calculated with a limit equilibrium program. When observations are available, new information is added in order to improve the precision of the analysis.

Limit equilibrium methods
Traditionally, the safety due to slope instability is calculated with a limit equilibrium method. The most popular is Bishop’s method that considers the equilibrium along a circular failure plane. It satisfies both the vertical equilibrium and that of the driving moments. To simplify the computations, the horizontal equilibrium is not considered. Other well known methods are Morginsern-Price, Spencer and Van’s method. They all have their own field of applicability.

These methods need strength parameters to determine the resistance against failure. The most common ways are using a cohesion and an angle of internal friction, or using undrained shear strength. Any description of the strength works with any limit equilibrium method.

The safety of the embankment is determined by the slip plane with the lowest safety factor. Beforehand, it is unknown which plane in the geometry has the lowest factor of safety. The lowest factor of safety is searched in space by a grid based search, by a gradient based method or by a genetic algorithm.

Observations
Limit equilibrium methods give an indication of the safety, but the embankment itself gives signals before failure. Examples of visual observations are cracks in the embankment. When the safety approaches its critical value, cracks parallel with the crest will develop. As the safety becomes more critical, perpendicular cracks develop that fully describe the imminent failure surface.

Other observations can be collected from sensors. If an inclinometer measures increasing rotations in the direction of a potential slip surface, the safety approaches the critical value.

Updating the safety
With the use of expert judgment and/or experiments, the observations mentioned before can be translated into a safety factor. It is likely that this safety factor is not identical to the one that follows from the limit equilibrium method as there is much uncertainty in such an analysis. An update of the strength parameters is possible in such a way that both methods can give the same safety.

An embankment that just failed serves as an example. At that moment, the driving forces are equal to the resisting forces. The stability parameters can be tweaked such that the stability in the limit equilibrium method equals exactly 1.0. In this case, the corresponding updated strength parameters are better than the ones assumed beforehand.

Another example is an embankment with cracks in the embankment. Experts estimate the current stability factor of an embankment to be about 1.05 due to the cracks. It is then possible to inversely calculate the strength parameters in order to fit this value. Consequently, the instant of failure can be predicted much better.

Genetic algorithm
As mentioned before, a search in space needs to take place to find the representative slip circle. The search required for this method is very complex and, therefore, not possible with a gradient based method. The chances of succeeding are largest by using a genetic algorithm.

Genetic algorithms process a mathematical representation of a solution of an analyzed problem. For Bishop's method, this representation is a vector containing the X and Y value of the centre of the circle, and the radius of the circle. This representation is called an individual; the sum of individuals form a population. An individual can be tested for its fitness, for example with Bishop's method.

The genetic algorithm improves the quality of a population in a similar way as nature does. Two individuals cross their DNA, there is a chance for mutations and a new individual is created. Two new individuals fight, and the fittest one continues to the next generation.

The genetic algorithm is faster and better at finding a global minimum. A disadvantage is that the results are not always reproducible. On top of that, there will be a very strong tendency to find the global minimum, while sometimes, a local minimum is interesting as well. This can be overcome using penalties steering the result in the desired direction. Because of its high speed, a genetic algorithm makes it possible to find a free slip surface with Janbu's or Spencer's method. The search space can be increased in complexity by adding the strength parameters to the search.

There is no unique solution to the inverse problem of finding the strength parameters resulting in a specific safety factor. Many combinations of strength parameters will result in the desired safety. The uniqueness of the solution can be improved by adding an extra boundary condition. E.g. only small changes in the strength parameters are allowed in matching the safety factor. In other words, while fitting, the algorithm will try to stay as close to the initial value as possible by using prior information.

In the traditional genetic algorithm, only the safety factor is minimized. In this case, a cost function will be minimized based on the safety and the distance from the initial value of the strength parameters. A weight in this function determines whether the measurements or the initial computation are more reliable.

Practical use
When using this program, the user or sensor needs to enter two values: an estimate of the safety, and a weight of this safety in relation to the initial computation. If the safety factor is known exactly, for example at the moment of failure, one can completely rely on the measurements. In this case, an update of all strength parameters will be given that produce the desired safety. If a sensor prediction of the safety is not exact, one can rely, for example for 50 % on the sensor and for 50 % on the initial computation. In that case, the strength parameters will be changed so the safety factor moves towards the measurement. This choice will be of a generic nature depending on the uncertainty defined by the user in the prior imformation, measurements and method used.

2.5.5 For piping – correlations of parameters with pipe formation

In Appendix 3 : , the parameters, which were measured at the IJkdijk piping experiments, are summarized. In the table, the suitability of the parameters is judged by levee experts from Deltares. In short, the driving parameter influencing the process of piping is pore pressure. Discharge and sand volume transported through the wells are also directly linked to the process of piping. Parameters which are indirectly influenced by piping, by the fact that water is flowing though the pipes, are temperature and SP. In this paragraph, new models are described to link measured parameters to stability of a levee. This is accomplished for discharge and attempted for sand production by a well.

The process of piping is visualized in Figure 2.2. It is distinguished into two main phases. At the start, the erosion process is restrained. A fluctuation in head drop may lengthen and deepen the erosion channel. This erosion will expire and a stable state remains. Beyond a critical head drop, however, the erosion will not stop unless the hydraulic head is reduced quickly, see Figure 2.9 (top). Then the situation becomes out of control, resulting in collapse of the levee.

For design and safety analysis of levees, the first phase (i.e. below the critical head drop) assures safe conditions. The piping model [Sellmeijer, 1988] focuses on that phase. During that phase, three processes are important when describing piping:

- Groundwater flow through the subsoil
- Pipe flow (Poiseuille) in the erosion channel (pipe)
- Equilibrium of rolling particles at the bottom of the channel and continuity of flow

These three processes are combined in a conceptual 2D-model, which predicts the critical head beyond which progressive erosion will occur, leading to failure of the levee. This model is incorporated into the computer program MSeep. In this program, arbitrary geometries may be applied. For special geometries, easy to use rules are derived. Examples are the simplified rule for a standard levee and the VNK rule for a two layer system, elaborated upon at the end of this section.

Determination of the critical head is sufficient for the design and safety of dikes. However, the model supplies other information, which is relevant for the process of piping. For instance, the degree of the critical state is correlated to discharge or volume. If such information is available, a proper guess of the risk for piping may be assessed.

This more extensive information is available during the MSeep computation. At first, the relation of head drop and slit length is determined. At the same time, relations for discharge and volume are known. These relations - in normalized form - are shown in Figure 2.9 for the geometry of the IJkdijk piping experiments. The critical head is the maximum value in the top graph for the head drop. The normalization is explained in Appendix 5 : .

During the IJkdijk piping experiments, all three of the key parameters (hydraulic head, total discharge and sand volume) were measured. According to Sellmeijer's rule, the relations between normalized pipe length and the normalized hydraulic head, discharge and well volume only depend on the scaled geometry. This is similar for all tests, so Figure 2.9 may be applied to all tests. The slightly thinner sand layer in tests 2 and 4 has a minor effect only.

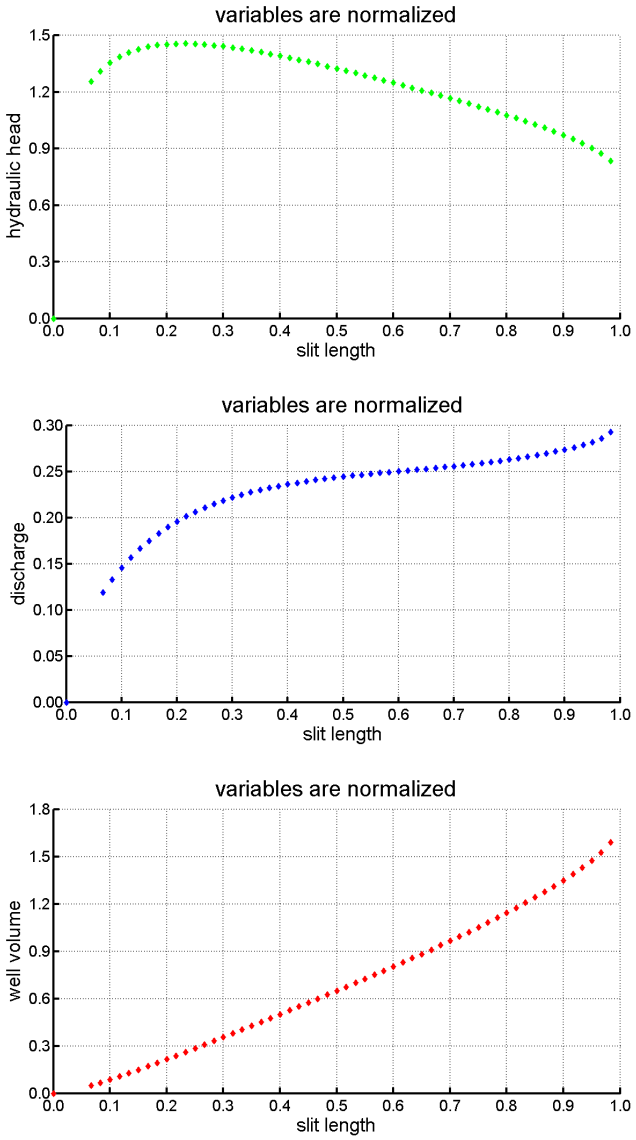

Figure 2.9 Normalized hydraulic head, discharge and well volume for the IJkdijk piping experiments

During the IJkdijk tests, times series of head drop were imposed and the total discharge and the total sand volume produced by the wells were measured. The total measured discharge is the sum of discharge through the erosion channels and through the top of the sand layer. From the MSeep calculations, it is estimated that about ⅔ of the total discharge results from flow through the erosion channels or the weak zones with preferential flow. These weak zones are present already before any erosion has occurred and can, for instance, be discerned from the early measurements by GTC Kappelmeyer during tests 1 and 4. In this model, only the discharge through the erosion channels is taken into account. Therefore, the measured discharge is corrected prior to inference of the erosion length.

The theoretical pipe lengths corresponding to the imposed head drop, the corrected discharge and produced sand volume are inferred from the relationships in Figure 2.9. The results of tests 1 to 4 are shown in Figure 2.10, Figure 2.11, Figure 2.12 and Figure 2.13.

The left hand chart shows the measurements consisting of the imposed head drop in green and the measured discharge in blue and, if available, the sand volume in red. The yellow level represents the predicted critical head drop from the 2D model. The time shown in the figures is roughly confined to the time span of the experiment during which the model is potentially valid, i.e. until the upstream reservoir had been reached. The critical hydraulic head was in all tests reached at the stabilization of the green line, as from that moment on the sand transport no longer ceased. It should be noted that due to the procedure followed to measure the sand

volume, the measured volume lags behind the actual volume and only a part of the produced sand volume has been measured.

The right hand chart shows the correlated values for the erosion length based on different sensor inputs. The colors correspond to their source: the green line is based on head drop, blue on discharge and red on volume. The cyan line corresponds to the pipe length which is determined using regression of pore pressure measurements along the line of pore pressure meters perpendicular to the direction of the levee [FC2009, Robust Monitoring]. The line of pore pressure meters which was closest to the location of breach during failure has been selected.

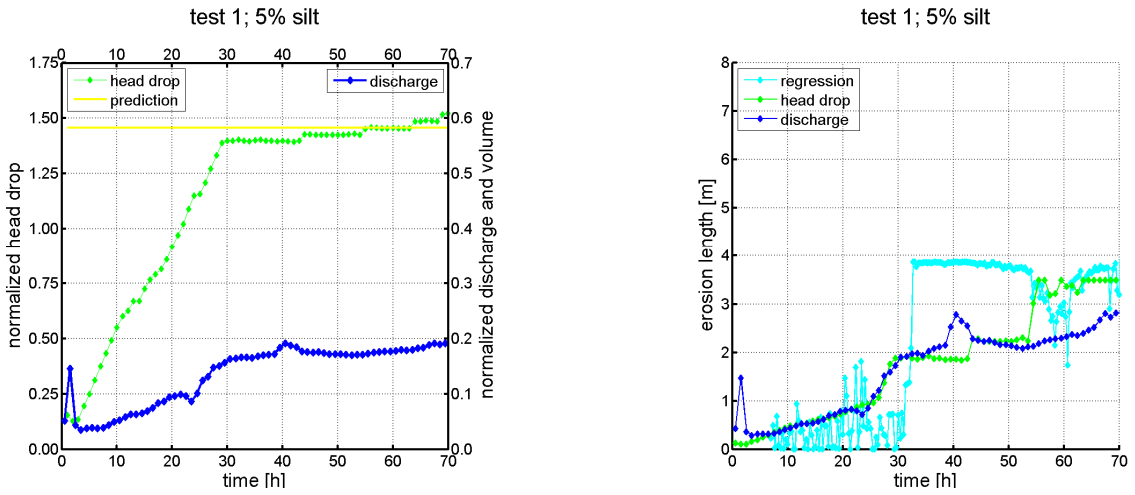

Figure 2.10 IJkdijk experiment 1 – Left: measurements of imposed head drop and discharge. Right: Inferred pipe lengths from hydraulic head, measured discharge and pore pressures at sensor line 5.

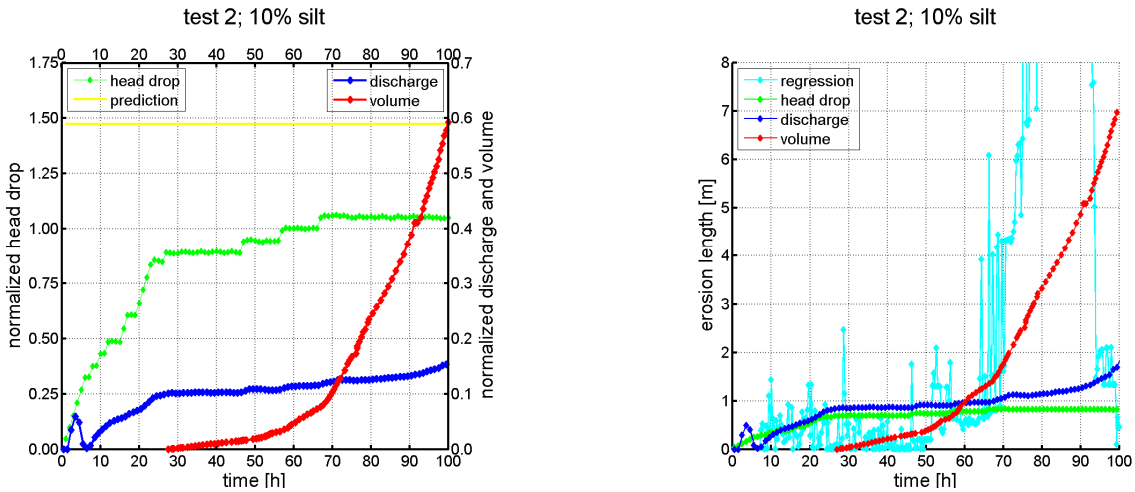

Figure 2.11 IJkdijk experiment 2 – Left: measurements of imposed head drop, discharge and well volume. Right: Inferred pipe lengths from hydraulic head, measured discharge, sand volume and pore pressures at sensor line 9.

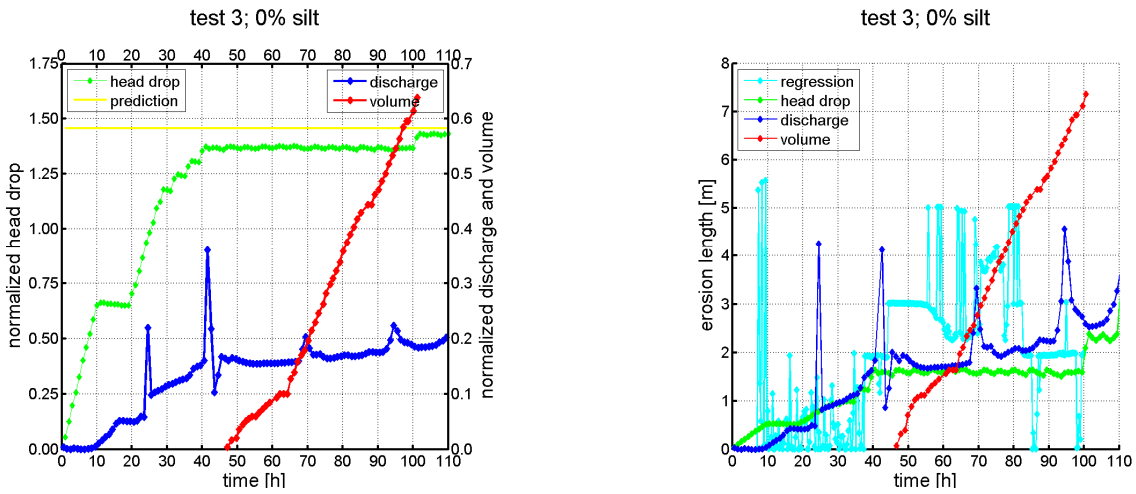

Figure 2.12 IJkdijk experiment 3 – Left: measurements of imposed head drop, discharge and well volume. Right: Inferred pipe lengths from hydraulic head, measured discharge, sand volume and pore pressures at sensor line 5.

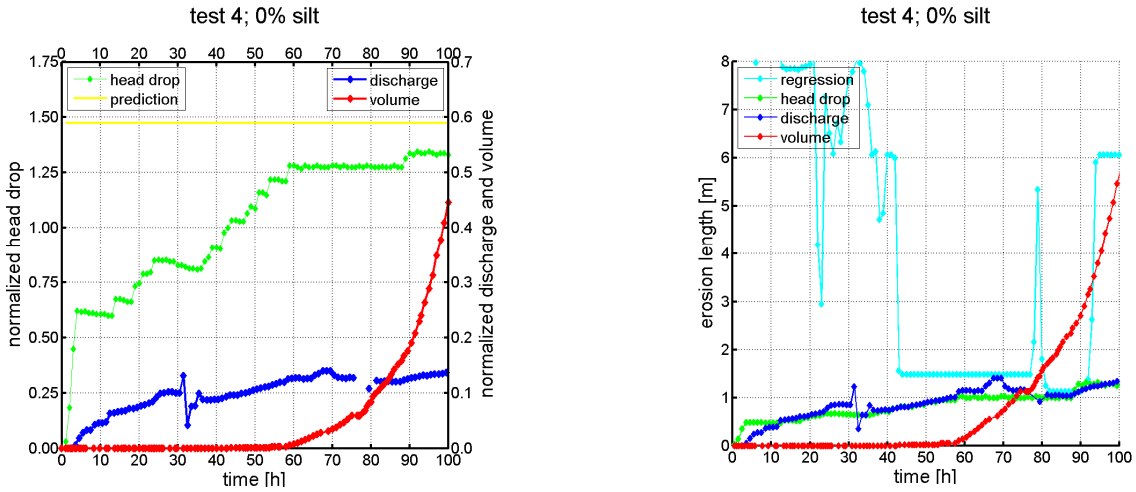

Figure 2.13 IJkdijk experiment 4 – Left: measurements of imposed head drop, discharge and well volume. Right: Inferred pipe lengths from hydraulic head, measured discharge and sand volume; pore pressures at sensor line 11.

The agreement between the theoretical erosion length predicted by the head drop and by the discharge is remarkably good, implying that the model parameters have been determined correctly (otherwise, these values would not agree), in spite of the deviation in critical erosion length between the model and the experimental values. For all four experiments, the green (head drop) and the blue (discharge) line are close together. For the first three experiments, the regression results based on pore pressures are of the same order. Since the regression has the tendency to revert to the position of the gauges, the curve is jumpy between those levels. In experiments 1 and 4 this effect is stronger, since the regression is obtained from the readings of four gauges only. In experiments 2 and 3, eight gauges were applied, so the jumpy effect is less severe. [FC2009 and Sellmeijer et al., 2011]. In the fourth experiment, the pipe length derived from the regression is rather large up to about 42 hours. This is probably due to the accumulation of silt, for which the pore pressures were not corrected. After 42 hours, the agreement between the pipe lengths determined by the various methods is rather good.

During experiment 1, the sand volume has not been measured. During experiments 2, 3 and 4 the sand boils were capped at a fixed level and the removed sand volume was measured. The erosion length based on these sand volume measurements deviates strongly from the curves based on head drop, discharge and pore pressures. The erosion length based on sand transport rises out of control.

The sand volume consists of two parts: a flat part and a strongly increasing part. For the model, the flat part is needed. However, the volume of the sand boils before capping is not included in the measurements. The true

eroded sand volumes are larger. The extra component initially increases slowly in time, becoming constant when the capping level is reached. The resulting volume is flat in the beginning, where the piping model is valid. Beyond the critical state the volume line will rise out of proportion. The early volume level is not known. Therefore, the measured volume does not supply a meaningful prediction of the erosion length.

Based on the IJkdijk results described above, it is concluded that the described correlation procedure has potential. Therefore, a procedure needs to be developed to transform specific measurements into predictions of, e.g. the critical head drop. For a specific geometry, it is sufficient to have the set of relations at one's disposal, such as shown in Figure 2.9. These relations can be determined using MSeep. The relations are dimensionless. They only depend on scaled geometry and permeability contrast. The specific piping parameters are clustered into multiplication factors.

For the IJkdijk tests, the input consisted of times series. Consequently, the outcome is also expressed as times series. However, in practice, such times series are not available. Probably, only a few individual data are collected. In that case, using a measured discharge, head drop or sand volume, the corresponding erosion lengths can be read out from the graphs of Figure 2.9. The curves even offer the opportunity, to some extent, to re-adjust the piping parameters. For instance, if the normalized head drop and discharge do not match, adjusted piping parameters might lead to a better fit.

So far, the use of extra measurements in individual cases is straightforward. A different approach is required for regional projects or in probabilistic studies, where thousands to several hundreds of thousands geometries must be considered. Then, it is convenient to refer to a retrieval system of results for a class of geometries. The desired retrieval system is in essence an interpolation tool.

One of the most compact and reliable tools is an Artificial Neural Network (ANN). An ANN is trained by a huge amount of MSeep calculations, which are performed in advance. The geometry in the calculations is schematized. The complete curves which are output of the MSeep calculations are not stored in the retrieval system, but only characteristic values to construct the curves. Up until the critical erosion length, the character of the curves is exponential for small erosion lengths and may be adjusted parabolically for larger values. In Figure 1 of Appendix 5 : an example is presented as thin solid lines. Beyond the critical erosion length - so beyond the stable phase of the erosion process - (large) differences may occur. This is not relevant for the correlation, because the model is not to be used for this phase of the piping process.

It is expected that the curves up to the critical erosion length can be characterized by three values each for head drop, discharge and volume. Two values for small erosion length will be needed in order to fix the exponential behavior. The third one is needed to fix the critical value. The required information density per axis depends on the complexity of the curve. A straight line needs two, a parabola three. Piping is more complex and requires a density of around 10. Consequently, for N variations in geometry, the order of 10^N calculations is required. In case of 4 degrees of freedom, this requires 10000 calculations.

If a generalization of the approach is required for the Dutch levees in general, the VNK schematization of the Dutch levees can be used [Calle et al., 2007]. In this schematization, the subsurface beneath a levee is described by two layers, where the top layer under the river is different from the one in the polder (Figure 2.14).

For the VNK schematization, the degrees of freedom are:

- D_1 / L (top layer height scaled by width of the dike)
- D_2 / L (sub layer height scaled by width of the dike)
- $\log(k_3/k_1)$ (permeability contrast of river layer and top layer)
- $\log(k_2/k_1)$ (permeability contrast of sub layer and top layer)

This geometry is called 'Holland Country Wide' and is very suitable for dike safety design in the Netherlands.

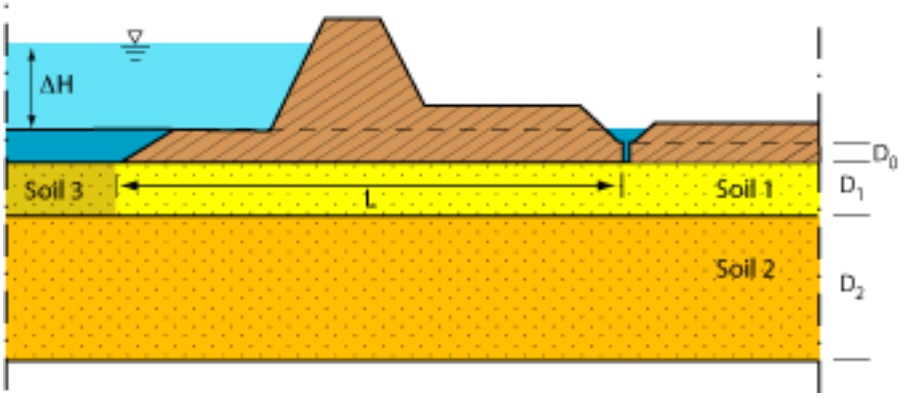

Figure 2.14 Schematization of levee and subsurface for piping calculations using PC-Ring and the module MPiping-VNK.

Based on Sellmeijer's rule, in several projects a number of models are built. For the VNK schematization of the Dutch subsoil, the parameter space was searched for the relation between the length of the pipe and the volume of sand per unit of length along the levee. This was done using neural networks [Calle et al., 2007]. Additionally, in the FC2015 project "Robust monitoring", performed in 2009, the length of the pipe was predicted from the measured pore pressures in arrays of sensors at the IJkdijk levee [FC 2009 and Sellmeijer et al., 2011].

2.5.6 For piping - use of SP and temperature measurements

When piping in the levee would be a 2D process, the discharge through the levee would be uniform along the entire length of the levee. In practice, the levee varies e.g. in width, actual sand composition etc. Therefore, the pipes are localized instead of 2D slits (as in the model described in the previous section).

The SP is a parameter which is influenced by the local flow of water. Theoretically, the strength of the SP signal is related to the amount of water flow. Stronger signals would indicate stronger flow. Variations in SP measurements along the length of the levee are expected to reflect these variations of flow through the levee. To use the SP to infer pipe lengths, first a possible link between the SP and the discharge needs to be established. This could then be used to distribute the measured discharge along the length of the levee. The second step is to infer localized pipe lengths from the localized discharge by an adjusted 2D model based on Sellmeijer's 2D model.

ITC and Fugro were measured SP during several of the piping IJkdijk experiments. ITC processed their SP data of experiment 4 in an attempt to pinpoint locations of more flow or less flow. Unfortunately, at first sight, no relationship between the *absolute* value of the SP and the discharge is manifest. The *relative* values of SP might be used to locate areas with increased or decreased flow. Therefore, the ratios between SP at locations near the final breach and further away from that point were calculated. The first results, however, were rather noisy and difficult to interpret. Further research is needed on the SP signal to extract local information of flow from the noisy signal. So far, a link between SP, discharge and pipe length has not been accomplished.

Another parameter which is influenced by water flow is temperature. Because of relative temperature differences between water present in the levee and the high water basin, a temperature anomaly will show when pipes form. In the piping experiments, clear temperature anomalies were detected by several parties. These can be used to determine the discharge, see Artières et al. [2010] and references therein. For the IJkdijk piping experiments, this approach was not explored.

3 REAL-TIME DIKE MONITORING

3.1 INTRODUCTION

In this chapter the results are presented of work package 3 of the MonsterCase project. Work package 3 focuses on long term and large scale monitoring of sensor dikes in real time. To test newly developed techniques on sensor data we used data from the LiveDijk Eemshaven project (Figure 3.1), instead of simulating sensor data. The LiveDijk project is a project from the LiveDijk Consortium. This consortium consists of the partners: Stichting Toegepast Onderzoek Waterbeheer, Waterschap (STOWA), water board Noorderzijlvest and Stichting IJkdijk. Also see http://www.LiveDijk.nl for more details about the LiveDijk.

Figure 3.1 Location of LiveDijk Eemshaven (blue line). Background image Google Earth.

The goal of this part of the project is to develop methods to gain real time information on the normal stability and condition of levees and to detect a threat of failure.

This work package focused on long term and large scale dike monitoring. By large scale we mean a situation in which a large number of dikes in the Netherlands are equipped with some kind of sensor system. A logical consequence of this situation is that the handling of a lot of different sensor streams and real-time analysis becomes complex and computational intense.

Because of the large number of sensor streams to be processed in the future we are aiming to develop pre-analysis techniques before heavy computational models are put to work. We first want to have an estimation of where potential problems may occur before we start an in-depth analysis. To do this we look at trend spotting techniques to detect trends in sensor data based on historical behavior. Deviations from the expected trend can then be used as a trigger to start further analysis. Trend deviations do not always mean there is a geotechnical problem, there could also be a technical sensor problem e.g. sensor drift or a communication problem.

When performing analysis on multiple sensor streams from different sensor systems you will run into time stamp related issues. Different sensor systems measure in different sample rates and possible do not have synchronized clocks, which makes it difficult to compare sensor data and do mathematical calculations on measurements which don't have similar timestamps. To cope with these time related issues we aim to develop a *timeline sensor data store* which implements the paradigm shift from measurement oriented storage to time oriented storage. This TimelineStore would get an interface which deals with time synchronization and interpolation. The need for trend spotting techniques and development of a timeline interface will be explained in more detail by describing the use cases in the next section.

In order to visualize the use of these newly developed techniques we use a Microsoft Multi touch table (Figure 3.2).

Figure 3.2 Microsoft Multi touch table

In this chapter, the need for trendspotting is illustrated with three use cases described in § 3.2. The TimelineStore is explained in §3.3. The building blocks in trend analyses and the concept of virtual sensors is explained in §3.4. The use cases are demonstrated in §3.5.

3.2 APPROACH AND USE CASES

This section describes situations (use cases) to explain the need for the development of trend spotting techniques and a timeline sensor data store. These use cases will be used in the next sections.

3.2.1 Use case 1: detecting normal behavior

Performing continuous in-depth analysis of sensor data demands a lot of computer processing power which might not always be available and is expensive. Beside this computer technical issue another, more important, issue rises. An in-depth analysis focuses on only one specific (geotechnical) problem, e.g. the calculating of the dike slope stability, risk of piping, etc. If we look at this from a point of view in which we envision large scale roll-out of sensor systems in dikes, this way of analyzing is not sufficient. We need a mechanism which monitors more aspects of the dike, the sensor system and the communication system. Moreover we want to know if something unexpected is occurring.

In order to know where something is happening what was not expected we first need to know what can be considered as normal behavior. Because different sensors produce different signals it is not an option to manually configure, for each sensor, its normal behavior. The normal sensor behavior will also depend on how and where it is installed in the dike. So, a requirement for a monitoring system is that the normal behavior of a sensor must be learned automatically when it is installed. This learning process should be based on his historical behavior.

To summarize for this use case: a monitoring solution should consist of a pre-analysis mechanism to be able to analyze sensor data on large scale and to detect unexpected and undefined problems. Therefore monitoring solutions should have:

> An automated process that learns what can be considered as normal sensor behavior.
> Detect when a signal deviates from what was expected.
> Create a trigger or signal to a module which performs in-depth analysis for specific problems.

3.2.2 Use case 2: prediction of the water level

In use case 1 we described desired system characteristics that make it possible to learn what can be considered as normal sensor behavior. Once this learning process is well trained, it should also be possible to predict how the signal will look like in the future, based on historical data. This can, of course, only be done under the assumption that the historical behavior is representative for future behavior.

An additional step in the use case could be to also predict the dike slope stability, based on Flood Control 2015 results. In 2009, a model was developed to calculate dike slope stability based on pore pressure using FEWS-DAM. This model is re-used for this use case. If we know what the pore pressure in the dike will look like in the future we could also predict the dike slope stability factor for a given point in the future. However, this is restricted to conditions comparable to already experienced conditions – extrapolation under extreme conditions never experienced before should be avoided, especially if not a model based on physics is applied.

For a monitoring solution we can add more desired system characteristics based on the use case, additional to the ones defined in use case 1:

> The system should have the ability to deliver historical data.
> The system should be able to calculate a virtual sensor value at the present time, using a alternative input signal.
> The system should be able to calculate a sensor value for a given time in the future.

Time series analysis is used to predict sensor values, which are then used in the stability calculations. The relationship between sensor values of different sensors is learned. When one of the sensors stops functioning, its value can be predicted from the value of the first sensor and the earlier learned relationship. The basics of time series analysis are described in §2.5.2.

3.2.3 Use case 3: correction of pore pressure with air pressure

Correcting a sensor value with an other sensor value seems like a simple operation. This operation is indeed simple if the sensors measure in the same frequencies and have synchronized clocks, so that timestamps match. When we imagine a situation where sensor networks will be rolled out on a much larger scale we can expect issues with shifted time series between this sensor networks. If you would have a sensor reading from sensor network A on timestamp T_a the chance that there will be a sensor reading from system B on a matching time will be very small.

A commonly used operation is the correction of the pore pressure, measured in a dike, with the air pressure measured in the neighborhood outside of the dike. Both parameters are measured by different systems and provided by different vendors. How does the correction look like if the time series from both systems don't match?

In order to be able to do this kind of operations we need a system that:

> Is able to shift time series for different sensor systems from different vendors.
> Is able to answer queries for sensor data on timestamps that not have been stored as a measurement.

So, the system should return a sensor value for any chosen point in time.

3.3 TIMELINESTORE

A very important part of working with sensor data is storing and reading it from the database. Sensor data has a typical write once, read many character. Sensor data can be used in a real time stream, but also for analyses afterwards: the historical view on the sensor data. Therefore a solid and easy to use storage mechanism has to be in place.

Almost all current databases which are used to store sensor data, are focused around the sensor measurements. Each time a sensor is being sampled, that sample – the measurement – is being stored in the database. The database can be queried to retrieve specific sets of measurements. For example all measurements between 1/1/2010 and 1/2/2010.

From a storage point of view this is a good solution. From an user point of view (the read part), this is not always the easiest way to deal with the measurements. Often the retrieved set of measurements from the database must first be "reworked" in order to be useful. Some examples:

- **Analyses**
  Fast Fourier analyses for example requires a set of measurements which are distributed in equal time intervals, and the number of samples should be a power of 2 (e.g. 256 or 512 samples). A set of sensor measurements are almost never organized in that way. Resampling is therefore needed.

- **Sensor data fusion**
  Combining the signals of two or more sensors is often a difficult task. Most sensors have different sampling moments. When the timestamp of the samples is different, only by a second, it is no longer obvious how to combine them. What is the value of sensor A – B + C at timestamp T? In order to answer that, a measurement is needed for each sensor A, B and C on timestamp T. Resampling is therefore needed.

- **Displaying**
  How to display the measurements in a nice and user friendly graph? One which can easily be zoomed in or out? With a sample rate of 1 minute, a graph of one year contains 525.600 measurements. Way too much to display on the screen. Smart aggregation is needed to produce a graph which can be fitted on a 1024x768 display.

So often the first action an user takes is to resample and/or aggregate the measurements set in order to be useful. Why not put this functionality behind a common interface? This is why we developed the Timeline concept, which will be explained in more detail in the remainder of this section.

3.3.1 Timeline concept

The heart of the TimelineStore is the transition from *observation oriented sensor data* to *temporal oriented sensor data*. Sensor data can be retrieved for *any* moment in time. The TimelineStore computes the value of the sensor by interpolating and/or aggregating the measurements.

In a traditional sensor data database (see Figure 3.3) the measurement for a sensor (S1) is stored in the database (Sample). A measurement consists of a timestamp and a value (e.g. 2010-07-16 at 20:30:45 time zone +1, 1033.56). The measurements are stored in the database for each sensor, see the table. A user can query the database for the measurements and retrieves the measurements, exactly as there are stored.

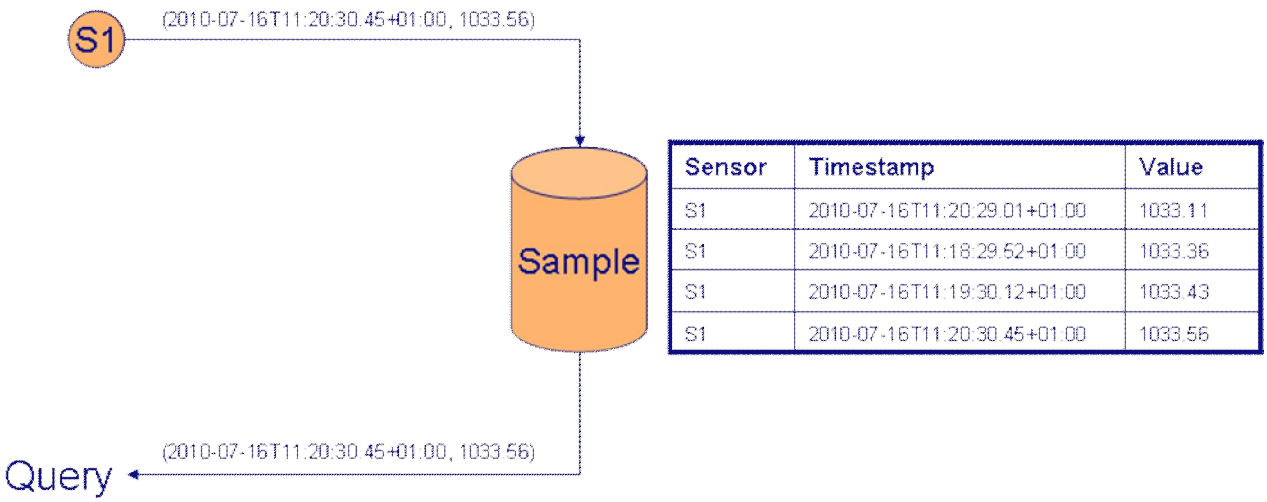

Figure 3.3 Traditional sensor data database usage

In the TimelineStore the storage of the measurements is the same, only the retrieval differs (Figure 3.4). Inside the database an interpolation engine is build which handles the queries about measurements which are not stored exactly. In this way a measurement can be retrieved on any time, the value will be calculated corresponding to the given timestamp.

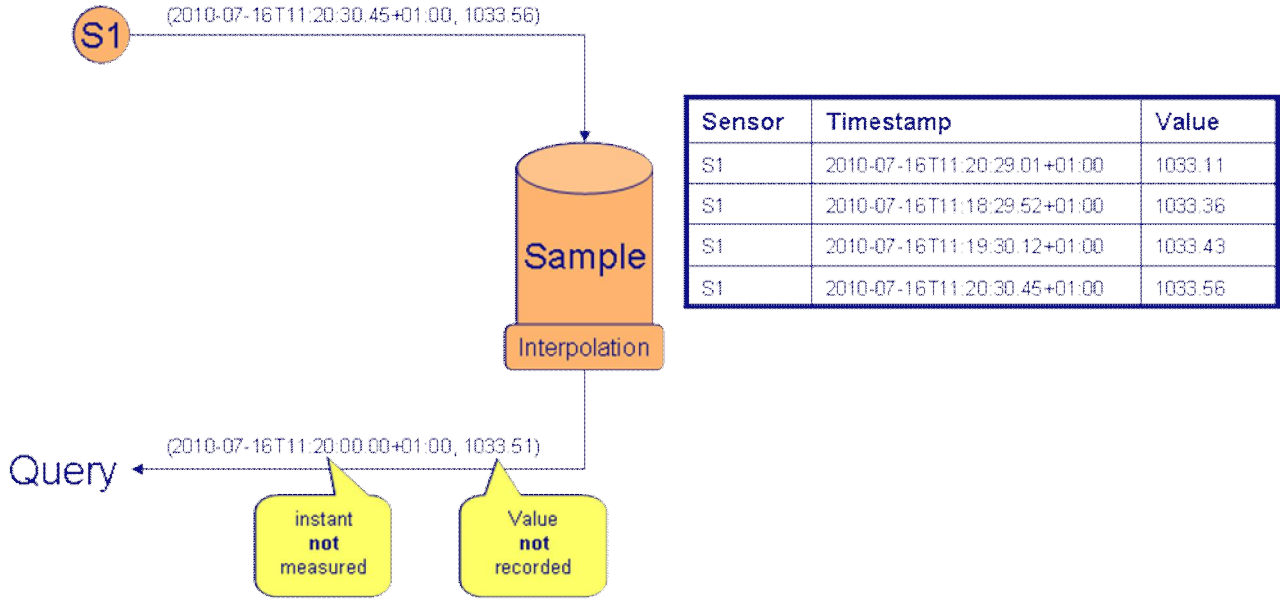

Sensor	Timestamp	Value
S1	2010-07-16T11:20:29.01+01:00	1033.11
S1	2010-07-16T11:18:29.52+01:00	1033.36
S1	2010-07-16T11:19:30.12+01:00	1033.43
S1	2010-07-16T11:20:30.45+01:00	1033.56

Figure 3.4 TimelineStore sensor data usage

3.3.1.1 Interpolation

Interpolation is a technique were a X,Y point in the graph (time, value) is being calculated based on surrounding available points (measurements). The interpolation starts with the *measurements*, the result of the interpolation are called *points*. Because there are many ways to perform the interpolation and many different sensor data types, the interpolation mechanism should be pluggable.

Different methods for interpolation are described in Appendix 9 : . For the timeline store pluggable modules for linear interpolation and sample-and-hold interpolation were built.

3.3.1.2 Aggregation

Besides interpolation, to determine points between two measurements, also aggregation is needed to determine a point representing many measurements. There are several ways to aggregate data. This report looks at the average mechanism: the hourly average, the monthly average, etc. Other techniques, such as wavelets, are also possible. This is left for further research.

To keep the database performing, these averages should be calculated each time a measurement is being stored in the database Figure 3.5). The sensor producing the measurements is not only connected to the sample database, but also to the hourly, daily and monthly average databases. They form the summary of the measurements.

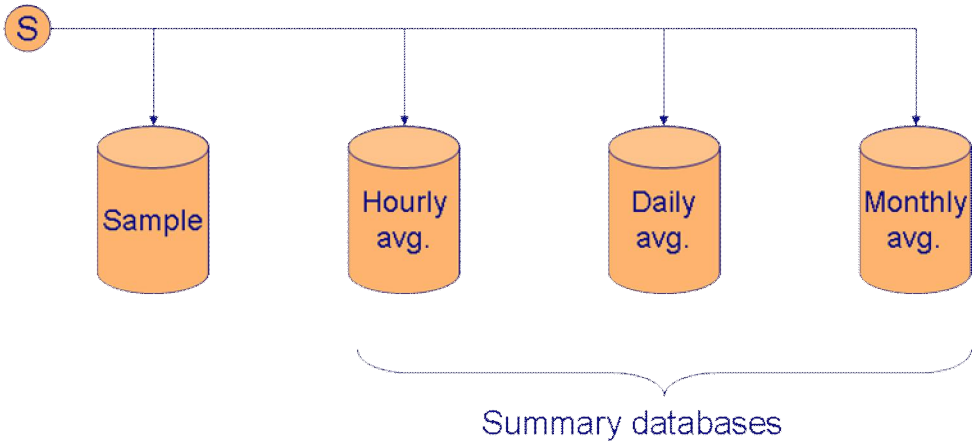

Figure 3.5 Averages as aggregation mechanism

Combing the aggregation and interpolation techniques, the following database architecture arises for the TimelineStore (Figure 3.6). Sensor measurements are stored in raw and in aggregational form. Each database has an interpolation unit, capable of calculating the points between the stored (aggregated) measurements. A resolution filter is used to determine which of the databases is used to process the request.

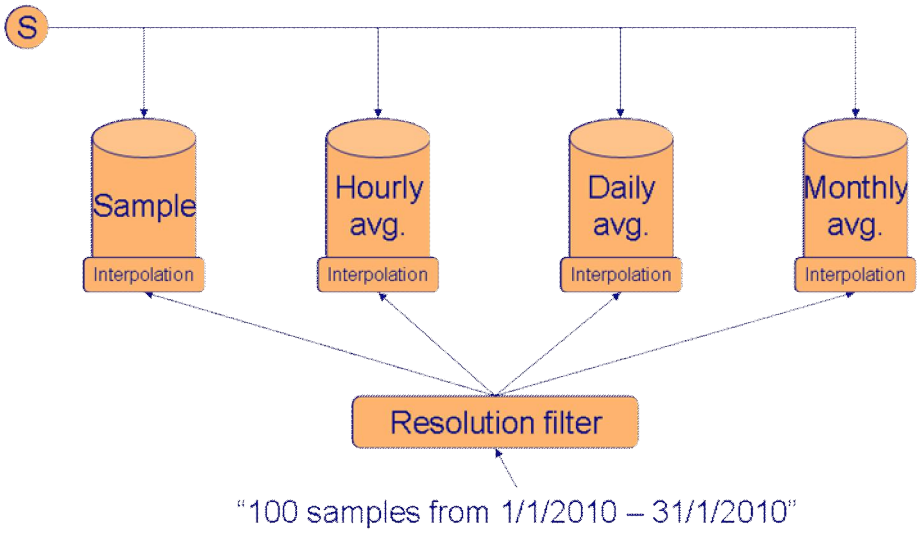

Figure 3.6 TimelineStore architecture with interpolation and aggregation

3.3.1.3 Timelines

Using the techniques from the previous subsections, a database is created that can produce points for each moment in time. In other words: the database presents access to the sensor via a timeline. To be more precise: this timeline contains all the historical sensor measurements (Figure 3.7). Requests in the future are not logical, the interpolation and aggregation techniques are not designed for that. But within the concept of a timeline it does: a timeline has no beginning nor end. From any point in history; to now; to any point in the future. Sometimes information about the future is present in the form of prediction models. Often based on historical data, something could be said about the future. It would be nice to present access to this data via the same interface, via the timeline. Two versions of the timeline should exist, the base timeline containing all the points based on historical measurements and a predicted timeline (Figure 3.8). The predicted timeline contains also points based on historical measurements, but also access to points in the future based on a prediction model (called the Base:Predicted timeline). This model has been run on a certain moment in time, based on the history available on that moment. Therefore this predicted timeline will freeze its content, new measurements are not taken into account by the prediction model and therefore not stored in this timeline. To access the new measurements the base timeline must be used. In this way the predicted points (Base:Predicted timeline) can be compared to actual measurements (Base timeline). If a new prediction is needed, based on the newly arrived measurements, a new predicted timeline (for instance Base:Predicted2) can be created, offering access to that data set.

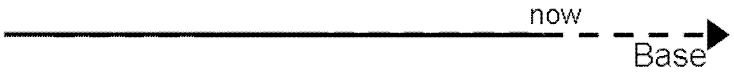

Figure 3.7 Timeline for history and now

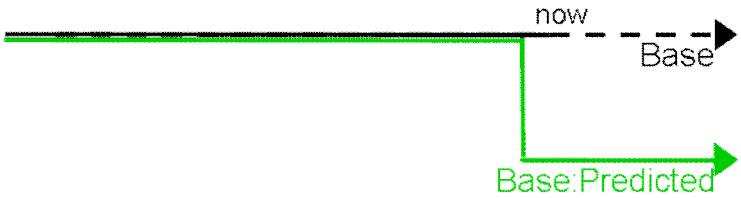

Figure 3.8 Timeline for history, now and future

A timeline offers a certain view on the sensor. The original measurements (Base) or a view in the future (Base:Predicted). This opens the route to other uses of the timeline. Often sensor measurements must be adapted afterwards, for instance because a disturbance (a car passing by) must be filtered out. Almost all the measurements stay the same, only a few of them must be recalibrated. A timeline could be offered containing precisely the recalibrated measurements, and all the other measurements which were not affected (Figure 3.9).

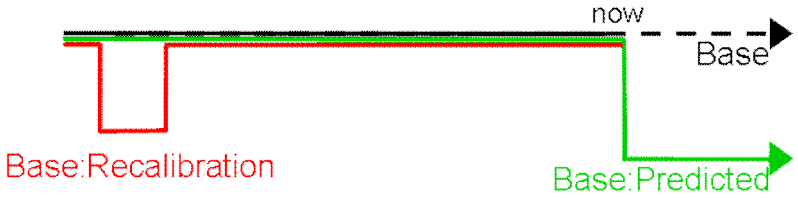

Figure 3.9 Timeline for recalibration

Finally the timeline concept could also be used for simulations (Figure 3.10). A simulation is a what-if scenario. Based on the situation at a certain moment in the past, what would have happened if this or that was different? What would have happened if this or that sensor had produced a different value? Using simulation models these changes can be calculated. Storing them in a timeline, containing the historical measurements up to the start of the simulation and the simulated results from that moment, gives a view to all the sensors in that simulation.

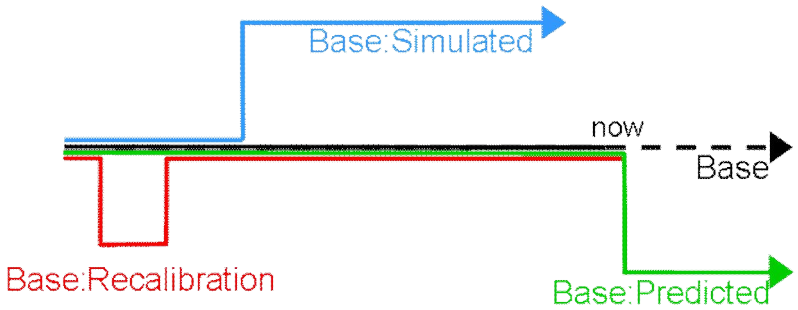

Figure 3.10 Timeline for simulation

Reuse of data by timeline interface

The main advantage of using timelines in this manner is that all these different situations (history, current, future, recalibrated and simulated) can be accessed via the same interface, the timeline. Therefore, visualization and analyses tools can be easily reused. Browsing through sensor data via a timeline can show history in the same manner as the future. By instantiating a new simulation timeline, the same viewer can be used to browse through the simulation. Even the same sensor analyses tools can be used to analyze the simulation, the analyses can be the same for the real life as for the simulated situation.

Database architecture

Combing the aggregation, interpolation and timeline techniques, the database architecture for the TimelineStore is depicted in Figure 3.11. Sensor measurements are stored both in raw and in aggregated form.

Each database has two units:
> An interpolation unit, capable of calculating the points between the stored (aggregated) measurements.
> A timeline mapping unit, used to determine which measurements come from which timelines.

A resolution filter is used to determine which of the databases is used to process the request.

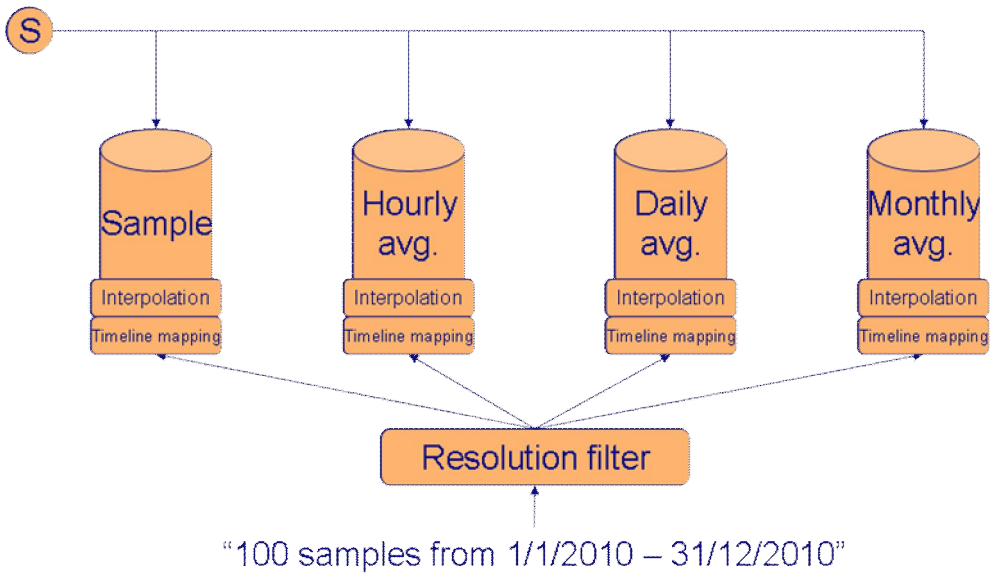

Figure 3.11 TimelineStore architecture with interpolation, aggregation and timeline mapping

Guiding principles
Dealing with sensor data from a timeline perspective leads to the following general guiding principles:
1. Never discard sensor data
2. Time is the point of reference of sensor data
3. Timelines can be stacked
4. Distinguish between measurements and "points".

3.3.2 Implementation of the TimelineStore

Based on the design introduced in the previous paragraphs, an implementation of a TimelineStore has been made.

3.3.2.1 Requirements

The most important requirements for a TimelineStore are:
> High performance
> Scalable, from single node to massive amount of nodes
> Robust and failsafe
> Easy implementation of the timelines concept

No database is of course ever too fast, but thinking about how to deal with these massive amounts of sensor data is important. Most current databases are SQL based, which makes them very flexible in the queries they can handle. Most current database are not easily made robust and failsafe. Special configurations, hardware and network infrastructures are needed for that.

A new type of databases begin to become available, the column based databases as proposed by Google in a paper in 2006. Google BigTable is a column oriented distributed storage system that was designed for the storage and maintenance of huge amounts of data. An open source implementation of these ideas are available under the name of "Cassendra". A further explanation of column oriented databases is described in Appendix 10 : .

3.3.2.2 TimelineStore

The TimelineStore is build around the Cassandra database (Figure 3.12), with additional software on top of it to implement the timeline mechanism and offer a nice API interface to the users. There are two versions of the API at the moment. A HTTP REST interface (see Appendix 11 :) and a java API, both can be used simultaneously. Each of these interfaces connects to a node in the Cassandra cluster and can connect to a different node if there is a failure. Cassandra can also be run as a single node, making development and demonstration easier.

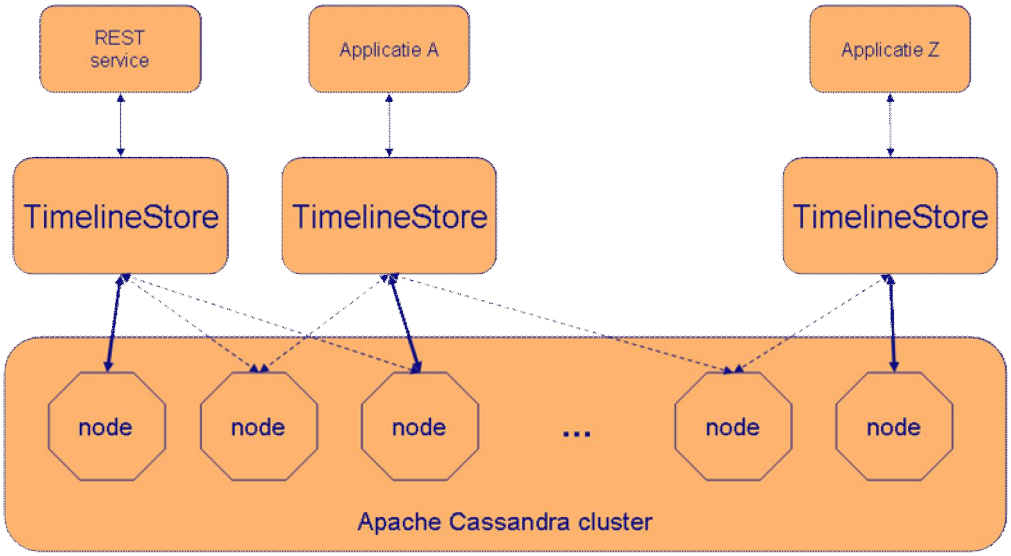

Figure 3.12 Cassandra cluster usage for TimelineStore

Different databases

The design is in such a way that Cassandra can easily be interchanged with other databases, even a memory based database (Figure 3.13). This gives the flexibility to store real sensor data in the robust Cassandra store. At the same time temporal virtual sensor outcomes of some analysis are stored in memory. Both have the same timeline interface, therefore both can be accessed by the same visualization and analysis components.

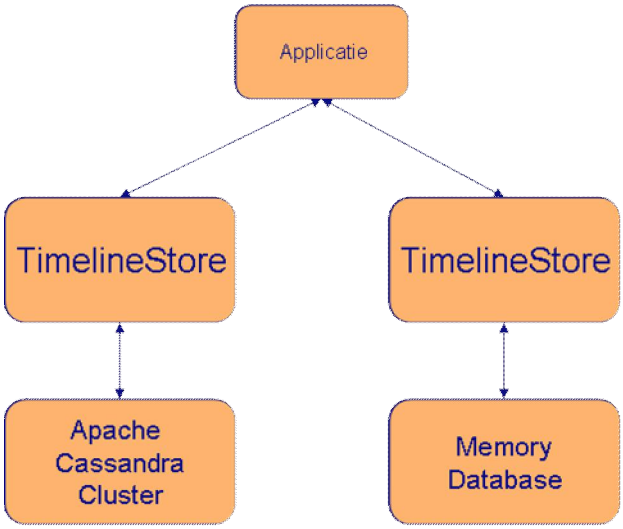

Figure 3.13 TimelineStore implementation options

3.3.2.3 Future developments

The current version of the TimelineStore offers the basic functionality as described above. Sensor measurements can be stored, points and raw measurements can be requested. The interpolation mechanism is pluggable with sample-and-hold and linear interpolation. The timeline mechanism can replace (recalibrate) sensor measurements.

This version together with the analysis described in this report proves that the idea of timelines is useful. The implementation in Cassandra is also feasible. Still a lot of questions need to be investigated to make sure this is a feasible approach in dealing with sensor measurements.

Some additions for the future:

- *Aggregation databases*
  The aggregation functionality is not present at the moment. Options are average databases or perhaps wavelets.

- *Forking of timelines*
  The current version can not fork timelines for simulation and prediction. This should be added

- *Add Metadata & reliability/accuracy data*
  Sensor measurements are only useful if the context is known. Often context is logged as metadata attached to a measurement. Using the timeline concept, meta data should also be converted from measurement based to time based. Therefore a timeline should also be able to store meta data (as a text sensor). The meta data can therefore via the time be related to all the sensor measurements/points. The same applies for reliability/accuracy of the measurements.

- *Add different interpolation techniques*
  Next to sample-and-hold and linear between 2 samples, also other interpolation techniques must be added such as splines, etc.

- *Add different sensor types.*
  The current TimelineStore can handle double (numbers fractions), long (discrete) and string (text) measurement types. More advanced types are desired such as motion (location, speed, direction), bar graph (FFT result), etc.

- *Scaling the Cassandra cluster into the cloud*
  The current version runs on a single Cassandra node. The Cassandra system is capable of running on many nodes. This makes the TimelineStore heavily scalable.

3.4 TREND ANALYSIS

As stated in the introduction of this chapter, we are aiming to develop pre-analysis techniques before heavy computational model are put to work, because of the large number of sensor streams to be processed in the future. We first want to have an estimation of where potential problems may occur before we start an in-depth analysis. To do this we look at trend spotting techniques to detect trends in sensor data based on historical behavior. Deviations from the expected trend can then be used as a trigger to start further analysis. Trend deviations do not always mean there is a safety problem, it also could be a technical sensor problem e.g. sensor drift or a communication problem.

In this section we will start with describing the concept of virtual sensors and monitors. Then a number of building blocks will be described. A virtual sensor can consist of 1 or more of these building blocks (or other blocks, to be developed in future). We will end this section with de description of a virtual sensor we developed in this project: the sample-rate-changeability-sensor, which signals whether there is a change in the sample rate (or not)

Traditional versus stream analyses

It is important to understand the difference between traditional (i.e. off line or batch) processing and stream processing of sensor values. Table 3.1, taken from the book "Learning from data streams" (by Gama, Gaber, 2007), explains the difference.

Table 3.1 Differences between traditional and stream data processing [Gama and Gaber, 2007]

	Traditional (=off line or batch)	Stream
number of passes	Multiple	single
processing time	Unlimited	restricted
memory usage	Unlimited	restricted
type of result	Accurate	approximate
distributed	No	yes

We see that a property of the stream data processing is an "approximate" result. *We want to emphasize that "fast but approximate answers are more useful than slow and exact ones"* (quote from the same book). This fast and approximate answer could trigger a traditional/batch process to get an accurate result.

3.4.1 Concept of virtual sensors and monitors

For detecting normal behavior and the deviation of this normal behavior we developed the concept of virtual sensors and monitors. Where a "normal" sensor is a physical part, a virtual sensor is not physical. Examples of existing virtual sensors are: throughput indicators of an IP-switch in your network, or the keystrokes per minute on a keyboard etc.

Other examples of a virtual sensors are shown in Figure 3.14, describing a fictive scenario. At the left side there is a physical pore pressure sensor. The measurements of this sensor are used by the Dike manager for monitoring the dike by calculating the slope stability factor of the dike segment. This Stability-factor is not only of use for the Dike manager, but also for the water board, who will receive slope stability factors of several dike segments, from several dike managers. These slope stability factors are the measurements coming from the virtual sensor (e.g. called the "Stability factor dike segment"). On its turn the water board will combine the results for different segments to calculate the flood chance for a certain area. This is also a virtual sensor, e.g. called "flood chance sensor". Next to the water board, also the head of a safety region is interested in the flood chance of the area for which he is responsible.

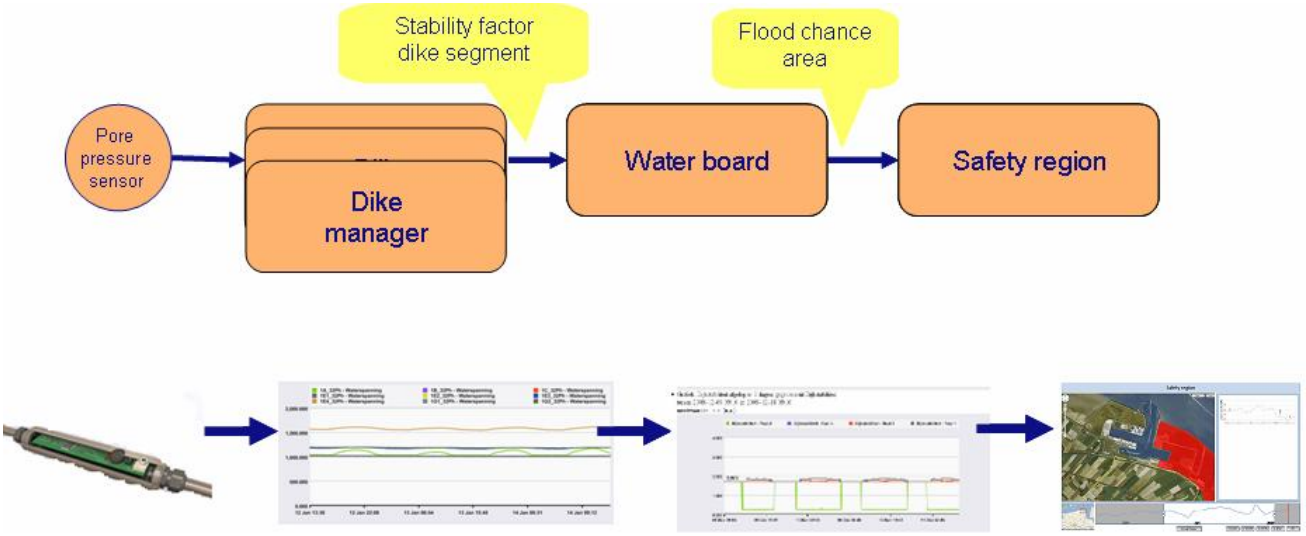

Figure 3.14 Physical pore pressure sensor and virtual sensors

The outcome of a virtual sensor is a value. For actual signaling that there is a problem or not, we use monitors. In a monitor one will configure what to do when a measurement passes a certain value. In the (fictive) scenario shown in the figure above, the Safety Region could use a monitor which sends a warning when the flood chance is between 25% and 50% and an alarm when the chance is greater then 50%.

This virtual sensor concept combined with monitors is ideal for using in trend analyses.

3.4.2 Building blocks

We defined and explored some building blocks which are very useful to make trend analyses possible. These building blocks can be used alone or in a combination and form a virtual sensor.

1. Sample and hold: interpolation mechanism for synchronization and missing samples
2. Moving average: average calculation over a time window and is used for noise reduction
3. Average and standard deviation: calculates the 'average' of the measurements and shows how much variation or 'dispersion' there is from the 'average'.
4. Subtraction: to subtract 2 signals
5. Fast Fourier Transformation (FFT): to transform a sensor signal (discrete time domain) into frequencies and amplitudes (frequency domain).
6. N-strongest frequencies: gives the N strongest frequencies and amplitudes (based on the output of the FFT)
7. Inverse Fast Fourier Transformation (IFFT): transforms a signal from the frequency domain into the discrete time domain
8. Number-of-Dominant frequencies: gives the number of frequencies (integer value) which are determining the sensor signal (based on the output of the FFT)

The building blocks are explained in more detail in Appendix 12 : . There, several examples are given as well.

Directions for further development:

> In future it should be investigated how this building block can be used as a part of a virtual sensor and combined to a monitor.
> One part of the investigation is how the normal number of frequencies can be calculated automatically (e.g. using a moving average).
> Another part of this investigation is what minimum and maximum levels should be used in the monitor. Should the minimum be at 0.5 times the normal number of frequencies and the maximum at 2 times?
> Finally what value should be used for ETA. If ETA is chosen smaller, the number of frequencies will decrease. The result will also be less sensitive for changes in the signal. And if ETA is increased, there are more contributing frequencies, and the result will be more sensitive for changes in the signal. In Figure 3.15 the same pore pressure signal is shown, but with a number of contributing frequencies for ETA =0.9.

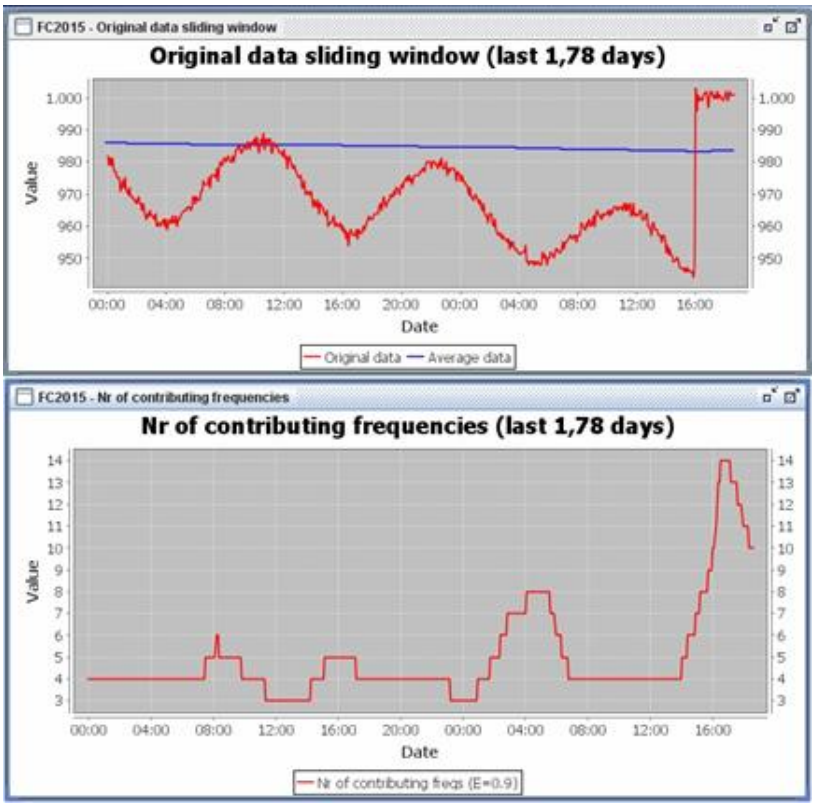

Figure 3.15 Pore pressure (top); Number-of-contributing frequencies for ETA=0.9 (bottom)

3.4.3 Sample rate-changeability-sensor

To determine a change in a signal, one should be able to determine what is "normal". To do so, the concept of changeability is introduced. To explain the concept, we will use the example of the "sample rate-changeability-sensor. This is a virtual sensor, which senses the changes in sample rate from a real (or virtual) sensor. The outcome of this changeability sensor is a value, which can be:

> zero: which means there is no change in the sample rate
> positive: which means that the virtual sensor is receiving more samples then expected
> negative: which means that the virtual sensor is receiving les samples then expected.

Note that this sensor is not looking at the value of the signal, but is analyzing the sample rate of the signal. This is used to detect if a sensor (or its connection) is still operational. Or if the sample frequency is changed.

The working of the sensor is as follows. Based on sample times of previous incoming measurement a prediction is made when the following measurement should be received. Then a timer is started which will go off after the predicted time. If the timer goes off, there should be 1 new measurement received. If so, the changeability = 0 (no change in sample rate). If the sensor received more than one measurement, the changeability is positive (the sample rate is increasing). If there is no measurement, the changeability is negative (the sample rate is decreasing). After receiving the measurement, a new wake-up time is calculated and the timer set. This means that we made the virtual sensor adaptive (self learning) for changing sample rates.

To make the sensor less sensitive for small differences between events a "window" is used (like the moving average). The size of this window (called *window-size*) is typically between 3 and 10. Note that the bigger the window-size, the "slower" the response on changes. The value -20 is used to indicate there were no measurements received at all within the window.

In Figure 3.16 an example is shown for the pore pressure sensor in the LiveDijk (top) where the measurements are coming every minute. In the bottom figure shows the changeability (using a window with *window-size=10*). The changeability moves between -0.1, zero and +0.1. In fact it means that (in average) the samples are coming every minute, but sometimes a sample arrives earlier than expected (+0.1) and another time it is arriving later (-0.1). In the following section the results of changeability sensor are explained in more detail based on a use-case.

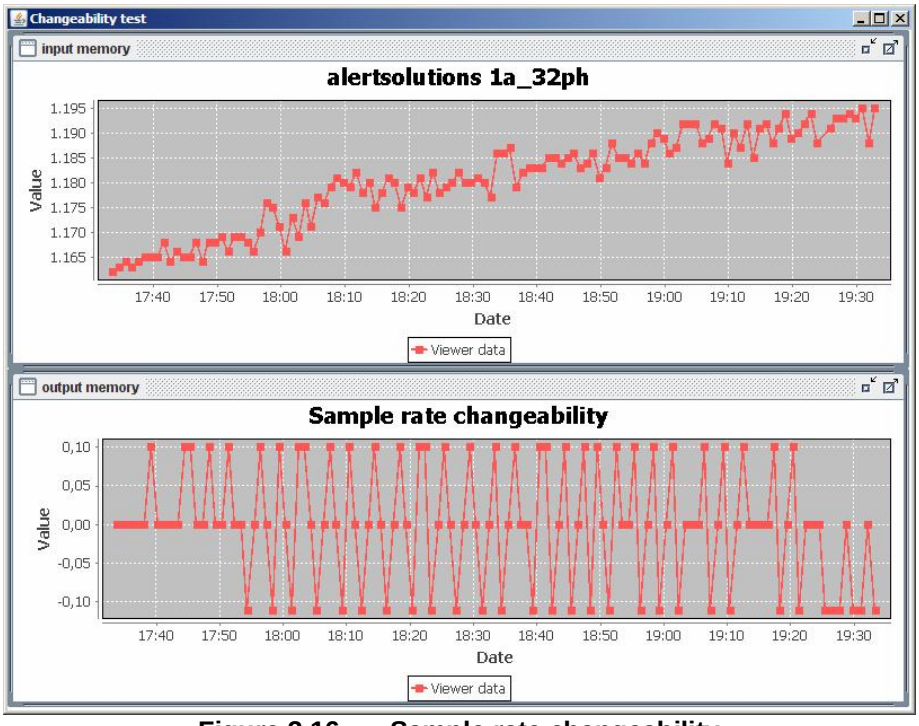

Figure 3.16 Sample rate changeability

3.5 USE CASE DEMONSTRATIONS

We use LiveDijk Eemshaven data and the use-cases of section 3.2 to apply the developed technics in the previous section. The LiveDijk Eemshaven is schematized in the following figures. In Figure 3.17, the geotechnical cross-section of the levee is shown. The levee consists of a sand body. Figure 3.18 and Figure 3.19 show the outline of the sensor arrays in top view and in cross section. The sensors are incorporated in the LiveDijk dashboard (Figure 3.20).

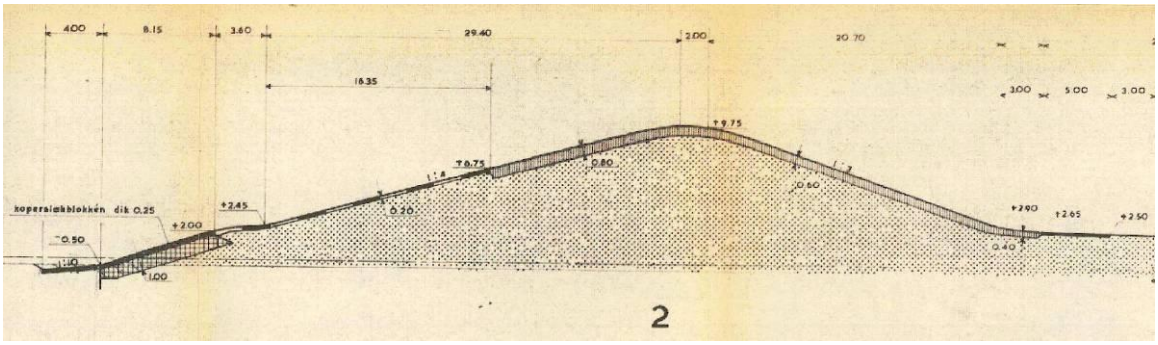

Figure 3.17 Geotechnical cross section of the LiveDijk Eemshaven

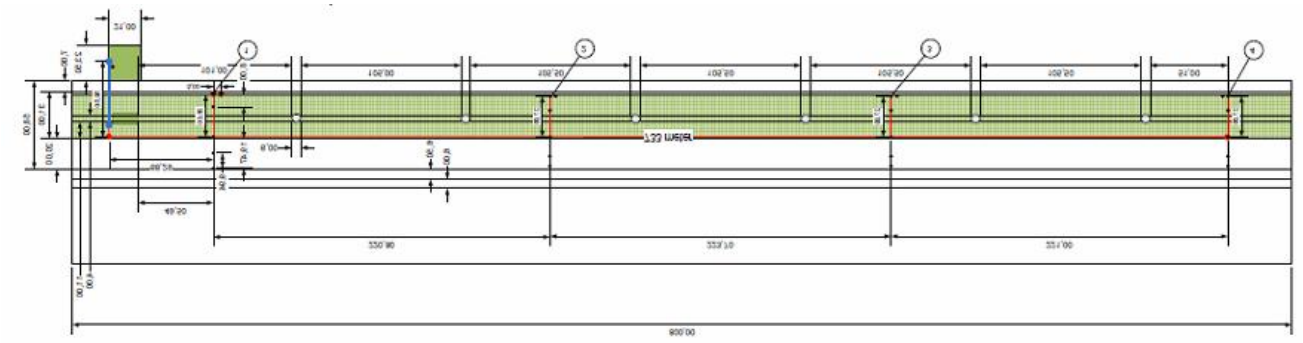

Figure 3.18 Top view of LiveDijk Eemshaven with the location of the four sensor arrays

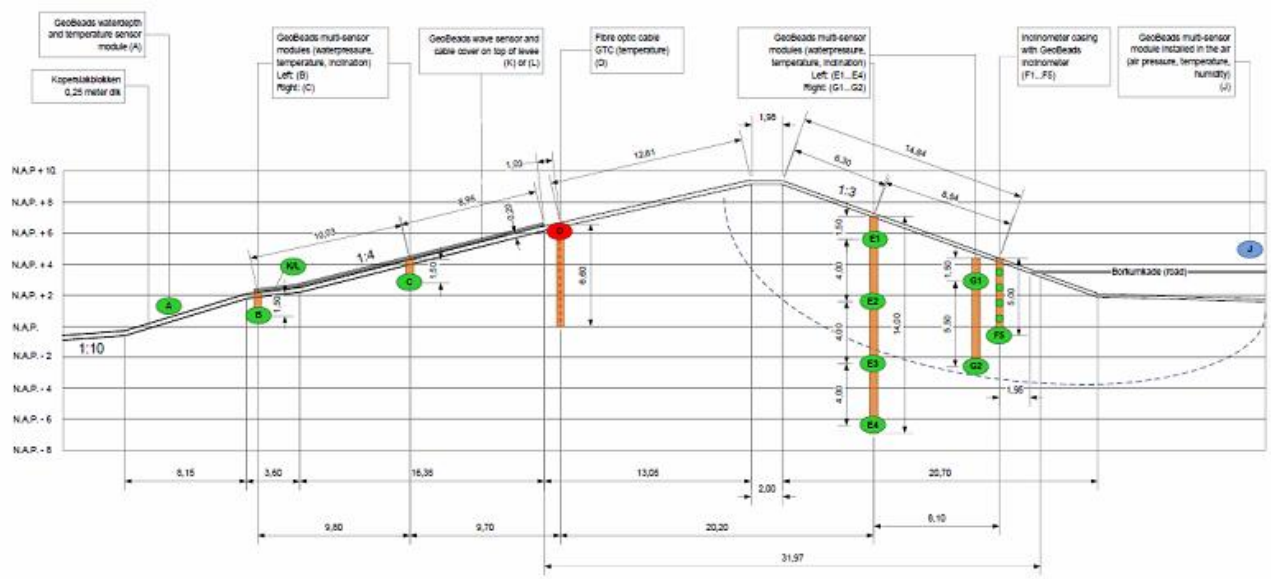

Figure 3.19 Cross section of LiveDijk Eemshaven with locations of sensors (green circles)

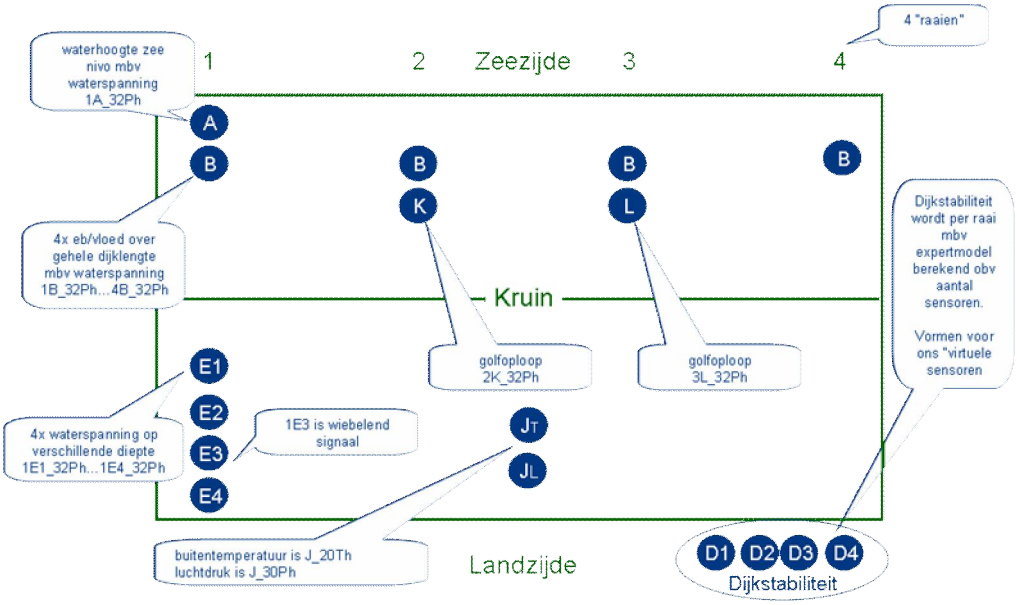

Figure 3.20 LiveDijk Eemshaven sensors in the LiveDijk (simplified top view)

The LiveDijk data and analyses are shown on a Multi Touch interface, since the TimelineStore itself has no visual component. Figure 3.21 shows the interface with some sensor graphs. At the bottom, the main timeline is situated. This controls the period in time displayed on the screen. Most objects are related to this timeline, the small sensor graphs will change accordingly. The red bar in the main timeline indicates the present time. The bigger sensor graph window appears when you enlarge a small sensor graph with your fingers. Then an interactive version of that graph appears, with its own timeline to inspect the sensor data in more detail.

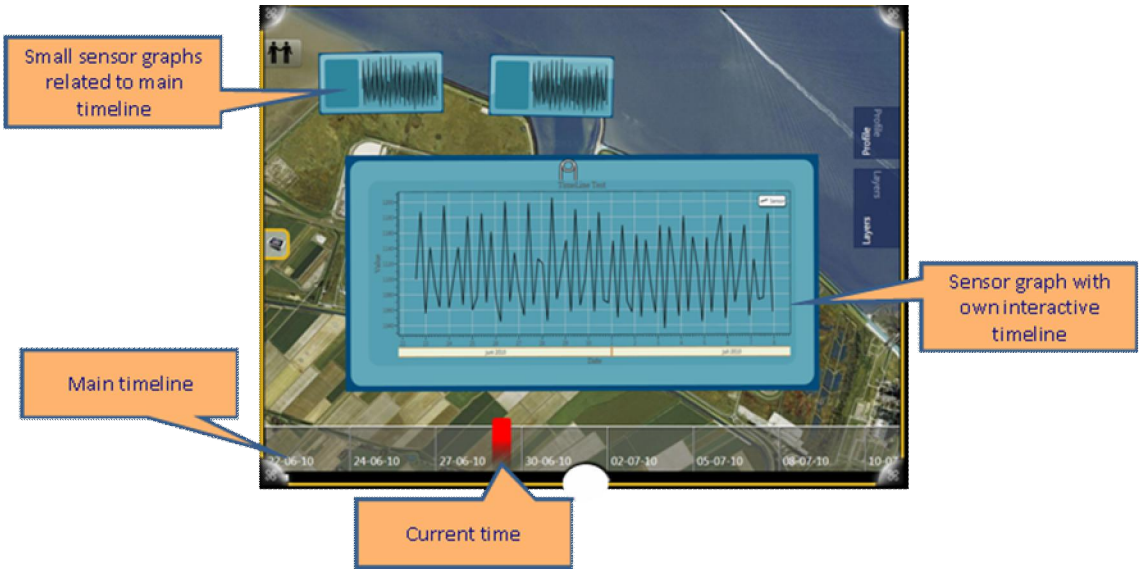

Figure 3.21 Main Timeline example on the Multi Touch table

Additional to these graphs also reference information can be shown, for instance a detailed schema of the internals of the dike (Figure 3.22). Web pages are also possible, to have a more interactive lookup of reference information.

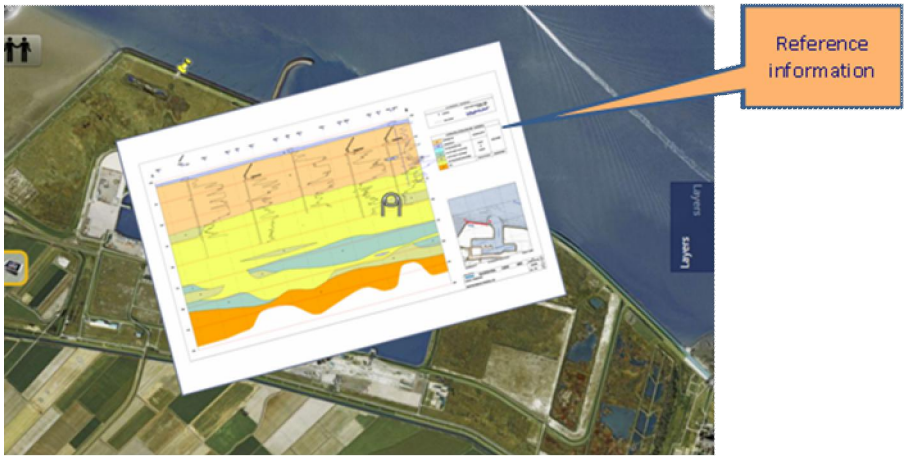

Figure 3.22 Reference information of the Multi Touch table

Live information can also be displayed (Figure 3.23), for instance the movement of ships around the "Eemshaven" (AIS vessel information). Using a layer window special selections can be made, such as relevant (filtered) twitter messages, rain fall (overlaying "buienrader" images), etc. Note that in the current version this information is not yet connected to the timeline. Extensions in the TimelineStore to store moving objects are necessary to realize this functionality.

Figure 3.23 Live information shown on the Multi Touch table

When available, it is possible to have concurrently a 3D view of objects on the map on the multi touch table (Figure 3.24). By placing tangibles - small objects with a special 2D barcode - on the table the view can be controlled as if it is a local camera. This helps in getting insight in the environment.

Figure 3.24 3D view: combining a monitor with the Multi Touch table

3.5.1 Normal behavior (use-case 1)

In this use-case we look at the normal behavior of the sample rate of a pore pressure sample. In theory the measurements are taken every minute. But how to detect (and signalize) when there are missing values or when the sample rate is changing?. In section 3.4.3 the sample rate changeability sensor is explained. This virtual sensor is used for the detection of normal behavior in this use-case.

Use-case 1a: detection of missing samples

In Figure 3.25, it is shown that at until T=1:58 hour the changeability of the sample rate is most of the time zero, some times -0,1 and some times +0.1 or +0.2. This means that until T=1:58 hour, the measurements are arriving at a "normal" and expected rate (in practice: one per minute, which is learned by the sensor in an adaptive way).

In the top panel of Figure 3.25, samples are missing for the period T=1.58 till T=2:07. This is sensed by the changeability sensor and shown in the lower picture by a negative output. At T=2:08 the measurements are arriving again in the "normal" frequency of 1 per minute. Because of the used window with *window-size=10* in the virtual sensor, it take some time until the change-ability is zero again (until T=2:35). This is typical behavior of the changeability sensor when there is a gap in the measurements: first a dip (indicating the missing samples) then a top (indicating the measurements are arriving again).

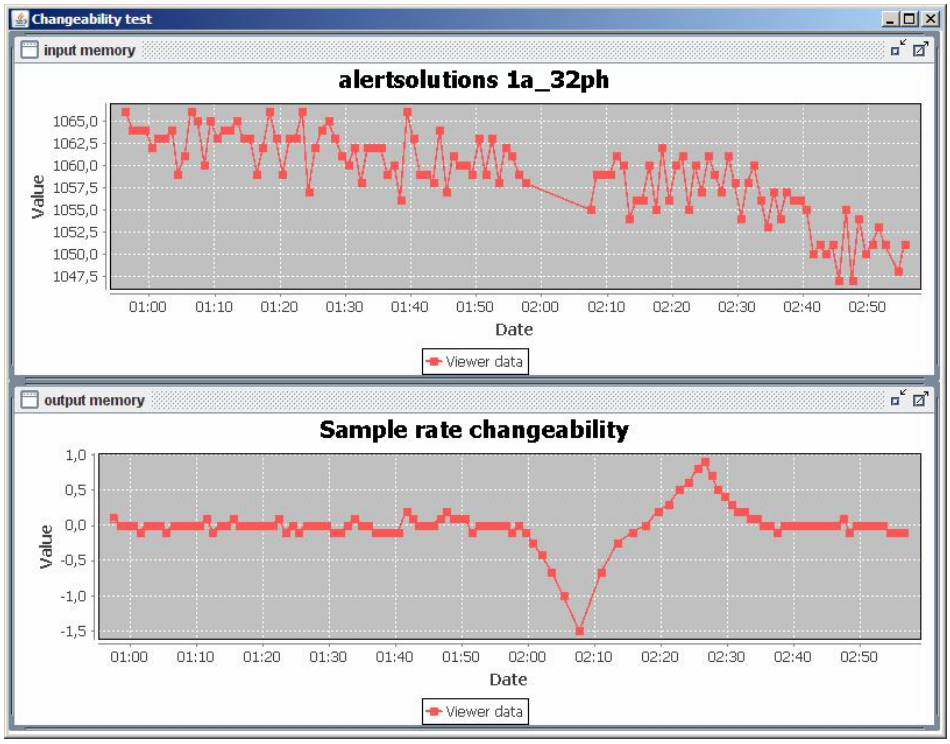

Figure 3.25 Sample rate changeability

Note that the changeability sensor is not able to tell *why* the measurements are missing, it only tells *that* they are missing. In the example it could be that there was a problem with sending the measurements from the LiveDijk via GPRS to the AnySense platform.

The sample rate changeability sensor can easily be monitored. Monitoring means that triggers can be set for a low and/or high level. Passing such a level invokes an email/sms/etc. In this project Nagios (see also www.nagios.org) is used for monitoring. This is a common open source monitoring application, heavily used to monitor computers. We added adapters to monitor also changeability sensors.

In Figure 3.26 the service monitor interface is shown. Four hosts (computers) are monitored, each running several service. The yellow service is our sample rate changeability sensor, indicating a warning for the change in the sampe rate, as shown in the previous figures. The LocalDike is a small table demo dike, which was not connected at the time, hence the red color indicating an error.

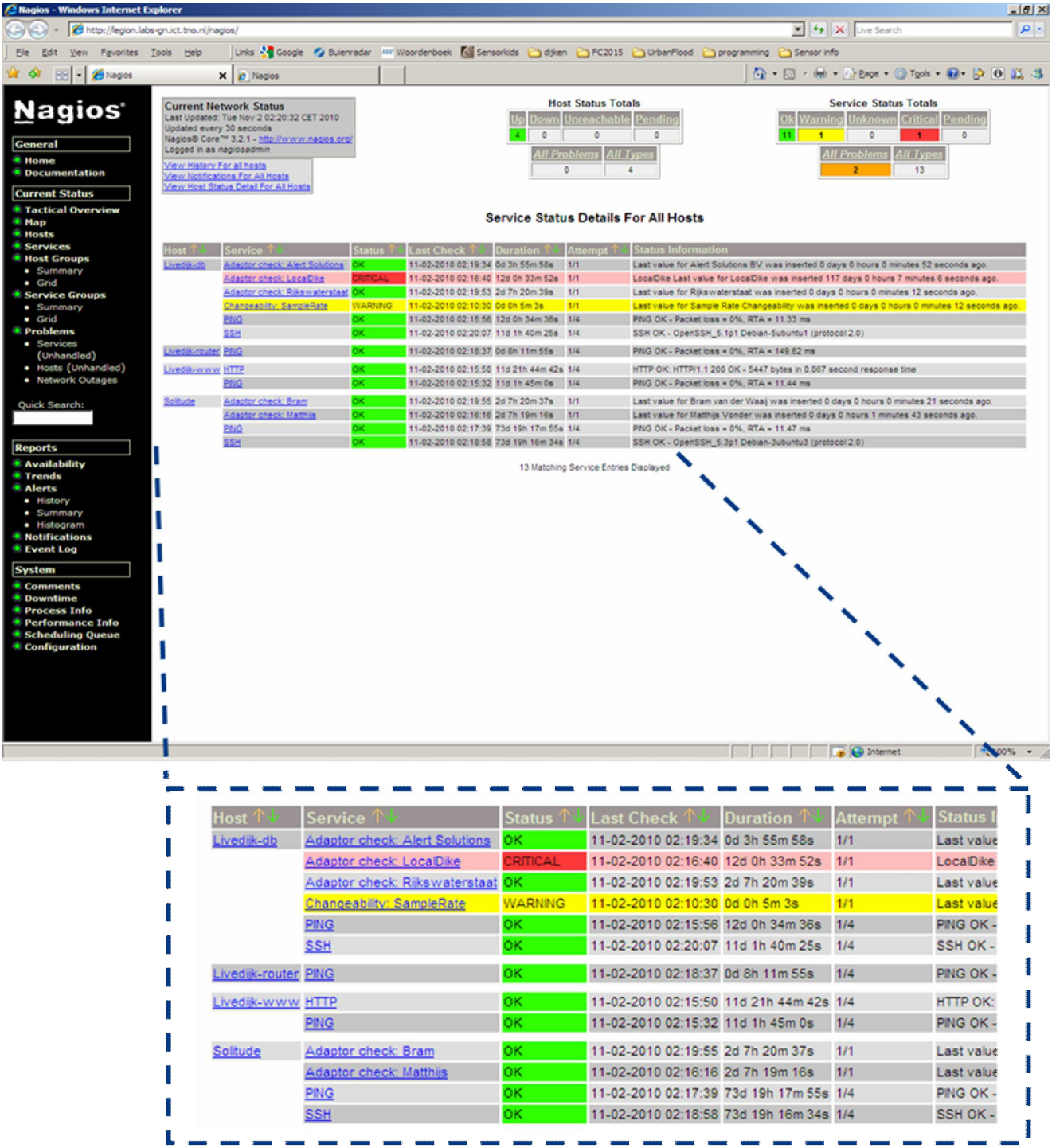

Host	Service	Status	Last Check	Duration	Attempt	Status I
Livedijk-db	Adaptor check: Alert Solutions	OK	11-02-2010 02:19:34	0d 3h 55m 58s	1/1	Last value
	Adaptor check: LocalDike	CRITICAL	11-02-2010 02:16:40	12d 0h 33m 52s	1/1	LocalDike
	Adaptor check: Rijkswaterstaat	OK	11-02-2010 02:19:53	2d 7h 20m 39s	1/1	Last value
	Changeability: SampleRate	WARNING	11-02-2010 02:10:30	0d 0h 5m 3s	1/1	Last value
	PING	OK	11-02-2010 02:15:56	12d 0h 34m 36s	1/4	PING OK -
	SSH	OK	11-02-2010 02:20:07	11d 1h 40m 25s	1/4	SSH OK -
Livedijk-router	PING	OK	11-02-2010 02:18:37	0d 8h 11m 55s	1/4	PING OK -
Livedijk-www	HTTP	OK	11-02-2010 02:15:50	11d 21h 44m 42s	1/4	HTTP OK:
	PING	OK	11-02-2010 02:15:32	11d 1h 45m 0s	1/4	PING OK -
Solitude	Adaptor check: Bram	OK	11-02-2010 02:19:55	2d 7h 20m 37s	1/1	Last value
	Adaptor check: Matthijs	OK	11-02-2010 02:16:16	2d 7h 19m 16s	1/1	Last value
	PING	OK	11-02-2010 02:17:39	73d 19h 17m 55s	1/4	PING OK -
	SSH	OK	11-02-2010 02:18:58	73d 19h 16m 34s	1/4	SSH OK -

Figure 3.26 The Nagios service monitor interface

Use-case 1b: detection of malfunctioning sensor

In the upper panel of Figure 3.27, the last measurement arrived from the LiveDijk at T=7:58. Since there are no more measurements arriving, the plot stops in the upper panel at this moment (it will continue when the next measurements arrives). In the lower panel, the sample-rate-changeability sensor still produces output. At T=7:59 the value is decreasing (indicating the rate is decreasing). Due to the window it will detect at T=8:29 that there are no more measurements arriving at all (within the window-size) by returning the value -20.

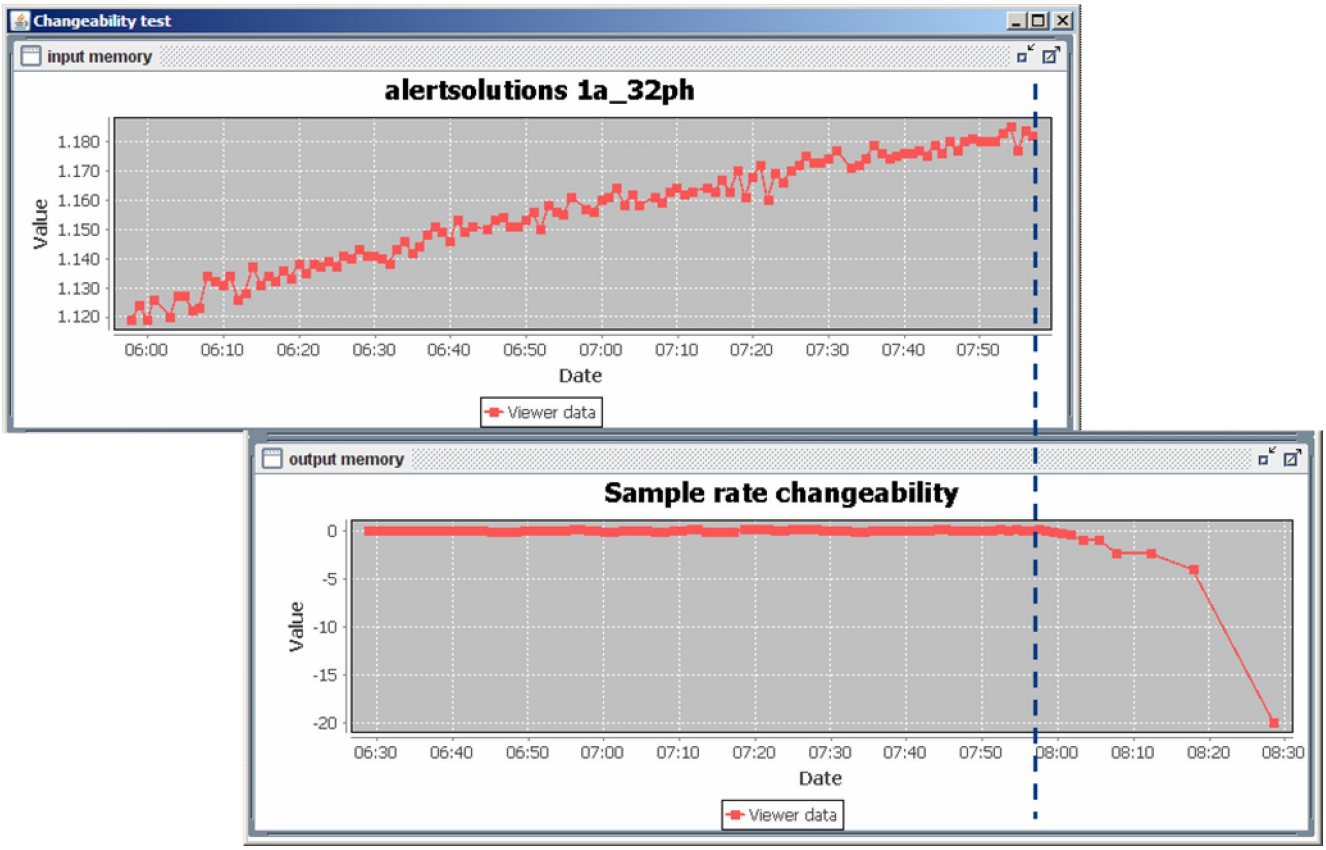

Figure 3.27 Sample rate changeability

Directions for future development

Note that in the use case described above we looked at normal behavior of the sample rate. For future work we recommend to make also a virtual sensor as input for monitoring the actual sensor values. A starting point for this could be using the "number-of-contributing-frequencies" building block (see section 3.4.2 and Appendix 12 :) to analyze the signal.

3.5.2 Prediction of pore pressure (Use case 2)

The LiveDijk Eemshaven has a relatively simple composition of sand. Therefore, there is nearly no delay to be expected between a sensor at the base of the levee and the pore pressure inside the levee. Furthermore, the levee rarely experiences hazardous situations and exhibits a high slope stability. Still, it provides a good test case to show the possibilities of time series analysis and the use of alternative input sensors to predict slope stability.

The values measured by the pore pressure sensors need to be corrected for the ambient air pressure (use case 3). Then, the pore pressures need to be converted to location of the water table, which is used in the levee slope stability calculations. When the water is rising, the pore pressure will adapt almost instantly, whereas the water level shows a delay dependent on the permeability of the levee body. Although the time series analyses can predict values inside the levee, more information about the permeability of the levee is necessary.

A complication factor is that a pore pressure sensor only provides a representative value when it is located below the water table. A sensor that is only temporary below the water table provides a less continuous time series.

Time series analysis based on equivalent sensors in sensor array 1

The time series analysis has been applied to cross section 1 of the LiveDijk levee. Figure 3.29 shows the results for a time interval of several tides. In the analysis, the measurements at location 1/E4 (the core of the levee) are explained by the measurements at location 1/A1 (the front of the levee), see also Figure 3.28. The purple line shows the real sensor data of sensor 1/E4. The green line is the result of a simulated output, solely

based on the input time series and the parameters α and δ. The light blue line shows the time series when updated with the real output. The graph shows that the data of 1/E4 can be predicted very well with the data of 1/A1. Moreover, when the parameters α and δ are estimated, gaps in the data can be easily interpolated. Sensor 1/A1 follows the water level outside the levee, unless the water level is lower than the sensor itself. Therefore, the values of sensor 1/A1 are truncated at the lower values, when the sensor is dry. Sensor 1/E4 is situated well below the water table, which makes the measured output much more symmetric. As expected there is nearly no delay between the sensors in different locations in the levee.

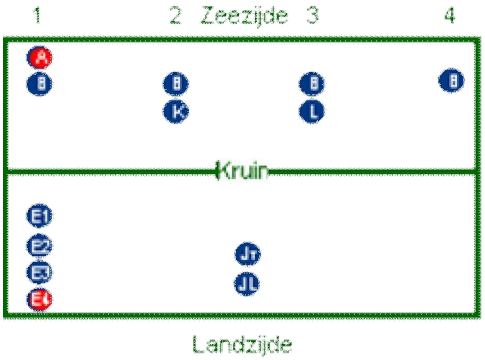

Figure 3.28 Location of the sensors A1 and E4 in the LiveDijk Eemshaven

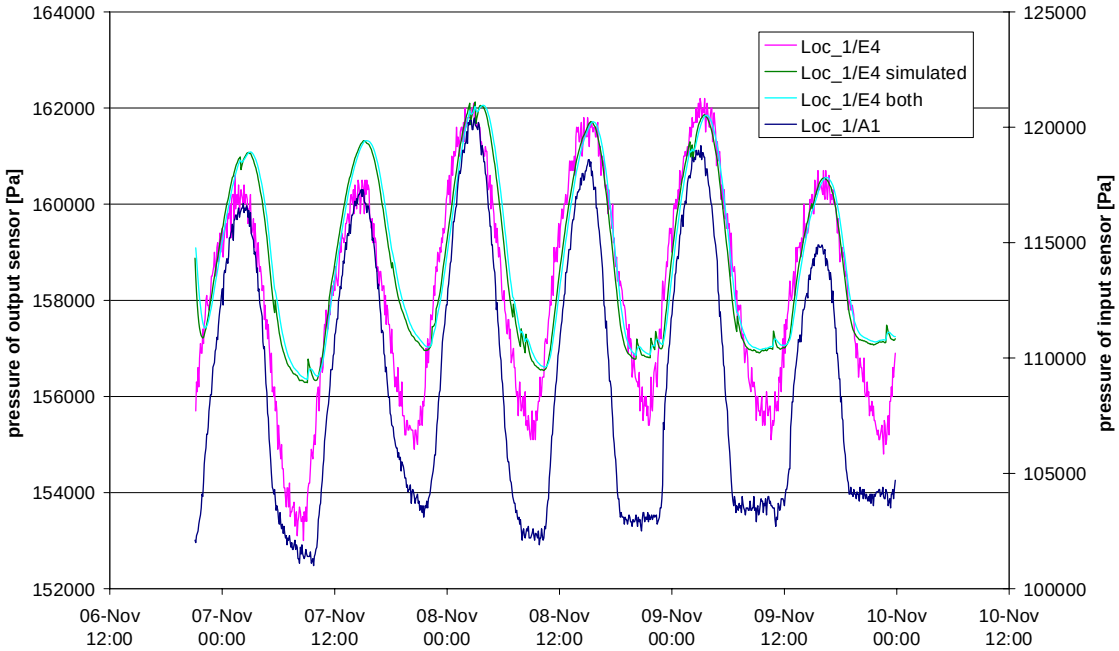

Figure 3.29 The measured input and output sensors and the simulated output at the LiveDijk Eemshaven

There is a difference in heights of peak values between the measured and the predicted pore pressures. This is due to the limitation of using sensor 1/A1 as a learning input: the measured values of sensor 1/E4 show a nearly sinusoidal curve, whereas the simulated version is biased by the values when sensor 1/A1 is dry. Because sensor 1/A1 is used to learn and predict the values of sensor 1/E4, the predicted 1/E4 also shows the bias towards “dry” values. Since we are mainly interested in the prediction of extreme conditions like floods, it remains the question how well this model responds to these conditions.

By varying different parameters, it was found out that 3 days of data – so approximately 6 cycles of the tide - is sufficient to learn the behavior of the sensor. The time interval between measurements is very dependent of the amount of noise on the signal. Generally, a data set with an interval of 15 minute is sufficient.

Timeseries analysis based on an alternative input source

In July 2010, the sensor network in the LiveDijk was struck by lightning, resulting in damage to the electronic system of the sensors. This occurrence shows the vulnerability of a sensor network. In order to make a system more robust, it should make use of different kinds of data to predict other datasets. Rijkswaterstaat measures the water level at the coast and rivers at about 100 places at a one minute interval. One of the Rijkswaterstaat monitoring points is located in the Eemshaven. This RWS sensor is very suitable as input to learn and predict the pore pressures inside the levee.

Figure 3.30 shows a time interval of RWS measurements (dark blue line) at the Eemshaven and the comparison between the water level sensor 1/A1, which falls temporarily dry (pink line). The graphs show 4 versions of sensor data. The measured pressure data at A1 is converted into water levels by subtracting the ambient air pressure and dividing by the gravity. Without correcting for atmospheric pressure, the calculated water levels can deviate about 20 centimeters. The pink line depicts the normally measured data as retrieved from the sensor. An artificial gap in the data was created starting at June 4th depicted by the green line. With the water level from RWS and the relationship between RWS and A1 data, the gap is filled by simulation (light blue line). The red line shows the simulated time series of A1 that is fed by the real output sensor data. To show the relationship between Rijkswaterstaat data and the sensor data as clearly as possible, both datasets use different axes. The relationship between the high tide and maximum pore pressures is clearly visible. The simulated time series that is updated by actual data tends a little closer towards the real observations.

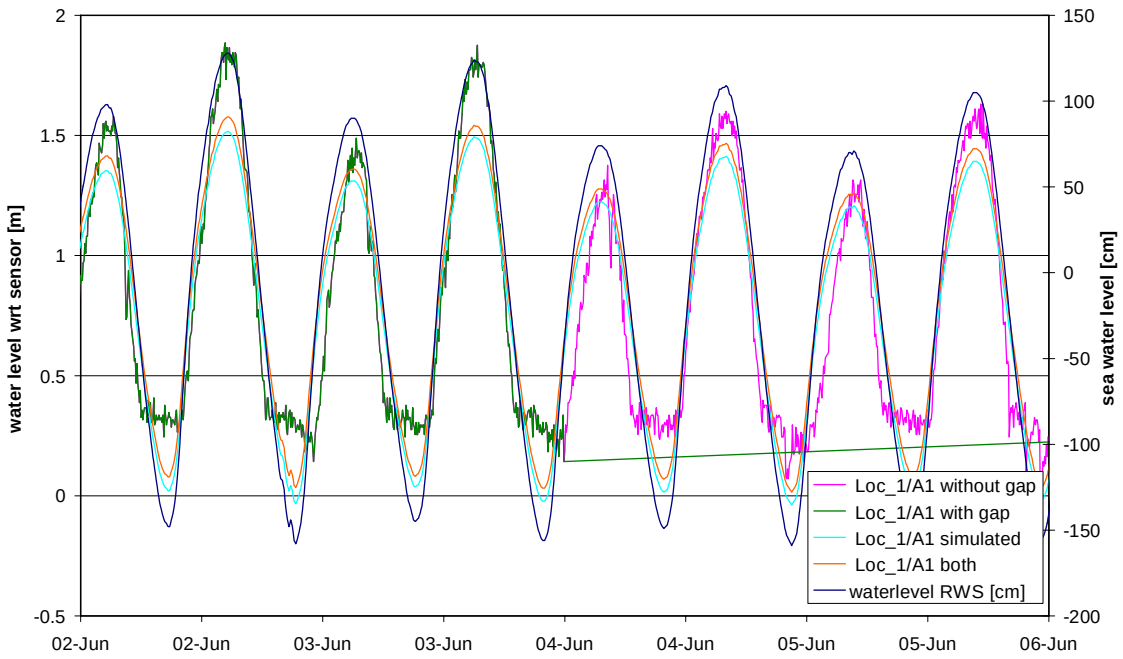

Figure 3.30 Time series of sensor 1/A1 with respect to water level data of Rijkswaterstaat

Because the RWS water level is used to learn and predict the 1/A1 sensor values, the predicted 1/A1 does not show the periodically “dry” values as in the measured 1/A1. The prediction mimics the behavior of the learning curve of RWS water levels, which is sinusoidal, without the bias when 1/A1 falls dry. From this analysis, it is clear that the water level measured by RWS can be used to predict the water level measured at location 1/A1 outside the levee in cross section 1. The next step is to use the RWS water level to predict the pore pressures inside the levee.

Figure 3.31 shows the result of the time series analysis in which the relationship between the measured RWS and measurements of pore pressure inside the levee are used to predict the pore pressure inside the levee in case of a gap in the data inside the levee. The color coding of the curves is identical to Figure 3.30. The predicted pore pressures at 1/E4 (light blue and red) are smoother than the measured pore pressures (pink). This is because of the smoothness the RWS signal which is used to predict pore pressures at 1/E4. From Figure 3.31 it can be concluded that the pore pressures can be predicted quite accurately.

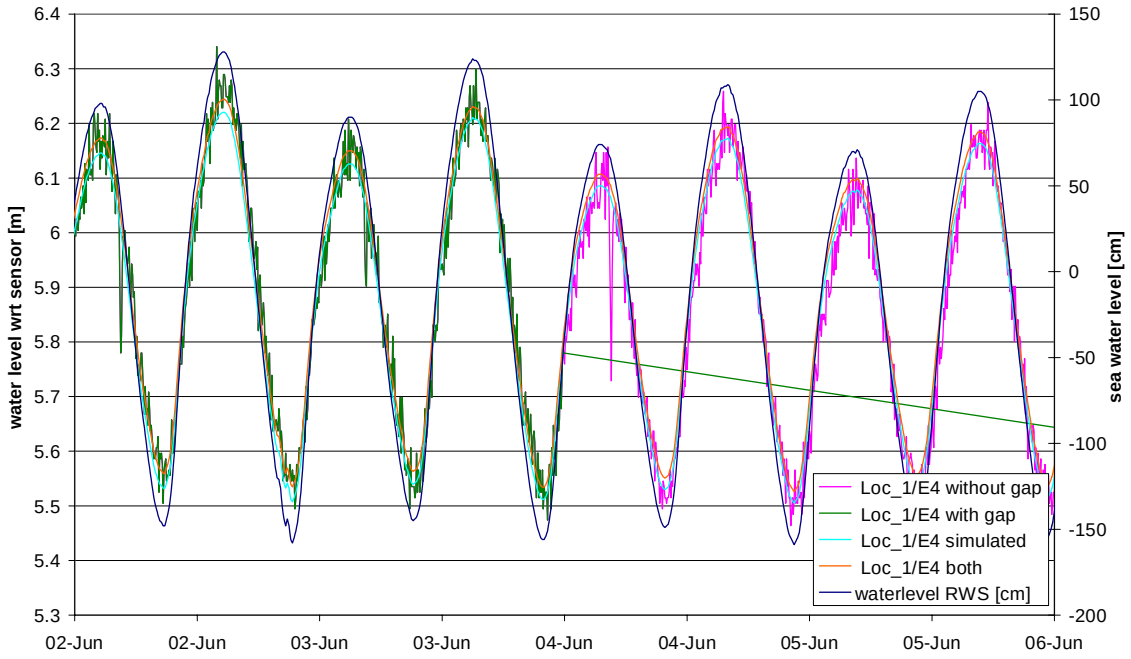

Figure 3.31 Time series of sensor 1/E4 with respect to water level data of Rijkswaterstaat

When all pore pressures in the levee are predicted from their learned relationship with RWS water level data, these simulated pore pressures can be used as input in the slope stability calculations. A comparison is made between the slope stability factor calculated by MStab using measured pore pressures and simulated pore pressures. While the levee continuously stayed well within safety limits (a slope stability factor around 1.8), the outcome of real data and simulated data were comparable. This offers the possibility to predict the slope stability even if one or several sensors are malfunctioning.

The time series analysis showed that different sensors can be used as input for the slope stability calculations. However, some precautionary remarks need to be made. The simulated values do not replace the measured values or decrease the necessity to install sensors. The relationship between the sensors used in the prediction needs to be updated to cover all external circumstances. In this example, the relation between RWS water level data and e.g. 1/E4 is only valid for conditions valid during the learning time span. In changing conditions, e.g. a big storm with high water levels, the relationship needs to be updated. The relationship between the sensors, which was learned during quiet conditions cannot be used anymore.

Future improvements for time series analysis

The previous model uses solely the data of the sensor without any knowledge of the physical process and structure of the levee. Although this model can be expanded with non-linear patterns, this approach is limited by aspects from a levee that can not be predicted by time series alone.

Sensor data can be exploited further by assuming that the measurements can be simulated by a physical model. The combination of observations and a model provides good insight in the accuracy of both sources of information. This data assimilation can be performed in various algorithms, amongst others Ensemble Kalman Filter, Bayesian Estimation and 3DVAR. The main idea of these algorithms is that they update the state from a model with the state of the observation. The one which has the best expected accuracy will have the higher weight in the weighting process. On a location near a sensor, the algorithm will rely more on the measurements, whereas the model is more important on intermediate locations.

Data assimilation can occur at different levels. In the first approach, only the dynamic state of the model (e.g. location of the water head) is updated. The water head fluctuates rapidly, and small errors in the model can lead to large errors in the state. Therefore, the measurements help to constrain the model close to reality. The next issue is to validate the model itself. The model uses some parameters e.g. permeability of the levee at different locations. If these parameters are estimated falsely, the model tends to give a structural bias. Therefore, the model parameters need to be updated as well. While all previous steps only provide predictions, this step provides real insight in the structure of the levee.

3.5.3 Correction of pore pressure with air pressure (use case 3)

In Figure 3.32 the measurements of several selected LiveDijk pore pressure sensors (1B-4B) and the atmospheric pressure sensor (JL) are shown.

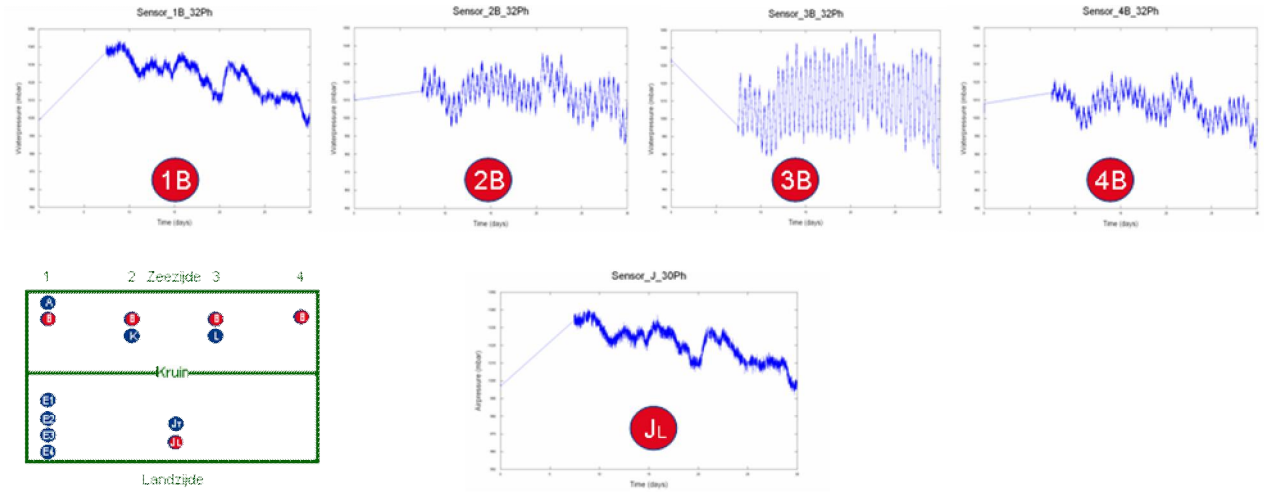

Figure 3.32 Pore pressure sensors and atmospheric pressure sensor at the LiveDijk

Normally, to make the correction of the pore pressure with the air pressure, the measurement of all sensors should exactly have the same timestamp. And no missing measurements are allowed. Fortunately, we can ask the Timeline store to give for each point in time a sensor value. The result is shown in Figure 3.33, constructed by subtracting the sensor JL from sensor 1B and sensor 1B.

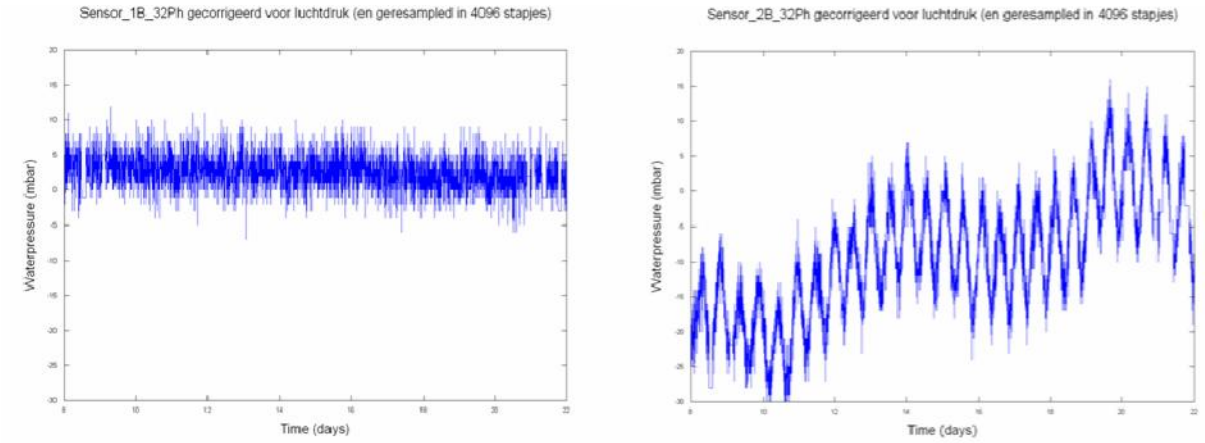

Figure 3.33 Corrected pore pressure for atmospheric pressure: left 1B and right 2B

In fact we see the result of two new virtual sensors measuring the corrected pore pressure.

Directions for further development

The figure above shows also the following:

- The corrected value for 1B is around zero. That means that the uncorrected 1B signal is almost the same as the atmospheric pressure. Which could mean that the 1B sensor is placed (just) above sea level, remaining dry in the measured period.
- The corrected value for 2B is most of the time below zero. Because the pressure could not be negative it could mean that either the atmospheric pressure sensor JT or the pore pressure sensor 2B should be (re)calibrated.

One could build a monitor (like in § 3.5.1) with the corrected pore pressure as input. When the corrected pressure is negative it will send a warning. An expert should then find out what is wrong and if a recalibration is necessary. If so, this correction could also be used in the Timeline store to correct measurements in the past (making a new timeline, like in Figure 3.9). When the corrected pressure stays around zero, it will send a warning. An expert should then find out if the sensor is perhaps wrongly placed.

4 REMOTE SENSING AND DIKE MONITORING

4.1 INTRODUCTION

In this chapter, the possibilities of using remote sensing data for the use of dike stability monitoring are discussed. The focus is on monitoring deformation as indicator for stability problems and soil moisture content or temperature contrasts as indicators for leakage. The use and limitations are illustrated by a case study of the levee of the Juliana Canal (Dutch: Julianakanaal) in the southern part of the Netherlands.

> The goal of this part of the project is to develop and apply remote sensing techniques for deformation and leakage in relation to dike stability.

First, the available techniques for earth observation (airborne, spaceborne and ground based) are considered and their expected applicability for monitoring deformation and leakage is assessed. This is based on literature and experience from Fugro and Deltares. Then the site Juliana Canal and the expected deformation and leakage locations are described. Subsequently, the results from the remotely sensed and the ground based measurements are given. The chapter is concluded by a discussion on the applicability of remote sensing data to an operational and real time Flood Control System.

4.2 TECHNIQUES FOR LEVEE MONITORING

4.2.1 Available remote sensing techniques

There are several remote sensing techniques available for the monitoring of levee. Some are already used, such as airborne laser altimetry. Others are tested in pilot studies, such as the use of Persistent Scatterer Interferometry (PSI) on several Dutch levees. These techniques are further developed in European projects such as Terrafirma (ESA funded) or SubCoast (EU funded).

Remote sensing techniques can be applied from different platforms. Sensors are mounted on satellites (spaceborne) or on helicopter or aircraft (airborne). Several airborne techniques can be applied from a terrestrial platform as well. In Swart [2007] an extensive overview is given of the remote sensing techniques and their platforms. A summary of the techniques is given here based on that report, completed with recent experiences from Fugro NPA and Deltares. The expected suitability of the technique is assessed for application on the monitoring of deformation and of leakage.

In Table 4.1 and Table 4.2 remote sensing techniques from an airborne platform are presented for deformation and for leakage. In Table 4.3 and Table 4.4 those for spaceborne platforms are summarized.

Table 4.1 Remote sensing techniques for deformation on an airborne platform

Technique	Suitability for deformation	Remark
Laser altimetry	✓	Technique used to make AHN-2 (digital elevation model of the Netherlands)
Digital photogrammetry	✗	Resolution too low and high costs

Table 4.2 Remote sensing techniques for leakage on an airborne platform

Technique	Suitability for leakage	Remark
Nuclear Magnetic Resonance	✓	
Near infrared	✓	Vegetation index, indirect indicator of leakage
Passive microwave radiometry	✓	Related to temperature and evapotranspiration
Thermal infrared	✗	Large difference in temperature required, only in e.g. cold winter

Table 4.3 Remote sensing techniques for deformation on a spaceborne platform

Technique	Suitability for deformation	Remark
Differential Interferometry	✓	Accurate data on movement of platform needed
PSI	✓	Depends on availability of persistent scatterers
High resolution optical images	✗	Suffers from reduced visibility due to clouds, resolution is still insufficient and costs are high

Table 4.4 Remote sensing techniques for leakage on an spaceborne platform

Technique	Suitability for leakage	Remark
SAR	✓	C-band, X-band
Polarimetry mode	✓	
Differential InSAR	✓	
Multispectral	✓	Related to vegetation
Passive microwave radiometry	✓	Related to temperature and evapotranspiration
Near infrared	✓	Vegetation index, indirect indicator of leakage. Resolution probably insufficient
ASCAT	✗	Insufficient resolution of 25-50 km
Thermal infrared	✗	Large difference in temperature required. From satellite suffers from effects of clouds and water vapour
ASAR wide swath mode	✗	Insufficient resolution, backscatter also depends on roughness and vegetation, SMC in top few cm. Sensor on Envisat satellite
MIRAS L-band	✗	On SMIS, insufficient resolution of 35-50 km

On http://gdsc.nlr.nl/FlexCatalog/catalog.html# an overview is presented with satellite missions and the sensors on board.

Deformation

For deformation, the most promising technique is Persistent Scatterer Interferometry, PSI. This is an advanced satellite SAR technique that uses interferometric processing of phase information to infer deformation of the land. A short description of the technique is provided below. A full description of satellite SAR techniques is provided in Appendix 6 :

SAR satellites send and receive radar waves in a certain frequency band (X,C,L band). A side looking antenna looks at the ‘scatterers’ or ‘backscatters’ of the radar signal as shown in Figure 4.1. Flat surfaces like water will reflect and will not return to the antenna, while rough surfaces will cause a backscatter to the antenna, depending on the properties and geometrical characteristic of the terrain. The frequency of coverage, i.e. the time between two exact same images, depends on the orbit of the satellite. When looking at cropland, the amount of backscatter depends on the type and growth stage of vegetation and on the amount of saturation of the subsurface. Different types of SAR sensors exist on different satellites, each having its own characteristics (frequency, polarization, coverage, repeating cycle, spatial resolution).

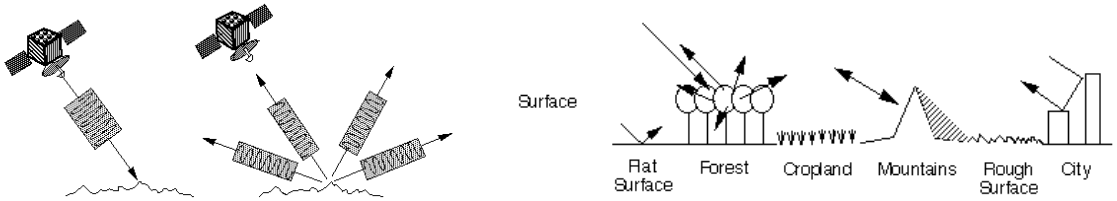

Figure 4.1 Satellite SAR technique. Left: Backscattering of a radar signal on a rough surface. Right: different surfaces cause different backscattering characteristics. Courtesy of ESA.

Persistent Scatterer Interferometry (PSI) is an advanced differential interferometric technique which involves the processing large volumes of multi-temporal Synthetic Aperture Radar (SAR) data to identify networks of persistently reflecting surface features (e.g. buildings, bridges, infrastructure and rocky outcrops), against which precise (millimetric) measurements of motion can be made. 'Persistent scatterers' are caused by objects that will give a high backscatter and do not change in scattering characteristic. This is in most cases a human made reflector such as a roof, a sound screen at the highway or a bridge. Also, for typical circumstances dikes can be considered as persistent scatterers. PSI looks at the phase difference of the radar signal per persistent scatterer. In this way, millimetric vertical movement can be measured per repeating measurement.

Monitoring ongoing and historical ground motion on and around a dike gives a valuable data source that can be used in determining the overall health of a dike and can provide a unique and invaluable addition to any risk assessment. Given the focus upon small spatial scale (from a SAR pixel perspective) linear features, PSI is considered the most appropriate InSAR technique capable of providing unique, complementary information within a smart dike monitoring system.

Leakage

Soil Moisture Content (SMC) is an environmental parameter which serves as a critical input to many applications which rely on detailed modelling and understanding of the upper soil layer, e.g. agricultural purposes. Remotely sensed optical or SAR data are affected by many surface parameters of which soil moisture levels is only one. Separation of the observed signal that depends on soil moisture is complex but necessary if monitoring of this parameter over large areas is to be cost effectively achieved.

The use of satellite data to infer soil moisture on specific locations is still a field of research. A literature review is provided in Appendix 7 : . A summary of the procedures for estimating and further potential for monitoring SMC using SAR with assumptions and limitations in Table 4.5.

The use of multipolarisation data is probably the most successful approach. However, these data are not available for the study area. Differential interferometry and the use of amplitude information in the SAR signal are also interesting approaches to retrieve information on soil moisture content. In §4.3.5 these techniques have been used on the study area.

An example of phase centre shifts from differential InSAR is provided for an area in Southern Iraq consisting of a partially agricultural area in an arid environment where it was anticipated that soil moisture was the dominant changing parameter. Fugro NPA processed the data looking for geological subsidence. Level changes, however, appeared in areas of temporarily increasing moisture which clearly correlated with the optical changes.

The optical image (Figure 4.2) with false color composite shows an unvegetated area that is prone to frequent flooding and significant variations in soil moisture (not just surface water). In the amplitude images (Figure 4.3) there is an increase in brightness in the near range on the second image of the pair, which can then be related to the rise in the phase centre on the DifSAR image (Figure 4.4). Whilst there are no field measurements to confirm whether or not the findings are related to soil moisture, the support of historical optical imagery (Figure 4.2) can be related to the phase centre shift in the DifSAR results. From this information and combining the supplementary datasets this supports the theory that this phase change is strongly related to soil moisture.

Table 4.5 Assessment of methods to derive soil moisture from SAR data

APPROACH	METHOD & ASSUMPTIONS	POTENTIAL
Amplitude Change	▪ Surface roughness assumed to be near constant ▪ Vegetation reduces SMC effects on signal, particularly for shorter wavelength signals ▪ Potential to utilize different incidence angles if short temporal separation is achievable. ▪ Matching radar configuration is required for each image	If surface roughness and vegetation cover are assumed not constant, attributing single wavelength SAR amplitude change primarily to soil moisture is not viable. Multi-look or multi-wavelength data have potential, however the difficulty in obtaining such data with sufficiently short temporal separation means this approach is also unlikely to provide an operational solution.
Multipolarization	▪ Semi-empirical scattering models (Oh & Dubois) model different mechanisms, inferring soil moisture from dielectric properties ▪ Extensive field work has been used to derive models for dielectric, surface roughness and volume scattering. ▪ Coefficients not always valid under new circumstances (have limited range of validity) ▪ Advances scattering models such as X-Bragg or X-PO improve applicability of scattering models to a wider range of roughness terms by incorporating H, α and A.	Multi polarization data allows the extraction of both scattering and soil moisture parameters A number of algorithms exist to extract quantitative soil moisture however research is ongoing. The potential for using Multi polarization and Multi frequency data is raised however the current difficulty would be obtaining data with short enough temporal separation to make this an operational solution.
Differential Interferometry	▪ SMC affects penetration depth and hence Phase Centre offset without ground displacement occurring ▪ Additionally ground displacement from clay swelling (also from increased soil moisture) can result in similar measurement changes ▪ Potential for using data from different wavelength sensors ▪ High quality DEM is required (SRTM)	Potential to monitor soil moisture changes at a scale of 50m or better with single polarization data. Biomass above 0.5kg/m could reduce detection. Requires validation in temperate agricultural regions.

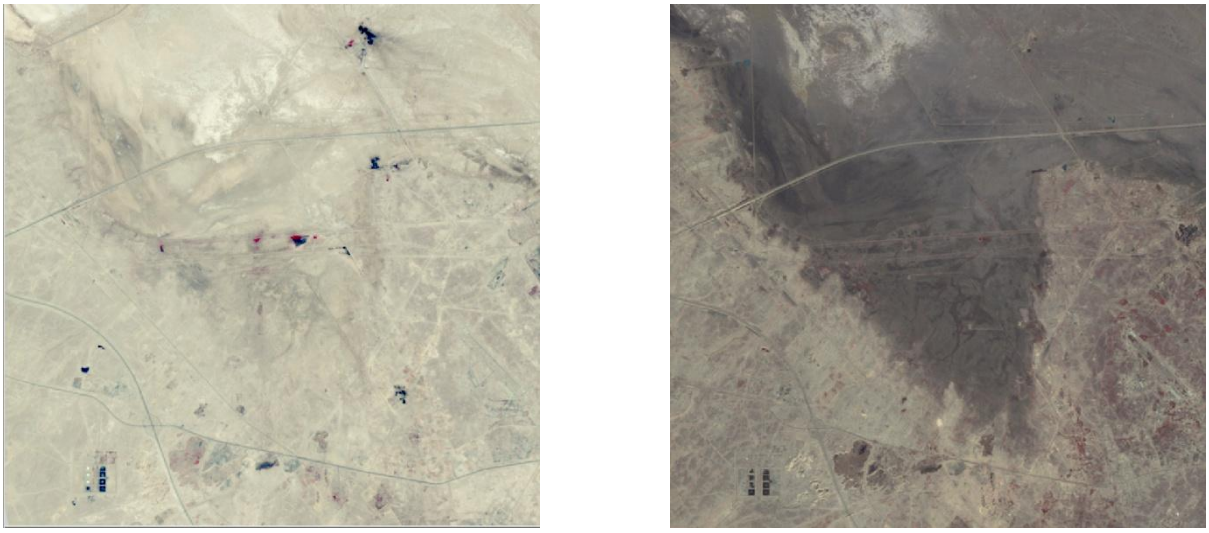

Figure 4.2 **Landsat ETM+ images showing changes from dry (left) to wet (right) over the same area**

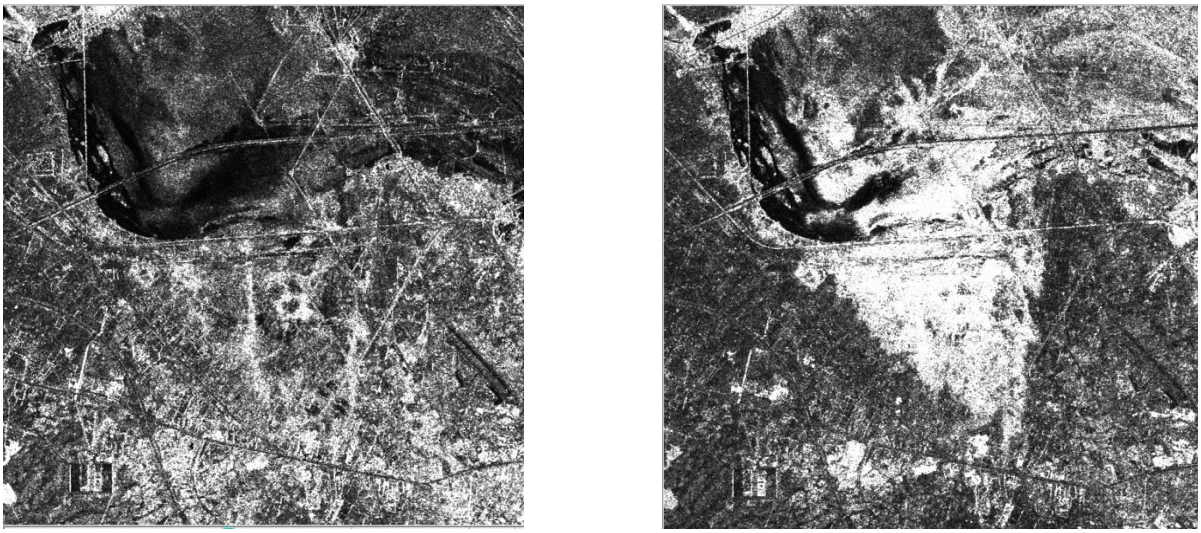

Figure 4.3 **Amplitude images of 19990313 (left) and 19990522 (right)**

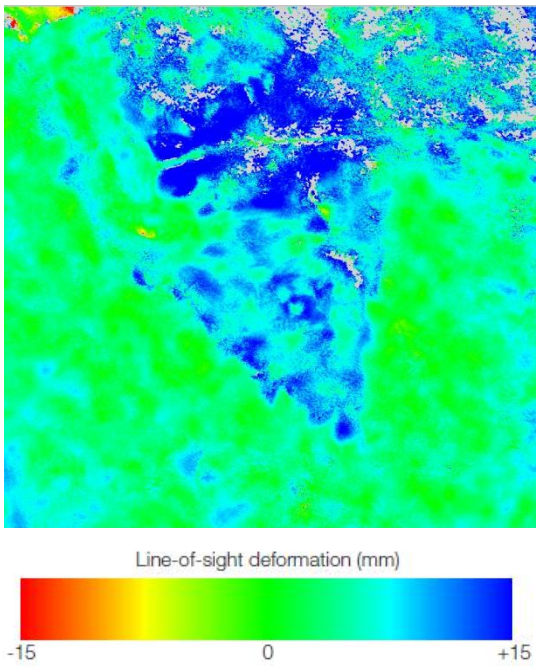

Figure 4.4 **DifSAR result showing phase change between 13 March 1999 and 22 May 1999.**

4.2.2 Available ground based monitoring techniques

Visual inspection of levees is a very important means of monitoring the state of levees in the Netherlands. Additionally, several ground-based techniques are available for detection of deformation and leakage. For deformation, the most important techniques are: leveling, GPS monitoring, tachymetry with prisms (3D movement), terrestrial laser scanning, use of inclinometers, close range photogrammetry and insertion of fiber optics cable into the levee.

For leakage, the self potential method may be successful, because of the fact that the electrical field is influenced by the flow of water. Several techniques give information on the soil moisture content (SMC): ground penetration radar (GPR), nucleonic methods, time domain reflectometry (TDR) and frequency domain sensors (FD).

Deltares studied preferential seepage at distinct locations in the Dutch polders. The “boils” exhibit characteristic temperature and Chlorine profiles. The vertical temperature and EC profiles were measured by “prikstok”, a geophysical measuring pole.

The dielectric permittivity is a proxy for soil moisture content. It can be measured on different scales: the small scale (large area) by SAR satellites, the intermediate scale by GPR and the largest scale (small area) by TDR.

TDR is a well established technique to measure SMC in situ [e.g. Heimovaara and Bouten, 1990]. It can simultaneously measure dielectric permittivity and bulk soil conductivity. It has a small measurement volume (< dm^3) and potentially a high temporal resolution.

In recent years, GPR has been used to estimate values of SMC [e.g. Huisman et al, 2003]. The SMC can be estimated from GPR measurements using reflected wave or ground wave travel time data, borehole GPR or surface reflections. The volume over which the ground wave averages the SMC is estimates to range from 0.1 to 0.5 m for a 225 MHz GPR antenna. Compared to satellite resolution and TDR, GPR indeed operates in the intermediate scale.

A full description of ground based monitoring techniques is provided in Appendix 8 : .

4.3 CASE STUDY JULIANA CANAL

4.3.1 Site description

The Juliana Canal is situated in the southern part of the Netherlands (see Figure 4.5). The Juliana Canal has been constructed in the 1920-30’s and opened in 1935. The canal forms a 36 km long bypass of a navigable section of the river Meuse between Maastricht and Maasbracht. It is an important transport connection between the ports of the Rhine delta and the industrial areas of southern Limburg and southern Belgium.

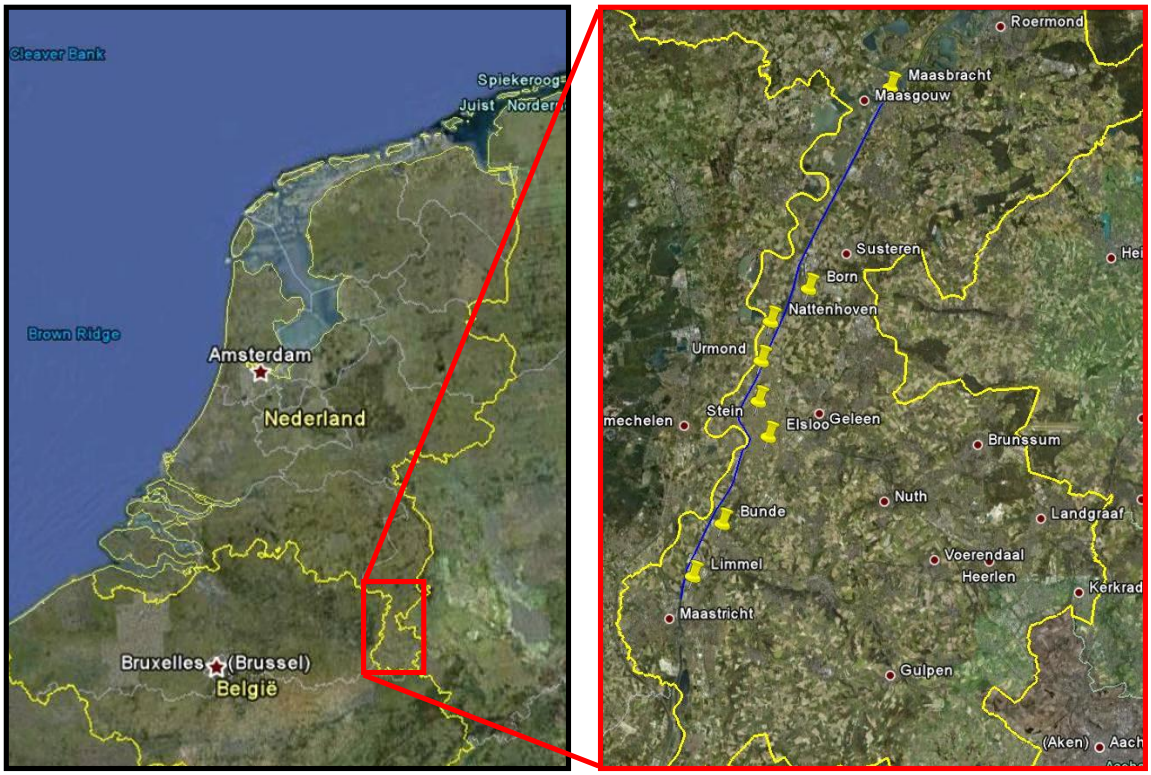

Figure 4.5 Location of Juliana Canal (blue line). Pinpoints are interesting locations for remote sensing measurements (right).
Background image – Google © 2010

The management of the levee belongs to *Rijkswaterstaat De Maaswerken* (RWS). RWS is taking measures to accommodate passage of ships of category 'Vb' through the Juliana Canal. This category of ships consist of a large Rhineship with a length of 135 m, a width of 11.4 m, a draught of 3.5 m and a deadweight capacity of 4000 tons. To this end, several construction works are planned for the widening and deepening of selected stretches between Limmel and Maasbracht. Also, the water level in certain parts will be raised. For these construction works, several studies are carried out.

The scenery of the Meuse valley is formed by a number of geological processes [de Kleine et al. 2010]. In the Tertiary (65-2.5 Ma), the region was covered by sea with fine sand and clay deposits. With falling sea level, rivers started to deposit sand and gravel. From these rivers, the Meuse forms. The Meuse does not only bring sediments, but also erodes during periods of uplift caused by faults. Also rain, wind and ice erode the landscape. Various periods of alternating relative uplift and subsidence created the Meuse terraces.

The lithological units in the subsurface in the region of the Juliana Canal are given in Table 4.6. The Juliana Canal is partly situated on or in the Meuse terraces. At other locations, the canal is constructed on or dug into the original subsurface. In general, the Juliana Canal will be infiltrating if leakage occurs.

In a Geo Risk Scan [Van Meerten et al., 2009], several locations were identified as enhanced risk sites. At these sites, expected problems are related to deformation by subsidence or insufficient thickness of the clay cover of the dike or canal bottom that can cause leakage.

Table 4.6 Lithological units near the Juliana Canal

	Formation	Description
young	Formation of Boxtel	Loam consisting of loess
	Formation of Boxtel	Debris fan of sand and gravel on or at the bottom of slopes
	Formation of Beegden	Loam, sand and gravel of the youngest terrace
	Formation of Beegden	Sand and gravel of middle terrace
to	Formation of Breda	Fine to moderately coarse sand, no glauconite
	Formation of Rupel	Weakly to strongly sandy clays, locally with glauconite
	Formation of Tongeren	Alternation of sands and clays with glauconite
old	Formation of Houthem	Marine limestone

The sites, which are interesting for investigation with remote sensing, are summarized in Table 4.7 and shown in Figure 4.5. For all sites, the establishment of the reference situation is recommended. Possibly, this can be done using remote sensing techniques.

For the 15 km long stretch of Born - Roosteren – Maasbracht, permanent leakage might be increased at existing leakage sites due to a water level rise in the Canal. Vulnerable sites are A2 north of Roosteren and the so called ‘Ecologische Hoofd Structuur’ (EHS), the National Ecological Network.

At several stretches in the canal, dredging is scheduled. This is between Limmel and Stein, at Urmond, and between Born and Roosteren. Permanent leakage can occur if the original cover of canal bottom is damaged during dredging. Vulnerable sites are identified at Hemelbeek (EHS), the terraces at Oud-Urmond and Berg aan de Maas, and the Kingbeek.

Table 4.7 Construction sites at the Juliana Canal (from south to north)

Site	Temporary leakage during wet construction work	Temporary drying out during dry construction work	Permanent leakage if canal bottom is insufficiently sealed	Permanent groundwater rise
Bunde	Affecting village and agricultural land	Affecting EHS	Risk present	No risk
Elsloërbos	Affecting Natura 2000 (Hemelveld+ Elsloërbos)	Affecting Natura 2000 (Hemelveld+ Elsloërbos)	Possibly affecting Natura 2000	No risk
Curve at Elsloo	Affecting Natura 2000 (Hemelveld / Hemelbeekdal) and EHS and possibly slope stability	Affecting Natura 2000 (Hemelveld / Hemelbeekdal)	Possibly affecting Natura 2000	Affecting slope stability
Stein	Raised ground water levels	No risk	Risk present	Risk present
Urmond	Affecting slope stability at terrace in Oud-Urmond and damage of foundations	Affecting agricultural land	Risk present	Affecting slope stability in Oud-Urmond
Nattenhoven	Affecting slope stability at terrace in Berg aan de Maas	No risk	Affecting slope stability in Berg aan de Maas	Risk present
Kingbeek	Affecting EHS, water quality in Kingbeek and agricultural land	No risk	Affecting Kingbeek	Risk present

4.3.2 Remote sensing data for case Juliana Canal

A wide variety of SAR data is available from a large number of earth observation satellites, operated by both public institutions (such as national or regional space agencies) and private commercial companies. Table 4.8 reviews the specifications of the key SAR satellite missions.

Table 4.8 Specifications of the key SAR satellite missions

Sensor	Radar wavelength	Lifespan	Spatial resolution (m)	Revisit time (days)	Scene size (km)	Program-mable
ERS-1	C-band	1991 - 2000	30	35	100 x 100	No
ERS-2	C-band	1995 -	30	35	100 x 100	Yes
Envisat ASAR	C-band	2002 -	30 to 150	35	100 x 100 to 400 x 400	Yes
RADARSAT-1	C-band	1995 -	10 to 100	24	50 x 50 to 500 x 500	Yes
RADARSAT-2	C-band	2007 -	3 to 100	24	20 x 20 to 500 x 500	Yes
JERS-1	L-band	1992 - 1998	18	44	75 x 75	No
ALOS PALSAR	L-band	2006 -	10 to 100	46	30 x 30 to 350 x 350	Yes
TerraSAR-X	X-band	2007 -	1 to 16	11	10 x 5 to 100 x 1500	Yes
COSMO-SkyMed	X-band	2007-	1 to 100	1 (at best)	10 x 10 to 200 x 2000	Yes

Deformation

The case study aims to demonstrate the capabilities of PSI for detecting, mapping and monitoring the stability of dike networks. Part of the levee along the Juliana Canal was selected to showcase this technology.

The Area Of Interest (AOI) is a 1 km buffer following a 35 km stretch of the levee along the Juliana Canal between Maastricht and Maasgouw in the province of Limburg (Figure 4.6).

Figure 4.6 Case study AOI (red line indicating the Juliana Canal dike, yellow line indicating the Dutch border).

Background image – Google © 2010

51 archive SAR scenes, acquired by the ASAR instrument onboard the European Space Agency's (ESA) Envisat satellite, spanning approximately five years (25th January 2004 to 14th December 2008) were acquired for PSI processing.

Table 4.9 lists the dates of the individual Envisat scenes. Table 4.10 provides an overview of the Envisat SAR data specification. Figure 4.7 shows the temporal distribution of the SAR data acquisitions (almost every 35 days during the full five year period). The spatial extent of chosen SAR scene footprint is show in Figure 4.8.

Table 4.9 SAR image dates

25/01/2004	13/02/2005	05/03/2006	29/04/2007	18/05/2008
29/02/2004	20/03/2005	14/05/2006	03/06/2007	22/06/2008
04/04/2004	24/04/2005	18/06/2006	08/07/2007	27/07/2008
09/05/2004	29/05/2005	23/07/2006	12/08/2007	31/08/2008
13/06/2004	03/07/2005	27/08/2006	16/09/2007	05/10/2008
18/07/2004	07/08/2005	01/10/2006	21/10/2007	09/11/2008
22/08/2004	11/09/2005	05/11/2006	25/11/2007	14/12/2008
26/09/2004	16/10/2005	10/12/2006	30/12/2007	
31/10/2004	20/11/2005	14/01/2007	03/02/2008	
05/12/2004	25/12/2005	18/02/2007	09/03/2008	
09/01/2005	29/01/2006	25/03/2007	13/04/2008	

Table 4.10 Envisat SAR data specification

Mode	Scene Size (km)	Ground cell resolution (m)	Incidence Angle (degrees from nadir)	Orbit	Polarization
Image Mode (IS2)	*100 x 100*	*30*	*19.2 to 26.7 (near to far range)*	*Descending*	*Single*

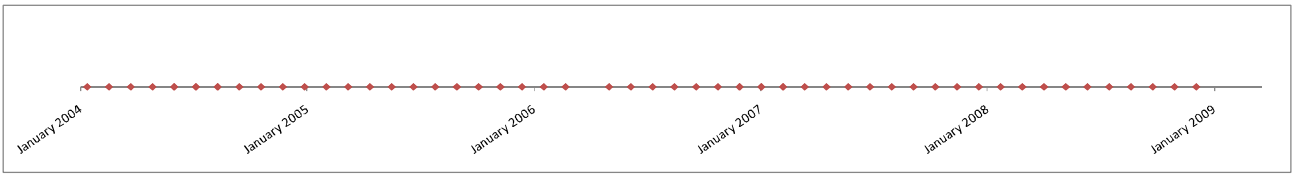

Figure 4.7 Temporal spacing of SAR data.

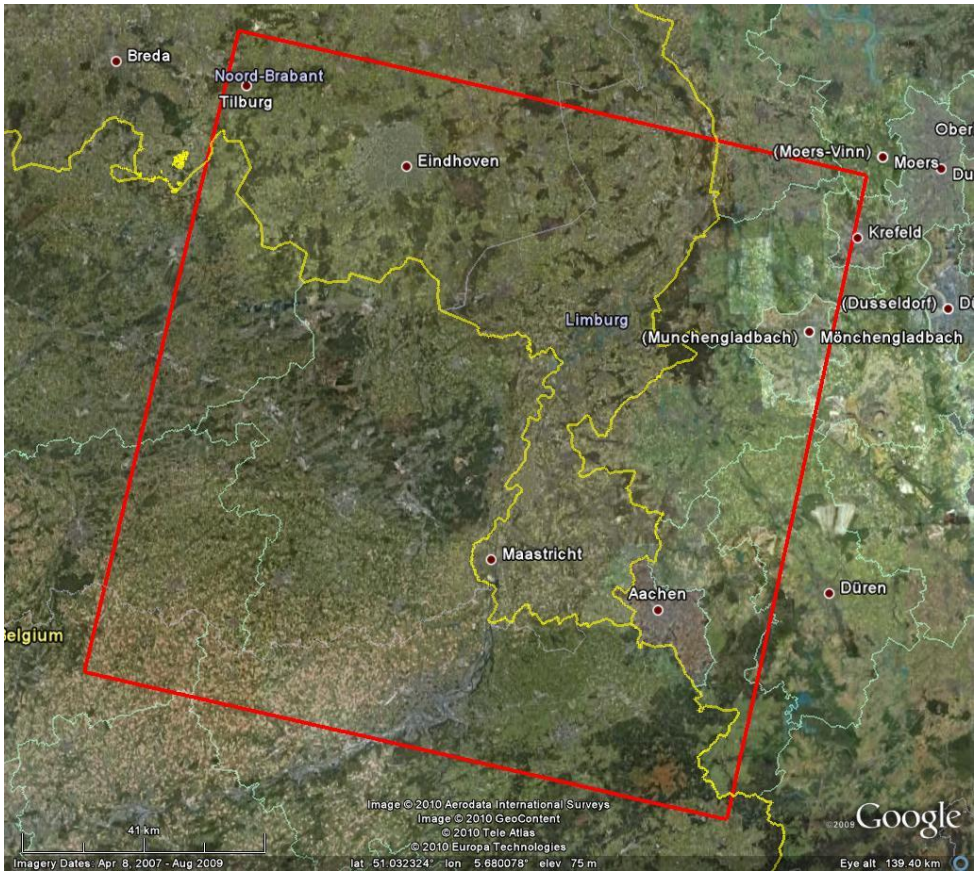

Figure 4.8 Envisat SAR scene footprint.
Background image – Google © 2010

Leakage

For the leakage study, two SAR data sets are used:

1. Same as PSI data set using Differential Interferometry, consisting of 51 archive SAR scenes, acquired by the ASAR instrument onboard the European Space Agency's (ESA) Envisat satellite, spanning approximately five years (25th January 2004 to 14th December 2008)
2. 48 ASAR scenes (both image mode (IMM) and wide swath mode (WSM)) were collected by the ASAR instrument on the Envisat satellite. The scenes span the period from 22nd February 2009 to 7thFebruary 2010. For this application, the incident angle appeared to be of minor influence, so scenes with different incident angles were combined in the analysis. HH polarization data are less affected by vegetation than VV or VH polarized data. Unfortunately, the images for the Netherlands are taken in VV polarization only which is most vulnerable to vegetation effects. The resolution of the SAR images for the leakage study is 150 m. The images are reprojected on the Dutch coordinate system (RD grid)

with a cellsize of 50 meters. This is to be able to compare images from passes with different inclinations of the satellite and to prevent even more resolution loss. This fact has to be taken into account when assessing the values of the pixels.

4.3.3 Available other data for case Juliana Canal

At the Juliana Canal, several ground based techniques were used by Deltares to investigate the hydrological and geomechanical properties. The investigation was funded by RWS. The results are summarized below.

Model analysis of leakage
A geohydrological desk study was performed to derive a simple method to predict the amount of leakage when a hole is made in the hydraulic resistive layers at the sites of planned construction works. The discharge is used to infer the area affected by leakage. Furthermore, the leakage should not exceed the norm of 25 m^3 per second.

The effects of a theoretical hole is analyzed by various 2D and 3D models of varying complexity. Leakage will not be a problem if a loam layer is present below the bottom of the canal. When gravel is present, leakage will be significant. It will lead to raised ground water levels in the vicinity of the leak. However, for short leakage periods the estimated discharge will be lower than the norm.

At the locations of Bunde up to Stein, the expected increase in moisture content due to leakage will be small. The ground level next to the canal is much higher than the groundwater level. At the locations of Urmond, Nattenhoven and Kingbeek, significant leakage will occur in case of a hole. Additional modeling and monitoring during the construction is recommended for these sites.

Ground penetration radar (GPR)
Measurements with GPR were performed on the canal with a 100 MHz antenna and on the embankment next to the water with a 250 MHz antenna (higher resolution, less penetration). The measurements on land were performed on trajectories perpendicular to the length of the canal, from the stone cover at the toe of the levee at the water level up to the crest. Ground-truth was provided by borings. At selected locations, the trajectory was extended to cover the outer side of the levee. The GPR results showed that the levees at the western side of the levees are partially covered by a loam layer at the inner side. The thickness of the loam layer varies between 20-30 cm at the toe of the levee just above the stone cover to 70 cm near the crest. The loam is sandy, with gravel in the lower part. At the outer side of the levee, the loam layer is situated on sand.

At the east side, the levee is lower than on the west side. The levee is difficult to access due to the motorway A2. At two selected locations, the cover on the inner side consists of asphalt on stones (lower part) and a thin loam layer of 12-30 cm thick overlying stones (upper part).

4.3.4 Deformation results for Juliana Canal

PSI processing was successfully applied to the SAR data stack.
Table 4.11 provides an overview of the key characteristics of the result.

The visual overview of the result is presented in Figure 4.9, plotting the average annual motion rate of the PS points across the full area of interest. Figure 4.10, Figure 4.11 and Figure 4.12 provide close-up images of different sections of the Juliana Canal.

The processing yielded a reasonable density of PS points across the area of interest. The majority are located across the towns and villages that the Juliana Canal passes through, although PS points are located directly on the dike walls in some locations. It is clear that the vast majority of the PS point locations coincide with built infrastructure. Regions of the dike that run in parallel with the orbit pass of the satellite have yielded higher PS densities (due to the imaging geometry of the sensor).

Table 4.11 Summary of the PSI data

Date range of analysis		25 January 2004 – 14 December 2008	
Satellite data used		ASAR-Envisat	
Georeference (X,Y) accuracy		10 m	
Reference data used for georeference		Landsat Enhanced Thematic Mapper (ETM+) Band 8 data. Refinement through the use of Satellite optical imagery (Google Earth)	
Projection system used		WGS84 - Geographic	
Area of result (AOI)		72 km^2	
Number of PS identified (AOI)		11741	
Mean PS density (AOI)		163 points per km^2	
Point motion statistics (mm/year motion classes)		***Points in each motion class***	
		Count	**%**
'High downward motion'	**-3.5 and more**	190	1.62
'Moderate downward motion'	**-3.5 to -1.5**	3192	27.2
'Stable'	**-1.5 to +1.5**	5165	44.02
'Moderate upward motion'	**+1.5 to +3.5**	624	5.32
'High upward motion'	**+3.5 and more**	2563	21.84
Regions not covered by InSAR results		Primarily agricultural areas and bodies of water.	
Processing notes		None	

Over the five year period analyzed, approximately 44% of the PS points exhibited minimal motion (average annual motion rates between -1.5 and +1.5 mm/yr), 29% expressed downward movement away from the satellite (average annual motion rates less than -1.5 mm/yr) and 27% expressed upward movement towards the satellite (average annual motion rates greater than +1.5 mm/yr). These figures illustrate that the area of interest is characterized by differential motion between 25th January 2004 and 14th December 2008.

Following the route of levee along the Juliana Canal from south to north, the area of interest is initially characterized by minimal motion, with isolated regions of individual PS exhibiting downward motion. Of most interest is an extensive region of uplift located along a 10 km length of the dike passing through the towns of Stein and Urmond. The maximum average annual motion rate exhibited by PS points across this area is 12.3 mm/yr, and the majority of PS points exhibit motion rates between 4.0 and 8.5 mm/yr. This is possibly linked to the dike failure near Stein at January 27th 2004 and the following reconstruction works. North of Urmond, the area of interest is characterized by general stability and some larger consolidated regions of moderate downward motion between Nattenhoven/Graetheide and Echt.

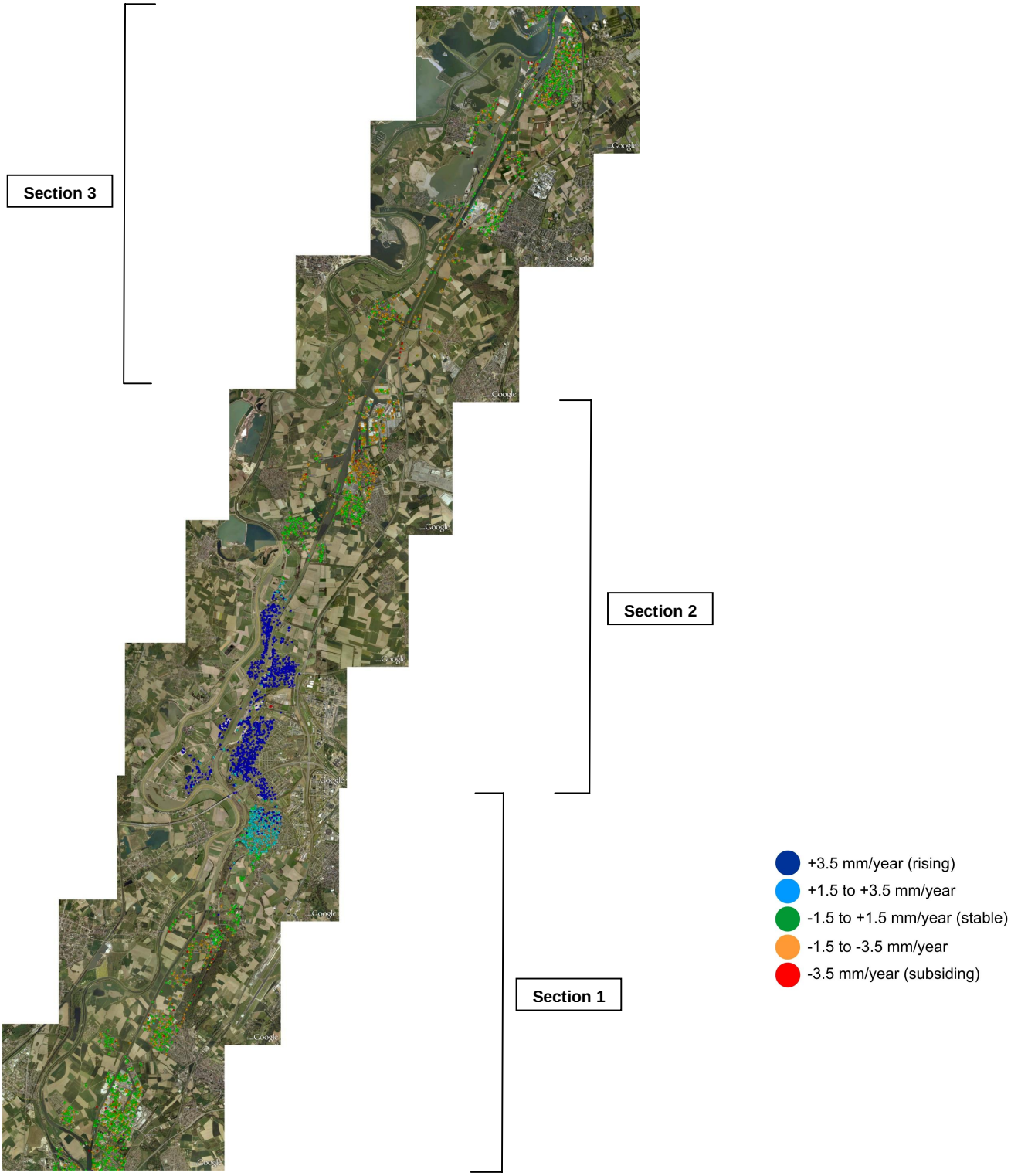

Figure 4.9 PSI result – Average annual motion rate (mm/yr)

Background image – Google © 2010

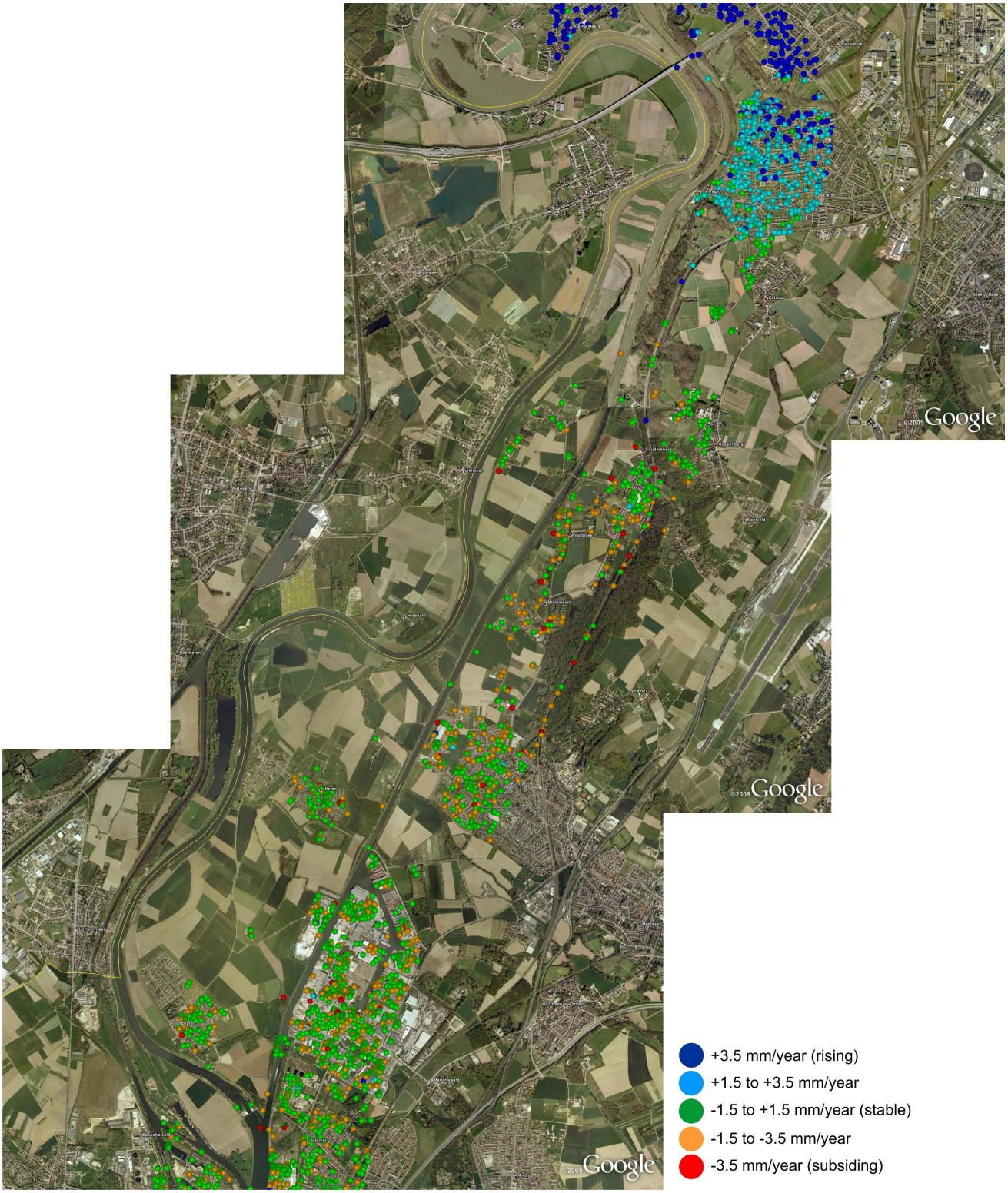

Figure 4.10 PSI result, Section 1 close up – Average annual motion rate (mm/yr)

Background image – Google © 2010

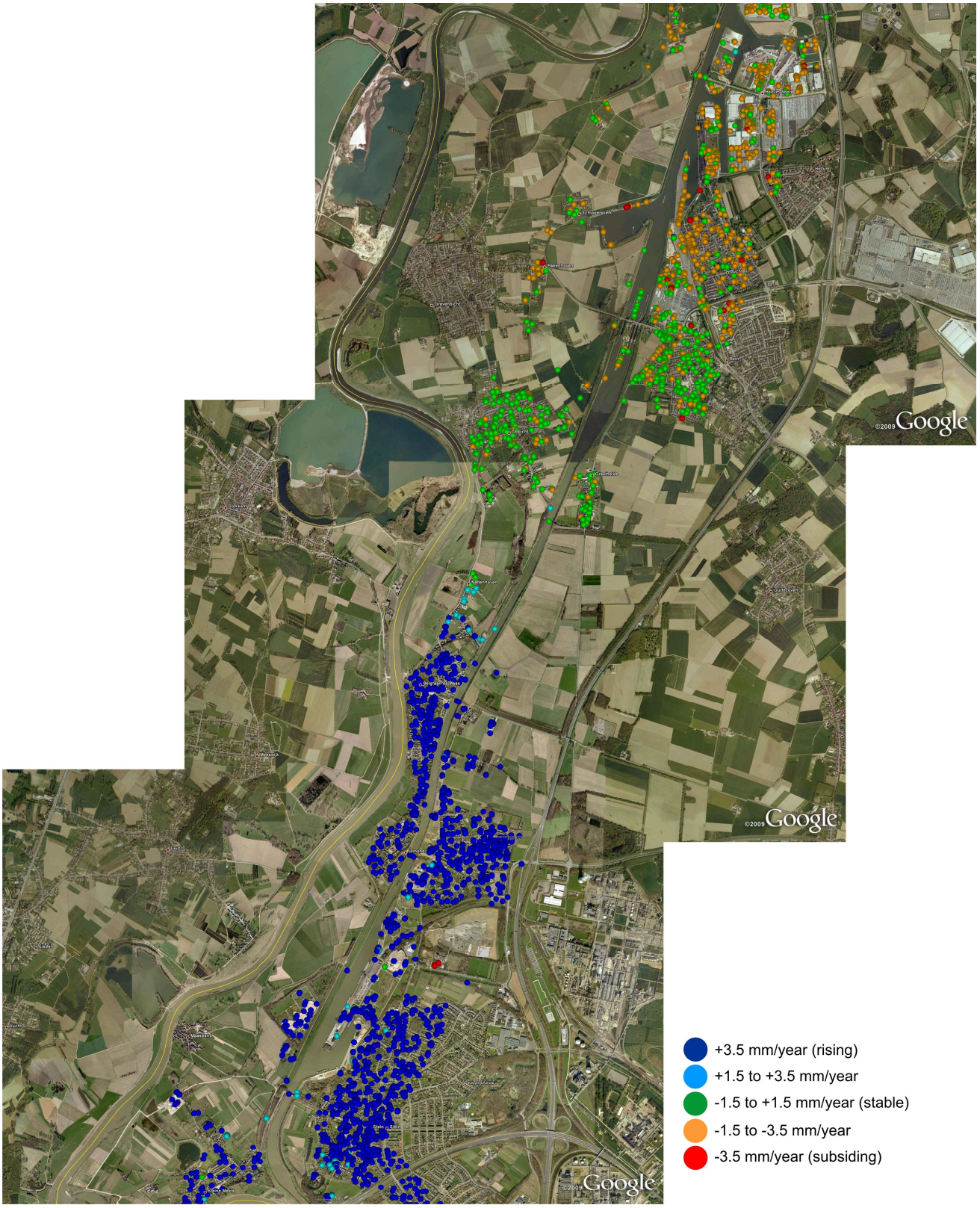

Figure 4.11 PSI result, Section 2 close-up – Average annual motion rate (mm/yr)

Background image – Google © 2010

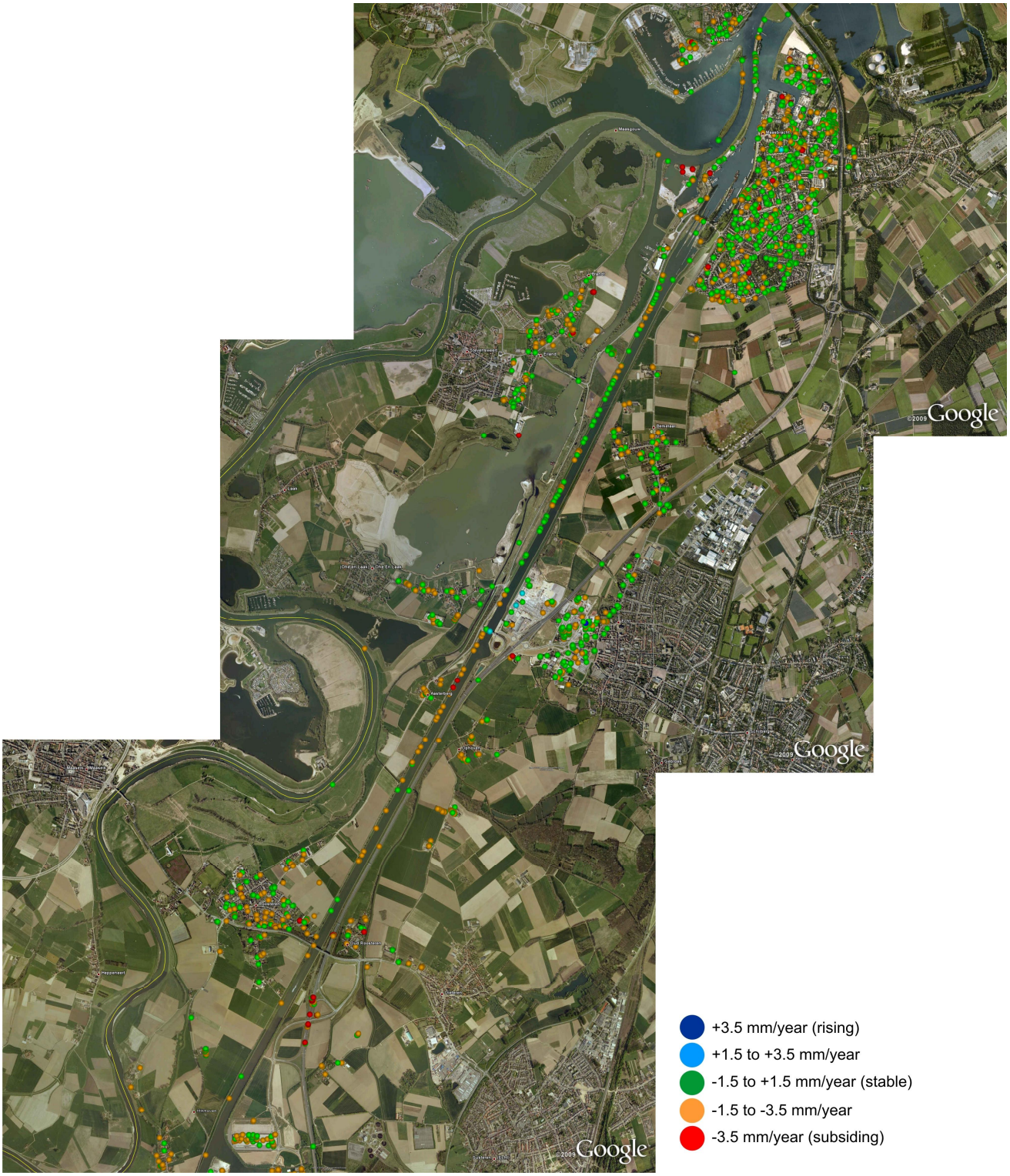

Figure 4.12 PSI result, Section 3 close up – PS average annual motion rate (mm/yr)

Background image – Google © 2010

4.3.5 Leakage results for Juliana Canal

The use of SAR data for leakage by changes in soil moisture content has been investigated in two ways:

1. Use of backscatter, using amplitude information
2. Use of differential interferometry (DifSAR), using phase information

Use of backscatter to study SMC

Images of Envisat's ASAR are used to see whether amplitude changes are caused by soil moisture. The acquired images have a resolution of 150m. The satellite passes the same location about 10 times per month with varying incident angles. Images with identical incident angles are collected with a repeating pattern of 35 days. Three areas near the Juliana Canal have been marked as vulnerable to seepage (Figure 4.13). From north to south the areas are the Kingbeek, a part southwest of Urmond and the western part of Stein. The northern area is covered with trees; the other two areas consist of grassland with some buildings. The northern area covers about 4 original SAR pixels, the middle 45 and the southern area 14.

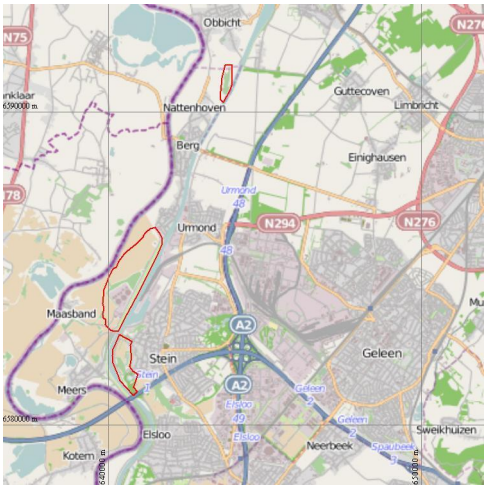

Figure 4.13 Three areas along the Juliana Canal vulnerable to leakage (indicated by red contours)

In Figure 4.14 eight subsequent backscatter images of the study area acquired in 2009 are shown. All images were acquired in a similar orbital pass: the local incidence angle and time of day is the same for all images. Unfortunately, some passes were unavailable, but still these eight images give some insight in annual variation. In general, urban areas give a higher reflection than rural areas, since buildings act as mirrors. Furthermore, rural areas show stronger reflections in winter than in summer. This is can be either a consequence from the annual variation in vegetation or from the annual variation in soil moisture content.

The average backscatter (sigma, on a logarithmic scale) has been determined for each image for the three areas and for a reference forest and reference grassland area. The results are shown in Figure 4.15 for the northern study area consisting of forest and in Figure 4.16 for the two grassland areas. The reference areas are picked in the north of Stein on a safe distance from the channel and with a low groundwater level. From these figures it is concluded that the annual variation is comparable for both grass and forest areas. The canopy of trees is normally too dense to show any signal of the soil, so it is unlikely that the annual variation reflects changes in soil moisture content. The grassland areas however show additional peaks on May 16th, May 22th, June 20th and August 29th. This difference is sufficient to rule out noise as cause since it happens on two independent places simultaneously. Without in-situ measurements, it is impossible to validate these measurements now.

Although the spatial and temporal resolution of ASAR images is theoretically insufficient to detect soil moisture at the required resolution, some anomalies might be related to soil moisture. With the launch of future SAR missions at higher spatial and temporal accuracy, this technique might provide an operational soil moisture detection system in the future.

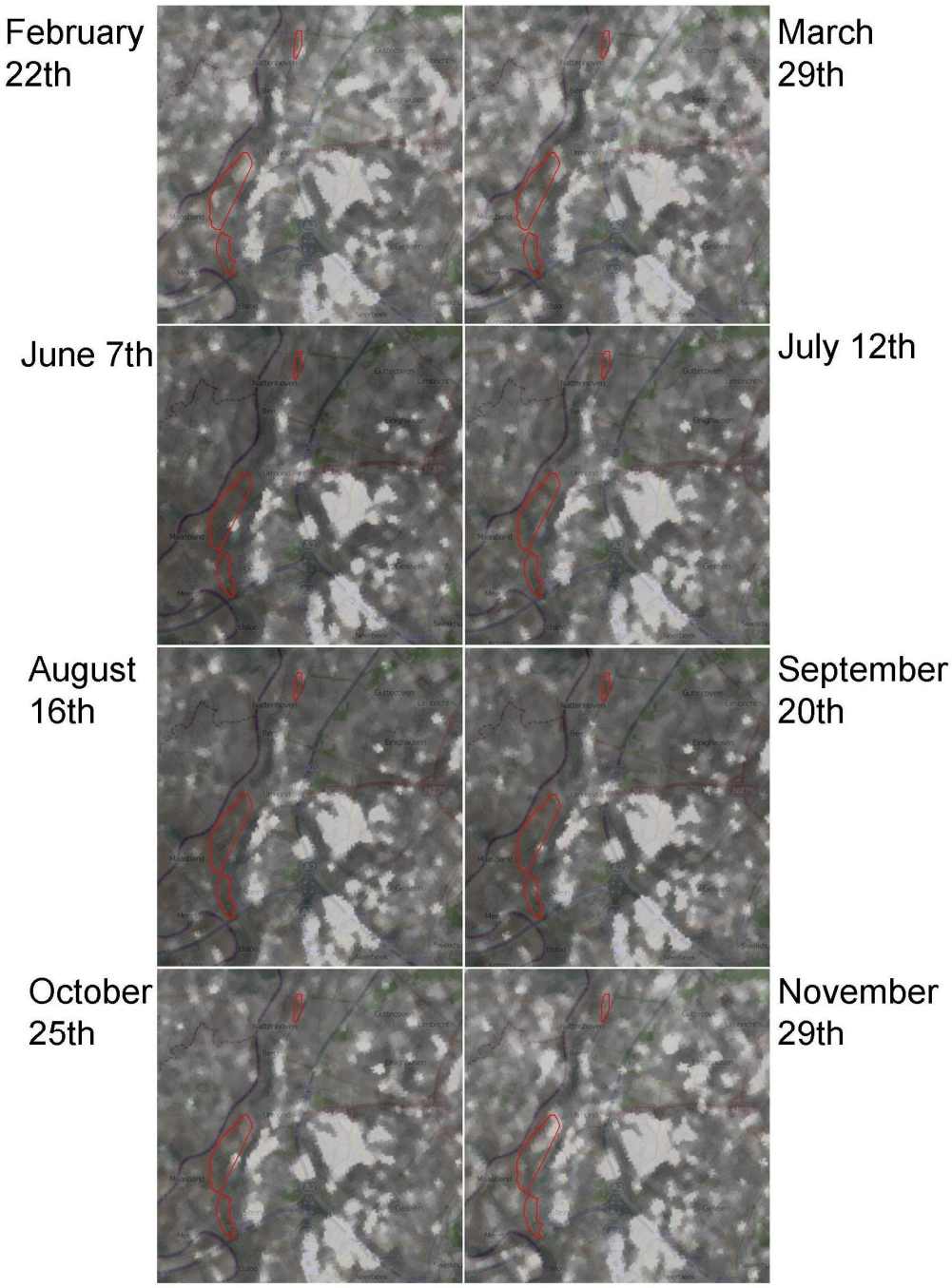

Figure 4.14 8 backscatter images from the ASAR wide swath mode, acquired in 2009. The locations vulnerable to leakage are shown by red contours. The road pattern is shown for reference.

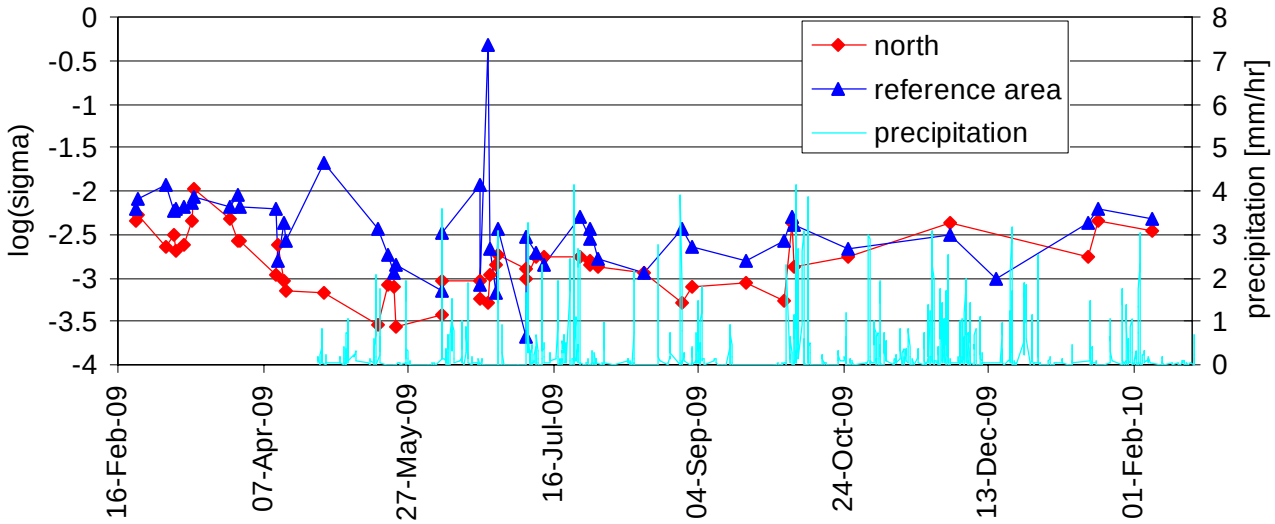

Figure 4.15 SAR backscatter of a forest area (northern study area)

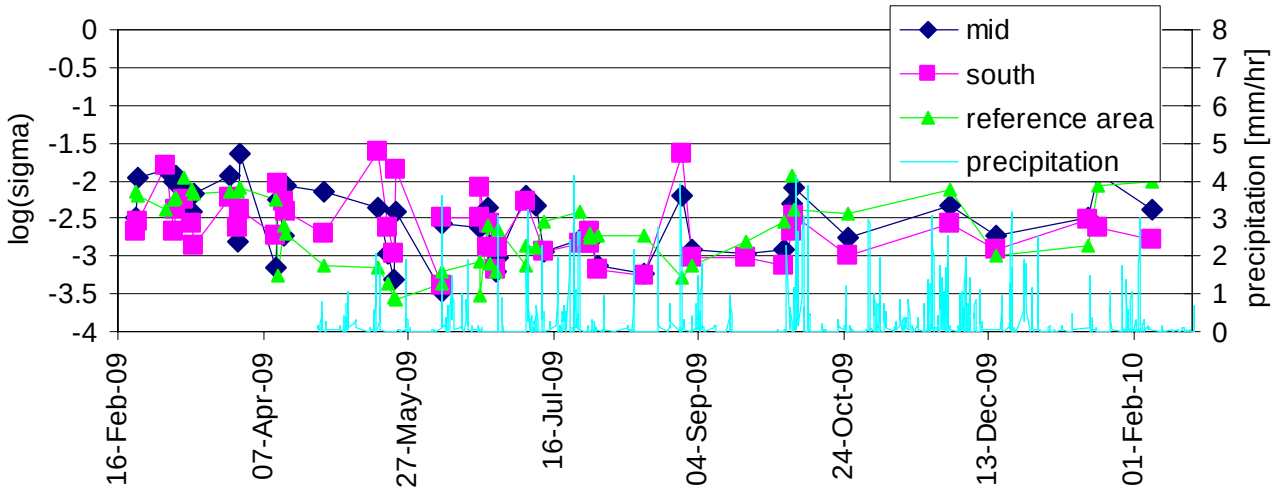

Figure 4.16 SAR backscatter of two grassland areas (middle and south study area)

Use of Differential Interferometry (DifSAR) to study SMC

Some of the SAR results over Juliana Canal were reprocessed as DifSAR results (35 day pairs of SAR images) to assess the variability in phase changes. The footprint and location is shown in Figure 4.17.

In addition to the SAR data, approximate temperature and rainfall (for day of acquisition and the 10 days leading up to acquisition) were collected from the KNMI (Royal Dutch Meteorological Institute) for the closest town to the region of interest. This data was collected from KNMI's online database. With the inclusion of approximate meteorological data we could begin to assess the relationship of soil moisture content and phase change.

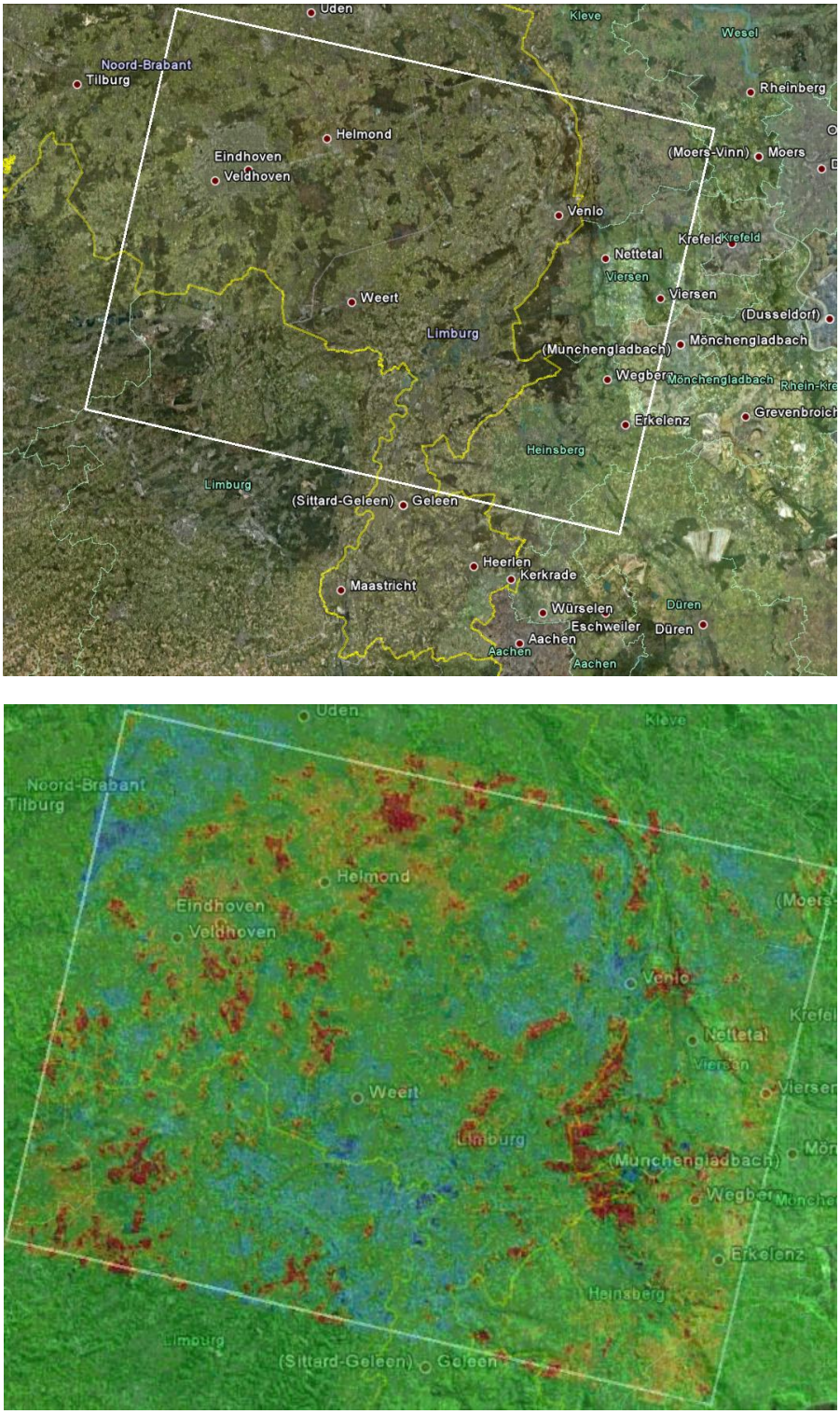

Figure 4.17 **Top: Footprint of DifSAR study over Juliana Canal. Bottom: DifSAR result projected on Google Earth background**

Figure 4.18 shows a sample of consecutive pairs that have been extracted. The relative deformation between three pairs of images is shown: in the left panel the difference between time t2 and t1 and in the right panel the difference between time t3 and t2. The interferogram pairs shown were selected because of the mirroring of the phase pattern. The higher frequency inversions are likely linked to soil moisture changes of the middle image. Based on the analysis of MODIS data, the low spatial frequency changes are probably related to clouds. In summary, these images show high and low spatial frequency changes of which we believe the higher frequency ones (except woodland) are worthy of further investigation if DifSAR is deemed a viable approach.

The results could have been affected by a number of factors such as those proposed by Nolan *et al.,* (2003). The potential effects of these factors are discussed in Table 4.12. On a small number of the pairs small features are seen to change such as wooded areas. However, selected pairs could be accounted for by precipitation patterns and the increase and subsequent decrease in soil moisture. In an attempt to explain this pattern the parameters listed in Table 4.12 were considered but do not appear to provide a clear explanation.

In summary, whilst no detailed precipitation data was available for this area there are some encouraging results that some high spatial frequency effects could be the result of soil moisture. For the higher frequency changes (except woodland) further investigation of DifSAR is deemed a viable approach.

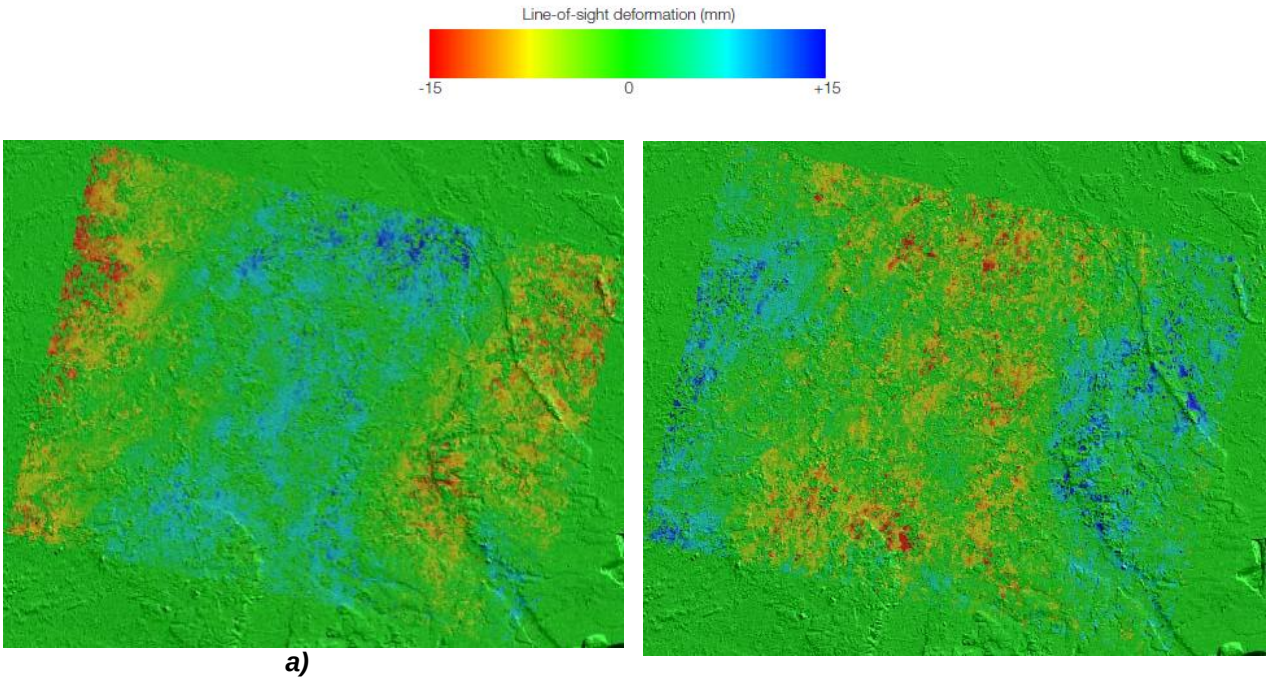

a)

20040613 - 20040718 ***20040718 - 20040822***

R: 15.10 - 45.70 ***T: 13.3 - 19.60*** ***R: 45.70 - 52.90*** ***T: 19.60 - 15.30***

Figure 4.18 Consecutive DifSAR results showing phase variations overlain with SRTM DEM shading. R = Cumulative rainfall in the 10 days leading up to acquisition of slave scene, T = Temperature on each data (^{O}C)

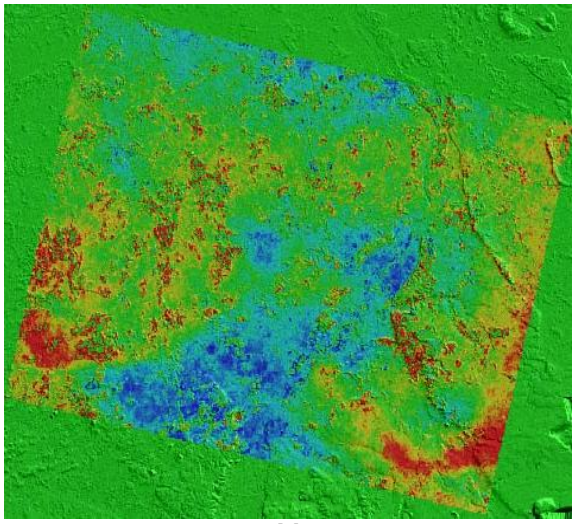

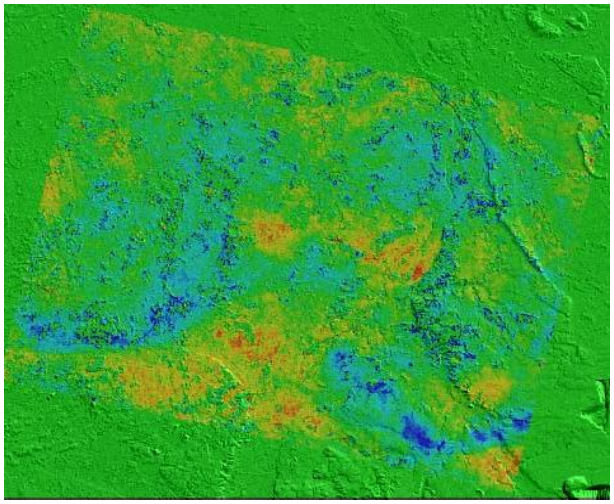

b)

20050109 - 20050213 ***20050213 - 20050320***

R: 8.60 - 48.60 ***T: 7.70 - 2.60*** ***R: 48.60 - 7.90*** ***T: 2.60 - 8.90***

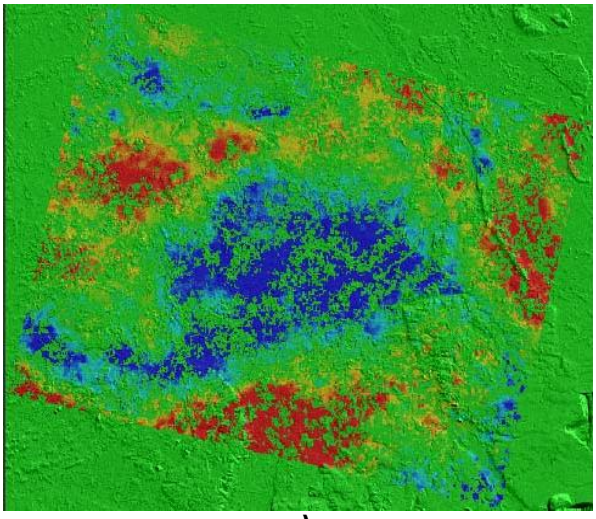

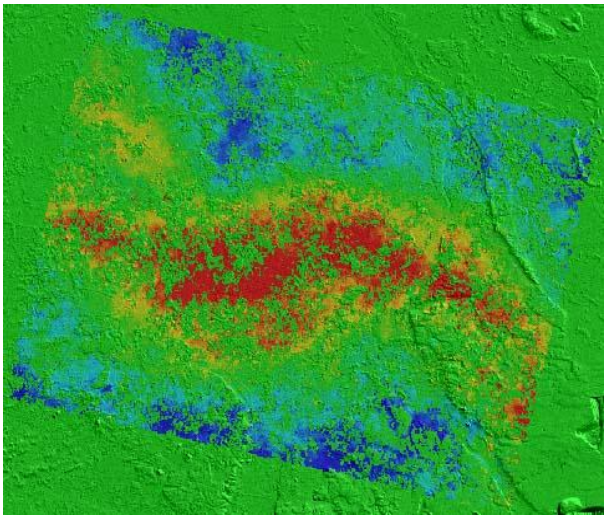

c)

20050807 - 20050911 ***20050911 - 20051016***

R: 39.10 - 2.80 ***T: 12.90 - 17.20*** ***R: 2.80 - 0*** ***T: 17.20 - 12.10***

Figure 4.18, continued Consecutive DifSAR results showing phase variations overlain with SRTM DEM shading. R = Cumulative rainfall in the 10 days leading up to acquisition of slave scene, T = Temperature on each data (^{O}C)

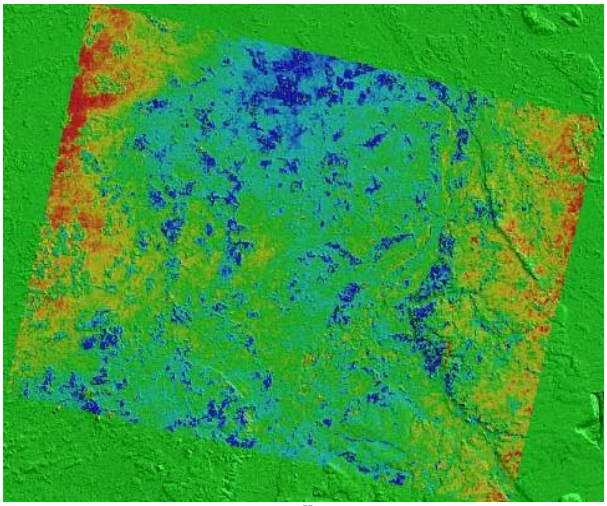

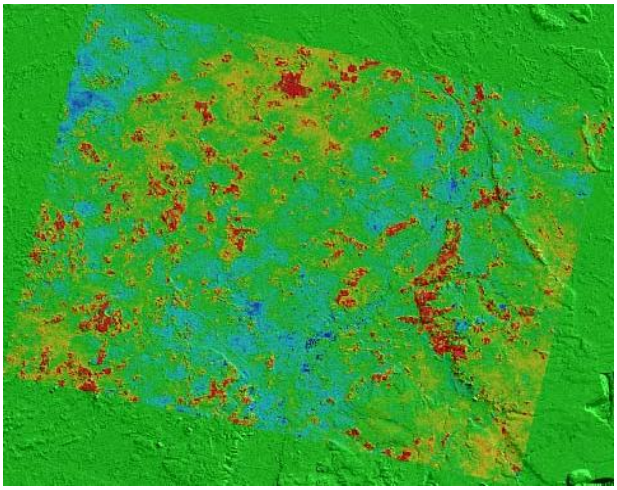

d)

20070114 - 20070218 ***20070218 - 20070325***

R: 31.40 - 30 ***T: 6.90 - 5.30*** ***R:30 - 13.80*** ***T: 5.30 - 8.70***

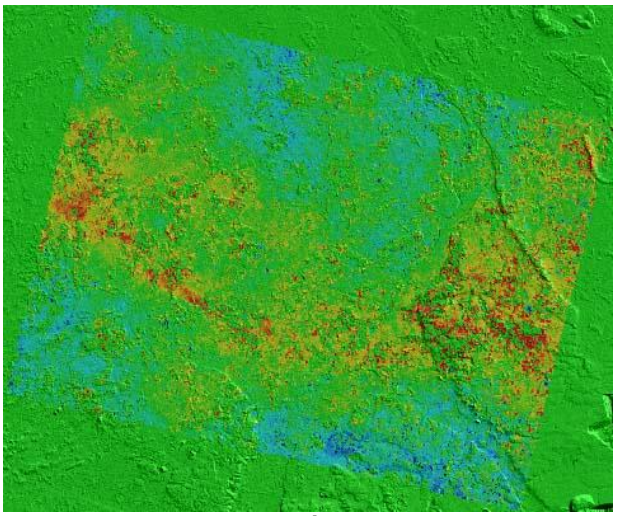

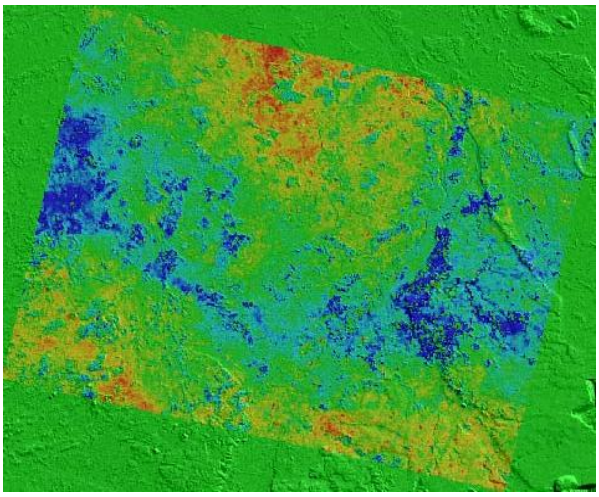

e)

20071021 - 20071125 ***20071125 - 20071230***

R: 4.50 - 19.10 ***T: 6.30 - 10*** ***R: 19.10 - 6.40*** ***T: 10 - 5.40***

Figure 4.18, continued Consecutive DifSAR results showing phase variations overlain with SRTM DEM shading. R = Cumulative rainfall in the 10 days leading up to acquisition of slave scene, T = Temperature on each data (^{O}C))

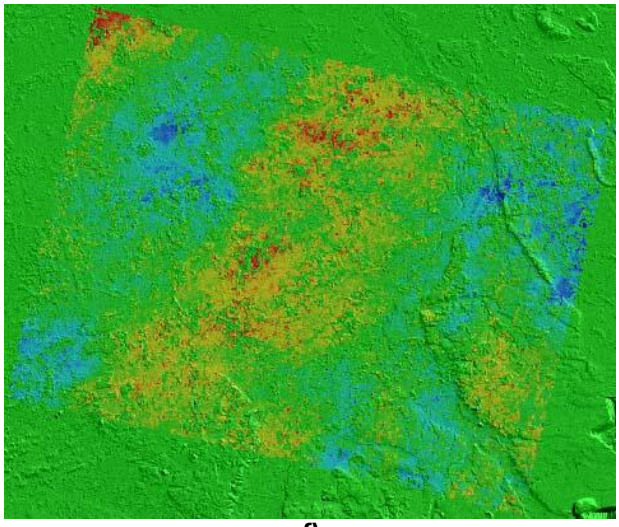

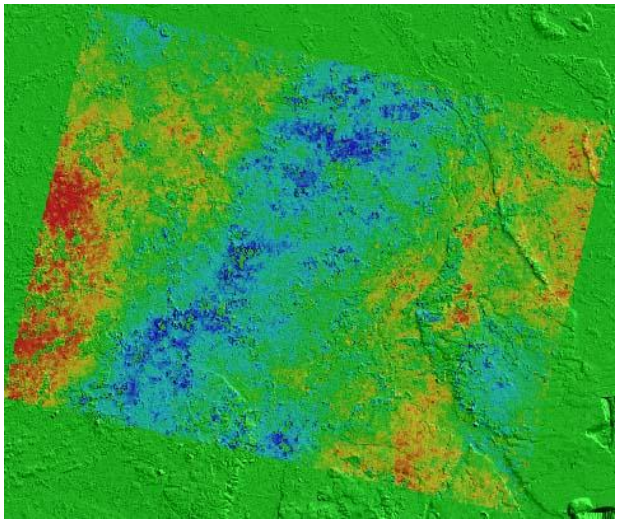

f)

20081005 - 20081109 ***20081109 - 20081214***

R: 51.80 - 13.20 ***T: 11 - 10.30*** ***R: 13.20 - 12*** ***T: 10.30 - 3.10***

Figure 4.18, continued Consecutive DifSAR results showing phase variations overlain with SRTM DEM shading. R = Cumulative rainfall in the 10 days leading up to acquisition of slave scene, T = Temperature on each data (^{O}C)

Table 4.12 Possible sources of phase variation and reasons for ruling out in this instance

Possible source	Effect on DifSAR	Discussion of effects at Juliana Canal
Atmospheric and Ionospheric anomalies	Create smoothly varying patterns of phase change of the amplitudes. The effects tend to be more on large scales e.g. kms or more. However, it has been found that some smaller anomalies could also be possible.	Small land parcels with very abrupt edges have displacement inversion that coincide with the larger inversion features. We would not expect such abrupt phase change at field boundaries if this was due to atmospheric anomalies. However, the larger scale variations across the image do show some correlation with atmospheric conditions/cloud cover as shown in the MODIS imagery for those days, suggesting that atmospheric anomalies could be a source of the larger pattern of phase changes seen.
Topographic residuals	Introduction of apparent features relating to differences between reference DEM and actual elevation of the terrain.	Single DEM was used to correct the data. Topographic residuals do not explain abrupt changes over land parcels. No two pairs with the same (or similar) baseline exhibit the same features suggesting topographic residuals are not causing the phase change.
Wind/Vegetation growth and surface roughness	Common effect causing decorrelation relating to growth or wind induced changes in land cover.	Whilst some of the changes do suggest some decorrelation from vegetation, other changes occur over bare agricultural fields suggesting that this error source doesn't explain the overall variability
Other surface phenomena (e.g. frost/dew)	Frost/dew never documented as DifSAR observable. However, likely that dew could cause decorrelation similar to wet snow.	Frost and dew may have been present on a couple of dates but doesn't explain the variability on the other dates.

4.4 EXPERT SESSION AND DISCUSSION ON THE SUITABILITY OF REMOTE SENSING

Expert session
An expert session was held to discuss the application of satellite InSAR techniques within a flood and coastal subsidence context. The meeting drew together a combination of individuals with expertise in InSAR, geology, geomathematics and geotechnics from organizations including TNO, Deltares, British Geological Survey, Institute of Geomatics (Spain), Lithuanian Geological Survey, Polish Geological Survey, Fugro and TRE Europa. The session reinforced the reported unique capabilities (and limitations) of satellite InSAR approaches, and discussed parallel activities, and potential future activities, that will further develop this technology from a flood and coastal subsidence context.

It highlighted the potential requirement for 'standardization' of services (to some extent at least), the value of integrating services and the importance of educating users in order to ensure that less well known technologies are applied and the results interpreted in an appropriate manner. It was also noted that monitoring requirements will of course vary between locations, however the partially realized potential of satellite InSAR was clearly apparent to all.

Deformation
This PSI case study for deformation successfully demonstrates that satellite InSAR techniques (and datasets) are capable of providing information relevant to assessments of dike integrity, and could form a key component of an integrated dike monitoring and risk assessment program.

The PSI case study has highlighted a number of (possibly) previously unknown ground and structure motion anomalies that impact upon the Juliana Canal region. Conclusions on the implications for dike safety can only made by dike experts (who should consider the PS data in parallel with all other available geo-datasets).

Although PSI will never be able to compete with the spatial and temporal resolution of ground-based assessments, its unique capability of remotely monitoring the long-term stability of very large areas, and large networks of features, makes it a key element of a total solution.

The case study demonstrates not only the capabilities of PSI but also some limitations. Depending upon the surface properties of a target area, InSAR may or may not yield measurements across features of interest. The analysis failed to yield any PS points across large portions of the dike system. If the dike itself is the feature of interest then this could be considered a failure, however the PS points located in the areas proximal to the dike provide a unique insight into local and regional stability. An understanding of regional motion information is likely to greatly enhance the effectiveness of monitoring smaller-scale features or specific locations, and satellite InSAR is ideally placed to provide the required wide-area coverage. InSAR is at its most powerful when combined with other datasets to produce a more complete picture of what is happening. In many cases PSI will be able to provide information on structural stability *and* regional stability; in others it may only be able to provide regional stability information.

Deploying artificial radar reflectors e.g. trihedral Corner Reflectors (CRs, Figure 4.19), across areas of the dike network which lack natural radar reflectors would ensure that suitable targets exist against which future stability measurements could be made.

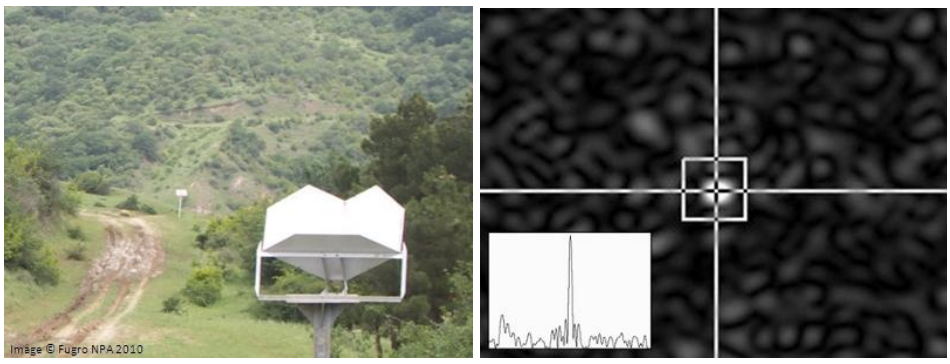

Figure 4.19 CR deployed across a region of low radar clutter, CR response within the SAR data.

The number of PS points along the dike system can also be increased by adjustments in the processing. By using different filters and cut-off thresholds between noise and signal, more PS points can be found.

It is worth bearing in mind that PSI processing of alternative satellite SAR data, for example that acquired by the TerraSAR-X (Figure 4.20) or COMSO-SkyMed satellites, would yield far greater densities of PS points (thousands of PS points per square kilometer in urban areas). However, the compromise is significantly reduced spatial coverage. Similar to the C-band SAR data, this X-band data is however unlikely to yield PS points across the dikes without the addition of CRs.

Figure 4.20 PS density achievable through TerraSAR-X Stripmap PSI processing.

Operational Service & Integration

The recommended operational service model is based upon the generation of 'baseline' PSI ground and structure motion datasets, and subsequent systematic updates to each dataset.

Given the spatial coverage capabilities of satellite SAR, this could be achieved on a national, regional and/or local basis. National and regional datasets could be generated using medium resolution SAR data e.g. RADARSAT-2 standard mode (100 km x 100 km scene footprint, 30 m spatial resolution, 24-day repeats). Local datasets could be generated using high resolution SAR data e.g. TerraSAR-X Stripmap mode (30 km x 50 km, 3 m spatial resolution, 11 day repeats).

The national and regional datasets would cover extensive dike networks, complete flood defence systems and primary sea defences. The local datasets would focus on hotspots, critical sections or specific flood infrastructure e.g. those with known integrity issues where enhanced spatial and temporal sampling is more critical. Networks of CRs should be installed across key features with a shortage of natural radar reflectors to enhance the measurement network.

The choice of relevant SAR satellite missions must tie in with the long-term monitoring requirements of an operational service. Envisat is currently nearing the end of its operational life (from an InSAR perspective), so RADARSAT-2 and TerraSAR-X are considered the best options at present as both have reasonably firm commitments for future continuation missions. In the medium term, ESA's Envisat ASAR replacement mission Sentinel-1, due to be launched in a 2012/13 timeframe, may prove to be the ideal SAR data source for long-term motion monitoring. Owned and operated by ESA, all the data will be made available for free, however the satellite is unlikely to be programmable. Instead it will attempt to acquire as much data as possible, generally using its Wide Swath Interferometric mode with a resolution similar to Envisat (30m) but with a scene footprint of 250km x 250km.

It should be noted that SAR data collection can never be 100% guaranteed and on rare occasions routine maintenance can impact upon data collection. Satellites can also develop hardware or software failures resulting in short, medium or long-term failure. Every effort is made by satellite operators to maintain data continuity but nothing can ever be guaranteed.

The dataset update frequency is flexible but could be on a rolling three, six or twelve-month basis, whereby new SAR data acquisitions are appended to the existing SAR data stack that undergoes processing.

Satellite InSAR is unlikely to ever be able to provide near-real-time motion information, primarily due to the lag time required to generate the precise orbit files that are critical to InSAR (ranging from one to six weeks depending upon the satellite mission), and the estimated time taken to produce and deliver the InSAR dataset from receipt of the SAR data & precise orbit files (typically ranging from four to six weeks). From a non-InSAR perspective, a number of satellite missions are capable of very rapid data delivery, within a few hours of acquisition in fact e.g. COSMO-SkyMed. This capability is valuable for a variety of applications including pollution monitoring, ice characterization and rapid flood mapping, although it should be noted that this capability comes at a premium, e.g. an additional fee of EURO 600 per COSMO-SkyMed scene.

The InSAR datasets could be delivered via an online server directly into an operational monitoring system. Automated post-processing steps could be implemented to 'flag' significant changes in motion characteristics in results e.g. increase/decrease in motion velocities and spatial extents, presence of new motion phenomena. Such observations could raise automatic alerts that could initiate more detailed ground investigations. In addition, automated hard-copy reports and maps with differing levels of information could be generated depending on the user requirements, background and knowledge.

It should also be noted that the extensive archives of SAR data could be utilized for a range of parallel applications including flood inundation mapping.

The decision on appropriate SAR data source, geographic coverage, update frequency etc. is dependent upon multiple factors, not least available budgets, but the inclusion of satellite InSAR datasets will increase the value of a monitoring system by taking advantage of the strengths of multiple, complementary technologies.

Leakage and soil moisture content

The test areas in this project are characterized by arable land that causes soil roughness and vegetation cover to be frequently altering due to tilling and crop growth. In addition, parts of the areas are covered by woodland that has high levels of biomass giving dominant volume scattering. For these reasons, the low resolution SAR amplitude data used in Smulders *et al.,* [2010] was unable to provide reliable SMC estimates. The Sentinel-1 sensor, to be launched in 2012, will be a C-band single and dual polarization (HH, VV or HH/VV, HV) radar system gathering freely available high spatial and temporal coverage data. For the case of the Juliana canal this will be too late, but similar future case studies will gain higher resolution and signal-to-noise ratio, making investigations of this data possible in the near future.

It is suggested that approaches that provide the greatest potential for detection of relative SMC change in such test areas dominated by cultivated arable land will be those that either utilize polarimetric decomposition, to infer relative SMC levels from dielectric change altering scattering properties, or using interferometry to assess relative changes in depth of penetration (phase centre shifts) of different wavelengths due to SMC.

Recommendations for use of SAR data for soil moisture content

- L band data is likely to be more applicable to these areas of interest because of the vegetation coverage, however, for bare fields and vegetation under 0.5kg/m^2 C band could also be used as a viable alternative.
- Eigenbased decomposition has, we feel, the best logic for quantifying soil moisture over this site. These methodologies need more investigation in vegetated areas and we feel that the use of L band, or where this isn't available C band, fully polarimetric data holds the best promise for further investigation at this site.
- The results of the DifSAR investigation over the Juliana Canal are inconclusive and further investigation would be needed. Initial results show that phase centre change does bear some relation to expected effects from soil moisture, but derivation of absolute values is difficult and other atmospheric and surface factors might be irresolvable.
- Another consideration could be the use of L band DifSAR by means of comparison with C band data over this area

Although the spatial and temporal resolution of ASAR images is theoretically insufficient to detect soil moisture at the required resolution, some anomalies might be related to soil moisture. With the launch of future SAR missions at higher spatial and temporal accuracy, this technique might provide an operational soil moisture detection system in the future.

5 MONITORING IN A SMART LEVEE

5.1 INTRODUCTION

In recent years, several initiatives have started regarding smart levees. During these pilot projects specific concepts of smart levees were researched, but are not yet feasible for commercial, large scale use. The results of subgoal 1 are described in the report “Feasibility study of smart levees concepts” [FC 2010]. The focus of that report is on the technical feasibility of smart levee concepts to step up from pilot to real life projects for day-to-day use. In this report, the monitoring of a smart levee is described.

A smart levee is defined as:

> A Smart Levee provides intelligence about its past, current and expected condition to its end users to make informed decision to maintain demanded flood protection levels.

In §5.2 the types of levees which can be smart are described. The monitoring techniques are summarized in §5.3. Monitoring plans are presented in §5.4.

5.2 TYPES OF LEVEES

Recently an international initiative has started to consolidate the best practices in levee management into an International Levee Handbook. One of the first tasks this group has done is to provide an international definition of a levee. We will use the definition they have developed.

> Levees are raised, predominantly earth, structures (sometimes called embankments or dykes) whose primary objective is to provide protection against fluvial and coastal flood events along coasts, rivers and artificial waterways that are not reshaped under normal conditions by the action of waves and currents.
>
> Levees form part of flood defence systems that may also include flood walls, pumping stations, gates, closure structures, natural features etc.

The work on the International Levee Handbook will progress until 2014 and might influence the definition of smart levee management. It is therefore advised to monitor this work and re-examine the definitions provided in this document at the end of the Flood Control 2015 program.

The principal objective of the International Levee Handbook is to provide a comprehensive and definitive guide to set out good practice in the evaluation, design, implementation, maintenance and management of levees (including guidance on site investigation).

5.3 TECHNIQUES

An overview of techniques and their suitability for monitoring from a technical point of view is shown in Table 5.1. In this table, the monitoring system, what it measures and how is it related to some levee failure mechanisms and corresponding models is shown. A description of the techniques can be found in Appendix 8 : . It should be noted that there are many more potential failure mechanisms for levees. Though not relevant for all levees (like the failure mechanisms (landside) slope instability, backward piping erosion and (wave or steady state) overtopping mentioned in the table), to name a few: landside toe liquefaction, waterside toe instability, static liquefaction, suffosion, horizontal instability due to draught (of peat levees), uplift instability and sink holes.

Measured parameters

The value of the measured parameters depends on the failure mechanism at hand, for instance backward piping erosion. When dividing techniques by parameter, they can essentially be divided in two groups; e.g. methods that measure the flow of fluid (direct and indirect) and methods that measure pore pressure (or a proxy of pore pressure, such as hydraulic head level). Pore pressure measurements in itself can not give information about water flow or water flow direction, but when pore pressure devices are placed in an array, it is possible to monitor the pore pressure through time and in more spatial dimensions. Herewith this technology can indicate flow of water.

The actual flow measurements can be direct methods or indirect. Direct flow methods measure flow quantatively, using an embedded flow meter (a propeller shaped flow sensor) for instance; the measurement parameter is flow. A disadvantage of such methods is that these devices have to be inserted into the embankment's body: that is more expensive and the internal structure will be modified by the needed penetration. Also, the fact that the device can get clogged by clay particles over time, after which cleaning or replacement is needed is disadvantage. For long term monitoring, sensors without moving objects would be ideal. Indirect flow methods are methods that measure other parameters than flow. Especially temperature and pressure distribution measurements seem to show promising results in monitoring embankment failure due to piping [Koelewijn et al., 2010].

When values for critical subsurface pore pressures for piping in embankments are known, pore pressure measurements can be effective in monitoring dike failure due to piping. Pore pressure measurements can be also be direct and indirect. Direct pore pressure measurements involve pore pressure devices embedded in the embankment's body and measure the pressure in situ. Indirect pore pressure methods can involve water content measurements or hydraulic head measurements from which in situ pore pressure can be derived by calculating water column weight.

Invasive versus non-invasive data acquisition

Many of the 'continuous' geophysical methods are non-invasive, their sensors are located on the surface and do not need to be implemented inside the embankment. This has several advantages over methods where embankment penetration is needed, invasive methods: installation as well as maintenance on the surface is much easier than installation and maintenance in the subsurface; and invasive techniques might for instance interfere with the piping process. The main disadvantage of non-invasive techniques is that the measurements are, in general, not made at or even near to the part of the soil volume where the failure mechanism starts to develop, especially in case of uplift induced slope instability, 'regular' slope instability, sink holes, static liquefaction and, to some extent, backward piping erosion.

Sensor spacing and spatial resolution

Another way to classify monitoring technologies is by sensor spacing, also referred to spatial resolution; is the resulting data discrete or continuous data (in space) and what is the distance between measurements? For

Table 5.1 Overview of levee monitoring techniques [based on Marnette, 2010]

Monitoring system	**Properties**						
	Measured parameter	**I**nvasive or **N**on-invasive	Internal structure disturbance **N**one, **M**edium, **S**evere	Influence zone of parameter **S**mall, **M**edium, **L**arge	Measurement **P**oint, **L**ine or **A**rea	Useful for Slope instability, backward **P**iping erosion or **O**vertopping	**R**eady to use **S**hort term or **L**ong term deployment
Piezometer	Pressure	I	M	S	P	S,P,O	R
Fiberoptics	Temperature	I	S	M	L	P,O	R
Fiberoptics	Deformation	I	S	M	L	S,P (O?)	R/S
Mems	Pressure	I	M	S	P	S,P,O	R
Mems	Temperature	I	M	S	P	P,O	R
Mems	Tilt	I	M	S	P	S	R
Mems	Inclination	I	M	M	L	S	R
SP	Self potential	N	N	M	P	P	S
IP	Dielectric	N	N	M	A	S,P	S/L
TDR	Dielectric	I	M	S	P	S,P	S/L
GPR	Dielectric	N	N	S	A	P	S/L
Internal flow meter	Water flow	I	S	S	P	P	L
Remote imaging	Visible/infrared light	N	N	M/L	A	S,P,O	S
Satellite imaging	Deformation	N	N	L	A	S,O	S/L
Satellite imaging	Soil moisture	N	N	L	A	P,O	S/L
GPS deformation	Deformation	N	N	M/L	P/A	S	S
Color tracers	Water flow	N	N	M	P/L/A	P	S
ERT	Dielectric	N	N	S	A	S,P	S/L
Electro-seismic	Dielectric & acoustic	N	N	M	A	S,P	S/L
Capacitive Resistivety	Dielectric	N	N	M	A	S,P	S/L
Microgravity	Density	N	N	S	A	S,P	L
Passive Microwave	microwaves	N	N	L	A	P	L

example, during dam failure due to piping, the fluid flow accelerates along the path of least resistance, making piping a very localized phenomenon, in the order of up to a few decimeters wide. When sensor spacing is too large in a discrete monitoring technology, the occurrence of piping may be missed, so failure due to piping may occur without detection. So, either the sensor spacing must be sufficiently small, or a continuous monitoring technique should be applied. Continuous monitoring technologies measure a parameter between two sensors, using geophysical phenomena, such as electrical or acoustical methods. The difference with ordinary technologies is that these geophysical methods sample its parameter over the full distance between two sensors. The resulting data is a signature of the mean value over the full sensor spacing of the parameter. When using data from between several sensors (in an array for instance), information can be extracted from the data with a higher resolution than with discrete measurements in comparable sensor spacing.

Another relevant issue is the localization. Is it important to be able to localize weaker areas within meters, or is it enough if a monitoring system can tell the user in which 100 m segment the failure threat level is raised? If it is chosen to monitor levees in large sections, mobile devices can be used for closer inspection for instance, reducing installation costs for the permanent monitoring system.

Temporal resolution and interpolation

Resolution can not only be defined in space, but in the case of monitoring, also in time. There is a choice of time scales in which monitoring can be done. The needed temporal resolution depends on the time scale at which the phenomenon that is to be measured occurs. Other considerations are: data storage limitations, computer power for data analysis (for larger data sets, data analysis takes longer), how important remediation measures are and in which time frame we need to take those measures.

Another consideration is whether or not it is useful to transiently adjust the measurement frequency: in periods of higher risk of vulnerabilities, during storms or high water for instance, it might be very useful to increase the measurement frequency, so more data will be gathered and better information about vulnerabilities can be given to the local authorities.

Although, in theory, it does not seem hard to calibrate timing of measurements from different monitoring techniques, the IJkdijk experiments showed that in practice it is not easy to get the timing right. This issue can be solved by using TimelineStore (§3.3) As an alternative, resampling data sets is possible, if sampling rates are high enough. Especially in cases, that it turns out that a correlation of two different data sets provides best information for failure prediction, different sampling rates and sample timings can be an issue.

When sampling rates are low, interpolation can predict values between periodic sampling. An important question is: what type of interpolation should be used when trying to predict levee failure? One could think of constant (last sampled value), linear, exponential, weighted functions etc.

Discrete data (point measurements) versus spatially continuous data (area measurements)

Monitoring systems can be distinguished based on whether they measure in discrete measurement points or spatially continuous data. Discrete measurements give data that represent the parameter sampled at exactly at the sampling location (think of a groundwater sample that is tested for dissolved metals for instance). Continuous data is generated by geophysical techniques that measure its parameter over a larger distance. The measured data represents the parameter, but over a larger distance (between sensors, between sensor and reference sensor or between source and receiver in seismic surveys).

One of the main reference parameters is pore pressure. Pressure essentially is a discrete parameter, but a relevant question is: what is the region of influence of a local pressure anomaly? Or more practical: how far away from the source of a pressure anomaly can this pressure difference still be measured? The IJkdijk piping experiments showed that pressure changes related to the initial phases of the failure mechanism could be discerned by pore pressure meters at a distance of up to two meters (either horizontal or vertical) in the sand layer. When (erroneously) placed in the clay layer the measurements were useless. The same holds for heat/temperature. Heat diffuses and a heat anomaly causes the surroundings to change temperature. What is the influence region of temperature anomalies? So these parameters are not strictly discrete.

Continuous parameters include electro and electromagnetic as well as acoustic data. Examples are electric resistivity tomography, self-potential and (active and passive) seismic data. The parameter is influenced along the distance between the sensors and the resulting data gives sort of an average value over this distance. Using smart data processing techniques, spatial information about this parameter can be obtained.

Spatial interpolation versus inversion

Whatever the parameter, the type of measurement equipment or resolution is, a data acquisition system measures data at discrete points: data is collected at the measurement points or at the resolution of the image (with instruments such as infrared cameras or satellite images). To get information about the parameter at locations where no measurement was taken, two things can be done: interpolation or inversion. Interpolation can be used with all data types and parameters, but inversion depends on the measuring technique. Different interpolation schemes (such as linear or quadratic) can be used. Interpolation estimates what the value between two discrete point measurements will be, according to the used interpolation scheme. Geophysical techniques, such as ground penetrating radar, seismic acoustics or electric methods measure their parameter between a transmitter and a receiver (an active system) or between a sensor and a reference sensor, such as the self-potential method (a passive system). This means that the resulting signal gives information about the measured parameter over the whole travel path of the, in this example, seismic or electromagnetic wave. Signals with travel paths that intersect both contain information about the intersection region. Inversion basically organizes and combines the information from several travel paths. The ultimate goal of inversion is to create the model that fits the data in the best possible way. The resulting image after

inversion shows more information than the an image of the original data. Furthermore, using inversion, one is able to extract information about the parameter at different depth levels and thus make a three dimensional image acquired with a two dimensional grid of sensors.

5.4 MONITORING PLANS

With the present state of the art, it appears that for each different levee a specific monitoring plan needs to be devised. This should start at determining the relevant failure mechanisms. Each mechanism should be addressed by a suitable monitoring plan. This may include in-situ instrumentation, or remote sensing, human inspection or even nothing at all, if any relevant data cannot be acquired or, on acquisition, time to take any action will be lacking. In the latter case, structural measures will be required to rule out that failure mechanism from happening.

Re-use of a monitoring plan for one levee at another levee should be done with care; only if conditions are well comparable (including subsoil composition and hydraulic conditions, to name but a few variables) this can be a sensible option.

Bearing this in mind, it will be impossible to present general schemes or tables showing the precise (or even indicative) amount of instrumentation to be applied for different failure mechanisms. For a specific levee Table 5.2 indicates some specifications of a suitable monitoring plan. This is for the Buitendijk along the South-East of the Dordrecht Isle near Rotterdam, a 4.5 km long levee. Because of the local situation, for piping a longer stretch needs to be monitored. More information on this site is given in Section 5.4 of “Feasibility study of smart levees concepts”, while several other examples of monitoring plans are presented in Section 3.5 of “Feasibility study of smart levees concepts”.

Table 5.2 Example of a summary table of a site-specific monitoring plan

Failure mechanism	Piping	Stability	Overtopping
Sensor system	fibre optics + piezometer	piezometer	visual inspection (once in fall and during severe SE to SW storm conditions)
Parameter	temperature + pore pressure	pore pressure	severity of overtopping and damage
Range of influence for each sensor	1 resp. 2 meters (2 m required)	1 – 10 meters	depends on weather
Accuracy	0.05 K resp. 0.02 kPa	0.1 kPa	Rough
Measurement frequency	5 min maximum during flood conditions	10 min maximum during flood conditions, otherwise once every hour	every half hour
Expected lifespan of sensor system	50+ years resp. 5-10 years	5-10 years	Sufficient
Amount of sensors needed	2x 5.5 km fibre optics + one piezometer every 200 m along 4.5 km + 2 extra = 11 km fibre + 25 piezometers	only relevant along a 1.3 km part of this levee, cross-section with 3 instruments every 30 meters, use can be made of piping piezometers => approx. 120 piezometers	two persons (together, for 4.5 km)
Costs per unit length along a levee	To be determined	To be determined	To be determined

6 CONCLUSIONS AND RECOMMENDATIONS

6.1 CONCLUSIONS

The general goal of the 2010 Flood Control project “Monitoring of a Smart Levee” (2010.02) is to define a framework for Smart Levees, including the development of new models for levee safety monitoring and underlying IT infrastructure.

The general goal can be subdivided into four subgoals, which are:
1. Define technical feasibility of Smart Levee concept. (separate report)
2. Model development based on IJkdijk experiments and LiveDijk Eemshaven (chapter 2 and 3)
3. Real time levee monitoring with improvement of robustness (chapter 3).
4. Develop remote sensing levee monitoring techniques (chapter 4).

The conclusions for the subgoals 2, 3 and 4 are summarized below.

Model development based on IJkdijk experiments and LiveDijk Eemshaven
Slope stability
For slope stability, both movements and pore pressures are key parameters. Humidity, soil moisture content, temperature and vibrations are not relevant for this type of failure mechanism.

The models discussed for slope stability are:
> Analytical model [Bourges and Mieussens, 1979] which is not suitable for levees.
> FEM which is not suitable (yet), still academic research level.
> Time series analysis: this approach was applied to the Livedijk Eemshaven data where no extreme conditions were found during the analyzed period. The analysis need to be expanded to extreme conditions such as storms to be able to give valid predictions under these circumstances.
> Use of observations (tilt) to improve slope stability calculation using Mstab.
> Statistical analysis of sensor data from field scale levee on subset of data only.

Piping
For piping, the key parameters are pore pressure and discharge. Self Potential, temperature and sand volume are potentially useful parameters.

The models discussed for piping IJkdijk data are:
> Adjusted 2D model to link pipe length to discharge, head drop and sand volume. The results are good for head drop and discharge. The pipe lengths from sand volumes could not be predicted correctly in these cases because of poor sand volume measurements.
> Possible use of SP and/or temperature to distribute discharge along levee. This is complex and no new models were developed.

Real time levee monitoring with improvement of robustness
In order to gain real time information a TimelineStore is developed and implemented. This is a necessary technical data retrieval interface (application-to-application interface) to be able to do multiple sensor analysis and time series analysis. Timelines are based on potential high available, high scalable, geodistributed database technology (Cassandra).

In the future, when large numbers of sensors might be installed, a pre-analysis technique is useful before heavy computational models are put to work. Two successful pre-analysis techniques are developed:
> A technical system: sample rate changeability sensor for detecting missing samples.
> Value of the signal: number of dominant frequencies.

These trend spotting techniques are very useful to detect anomalies without the need of having in-depth knowledge of the levee and its build-up.

The Multi Touch table offers an interactive way to browse the TimelineStore. The operations on sensor data, performed on the table, rely strongly on the timeline functionality.

Develop remote sensing levee monitoring techniques

Satellites
The choice of relevant SAR satellite missions must tie in with the long-term monitoring requirements of an operational service. Envisat is currently nearing the end of its operational life (from an InSAR perspective), so RADARSAT-2 and TerraSAR-X are considered the best options at present as both have reasonably firm commitments for future continuation missions. In the medium term, ESA's Envisat ASAR replacement mission Sentinel-1, due to be launched in a 2012/13 timeframe, may prove to be the ideal SAR data source for long-term motion monitoring.

Deformation
This PSI case study for deformation successfully demonstrates that satellite InSAR techniques (and datasets) are capable of providing information relevant to assessments of dike integrity, and could form a key component of an integrated dike monitoring and risk assessment program.

Despite the fact that not enough relevant scatterers where available for all locations, the PSI case study has highlighted a number of (possibly) previously unknown ground and structure motion anomalies that impact upon the Juliana Canal region.

Although PSI will never be able to compete with the spatial and temporal resolution of ground-based assessments, its unique capability of remotely monitoring the long-term stability of very large areas, and large networks of features, makes it a key element of a total solution.

Leakage and soil moisture content
Detecting leakage, 3 possible approaches are available:
- Use of backscatter (Amplitude information) from ASAR: Although the spatial and temporal resolution of ASAR images is theoretically insufficient to detect soil moisture at the required resolution, some detected anomalies might be related to soil moisture variations. With the launch of future SAR missions at higher spatial and temporal accuracy, this technique might provide an operational soil moisture detection system in the future.
- Multipolarisation: data were not available for this site.
- Differential Interferometry based on phase centre shifts: encouraging results that some high spatial frequency effects could be the result of soil moisture.

6.2 RECOMMENDATIONS

Based on the research, the following recommendations for subgoals 2, 3 and 4 are made:

Model development based on IJkdijk experiments and LiveDijk Eemshaven
- Statistical analysis on sensor data (IJkdijk or Bregambacht) combined with physical knowledge.
- Time dependent behavior of pore pressures at changing water conditions for slope stability and piping.
- For the piping, process a generalization of approach to all levees in the Netherlands using artificial neural networks.
- Implementation op SP and temperature in a more detailed piping modeling.

Real time levee monitoring with improvement of robustness
- Further investigation of the use of FFT analysis for the detection of sensor malfunction (e.g. the number of contributing frequencies)
- Multi sensor trendspotting: correlation between sensors; sensor values could be judged be correcting them with other sensor values.
- TimeLineStore: implementation of the concept of forking timelines in order to do simulation and investigation of all the capabilities of the Cassandra database for the use of dike monitoring.

Remote sensing levee monitoring techniques

Deformation

- Recovery of more PS points by advanced PSI processing.
- Use of different satellites, such as high resolution Terrasar-X to improve the number of PS points.
- The technique provides a useful means to monitor levee deformation. However, due to revisit times and the delay between data collection and availability of precise orbit information, the monitoring will be near real-time at best.

Leakage and soil moisture content

- L band data is likely to be more applicable to these areas of interest because of the vegetation coverage. For bare fields and vegetation under 0.5kg/m^2, however, C band could also be used as a viable alternative.
- Eigenbased decomposition has the best logic for quantifying soil moisture over this site. Fully polarimetric data hold the most promise for further investigation at this site with vegetated areas. L band data is preferred, but C band might also be useful when L band data is not available.
- The results of the DifSAR investigation over the Juliana Canal are inconclusive and further investigation would be needed. Initial results show that phase centre change does bear some relation to expected effects from soil moisture, but derivation of absolute values is difficult and other atmospheric and surface factors might be irresolvable.
- Use of L band DifSAR by means of comparison with C band data over this area.
- With the launch of future SAR missions at higher spatial and temporal accuracy, the DiFSAR technique might provide an operational soil moisture detection system in the future.

The Sentinel-1 sensor, to be launched in 2012, will be a C-band HH radar system gathering freely available high spatial and temporal coverage data. For the case of the Juliana Canal this will be too late, but similar future case studies will gain higher resolution and signal-to-noise ratio, making investigations of this data possible in the near future.

APPENDIX 1 : REFERENCES

APPENDIX 2 : PARAMETERS FOR STABILITY

APPENDIX 3 : PARAMETERS FOR PIPING

APPENDIX 4 : STATISTICAL ANALYSIS REPORT

APPENDIX 5 : PIPING – SELLMEIJER RULE

APPENDIX 6 : REMOTE SENSING TECHNIQUES – SAR AND INSAR

APPENDIX 7 : REVIEW OF APPROACHES FOR SMC RETRIEVAL FROM SATELLITE DATA

APPENDIX 8 : DESCRIPTION OF MONITORING TECHNIQUES

APPENDIX 9 : INTERPOLATION AND TIMELINES

APPENDIX 10 : COLUMN BASED DATABASE

APPENDIX 11 : TIMELINES REST INTERFACE

APPENDIX 12 : BUILDING BLOCKS IN TREND ANALYSIS